# Power Spectral Density Analysis
# of Wind-Shear Turbulence
for Related Flight Simulations

ME-EM

DEPARTMENT OF
MECHANICAL ENGINEERING AND ENGINEERING MECHANICS

MICHIGAN TECHNOLOGICAL UNIVERSITY

POWER SPECTRAL DENSITY ANALYSIS

OF WIND-SHEAR TURBULENCE

FOR RELATED FLIGHT SIMULATIONS

by

Tony R. Laituri ✓

A THESIS

Submitted in partial fulfillment of the requirements

for the degree of

MASTER OF SCIENCE IN MECHANICAL ENGINEERING

MICHIGAN TECHNOLOGICAL UNIVERSITY

1988

This thesis, "Power Spectral Density Analysis of Wind-Shear Turbulence for Related Flight Simulations," is hereby approved in partial fulfillment of the requirements for the degree of MASTER OF SCIENCE IN MECHANICAL ENGINEERING.

Department: Mechanical Engineering - Engineering Mechanics

_____

Dr. George Treviño
Thesis Advisor

_____

Dr. John H. Johnson
Department Head

Date_____

I was born in a crossfire hurricane ....

It's all right now (in fact it's a gas).

— The Rolling Stones

ACKNOWLEDGEMENTS

To The Stones: thanks for the help on those late nites.

And finally to my parents: thank you for the
inspiration and assistance throughout the years. As
concerned parents, you always wanted to know what I was up
to; well, this paper should explain the last year or so. It
may not be of much practical value to you, but it'll be good
for grins.

Sincerely,

Tony R. Sartori

S '88 MTU

ABSTRACT

Meteorological phenomema known as microbursts can produce
abrupt changes in wind direction and/or speed over a very
short distance in the atmosphere. These changes in flow
chararteristics have been labeled "wind shear." Because of
its adverse effects on aerodynamic lift, wind shear poses
its most immediate threat to flight operations at low
altitudes. The number of recent commercial aircraft
accidents attributed to wind shear has necessitated a better
understanding of how energy is transferred to an aircraft
from wind-shear turbulence. Isotropic turbulence here
serves as the basis of comparison for the anisotropic
turbulence which exists in a low-altitude wind shear. The
related question of how isotropic turbulence "scales" in a
wind shear is addressed from the perspective of power
spectral density (psd). The role of the psd in related
Monte Carlo simulations is also considered.

TABLE OF CONTENTS

LIST OF FIGURES

- xi -

LIST OF TABLES

F	"F-Factor" hazard index
F_o	Specified hazard threshold on F
f	Longitudinal correlation function for isotropic turbulence
g	Transverse correlation function for isotropic turbulence; Magnitude of gravity
$\underset{\sim}{g}$	Gravity vector
H(s)	Shaping filter transfer function
H_I, H_A	Isotropic and anisotropic shaping filter transfer functions, respectively
$H(\varkappa)$	Frequncy response of the airframe
I_{ij}	Isotropic component of the C_{ij} correlation tensor
k	Wave number
k^4	Kurtosis (or "flatness") function
l	Inverse Laplace Transform of $L(s)$
L	Transverse correlation length for anisotropic turbulent downwash
M_n	Statistical moment of order "n"

M_1, M_2 Shear-flow velocity gradients

n Gaussian white noise source

n_I, n_A Gaussian white noise source signals corresponding to isotropic and anisotropic turbulence components, respectively

p Pressure

P, P' Points in a turbulent flow located by $\underset{\sim}{x}$ and $\underset{\sim}{x}+\underset{\sim}{r}$, respectively

$P(\cdot)$ Probability density function of $(\cdot)$

$\underset{\sim}{r}$ Separation vector for turbulence velocity correlation

r Magnitude of $\underset{\sim}{r}$

R Normalized correlation function

R_{ij} Normalized second-order, two-point velocity correlation tensor

s Laplace variable

s^3 Skewness function

S_{imj} Third-order, two-point velocity product correlation tensor

t	Time
T	Averaging time period
$\underset{\sim}{u}$	Turbulence velocity vector
u_i	Turbulence velocity
$\bar{U}_i$	Mean-flow velocity
U_i	Total fluid velocity
u,v,w	Longitudinal, lateral, and vertical turbulent velocity components, respectively
U,V,W	Longitudinal, lateral, and vertical components of turbulent wind, respectively
V	Constant forward flight speed of the aircraft
X,Y	Input and output, respectively
α	Glide-slope angle for approach and departure
β	Constant defined for axisymmetric turbulence theory, i.e., $\underset{\sim}{\lambda}\cdot\underset{\sim}{r}\equiv\beta r$
$\Delta(\cdot)$	Energy scaling factor

ι $\sqrt{-1}$

$\underset{\sim}{\lambda}$ Unit vector defining the preferred direction of turbulence anisotropy

Λ Longitudinal correlation length (integral scale) of isotropic turbulence

$\Delta\Lambda$ Change in integral scale due to anisotropy

ν Reduced frequency $\equiv \omega \, c/(2\ V)$

Φ_o Constant psd value for Gaussian white noise

Φ_{qq} Aircraft response psd

Φ_{ww} Power spectral density of downwash turbulence

$\Phi_{ww}^{(a)}$ Anisotropic component of Φ_{ww}

$\Phi_{ww}^{(i)}$ Isotropic component of Φ_{ww}

Ψ Scaling constant for simulation

$\varkappa$ Non-dimensionalized wave number $\equiv \omega\Lambda/V$

k	Single function required to define the isotropic turbulence self-interaction tensor
μ	Fluid vicosity coefficient
η	Velocity scaling factor of the correlation function
ρ	Fluid density
σ	Turbulence intensity
$\Delta\sigma$	Change in turbulence intensity due to anisotropy
τ	Time displacement
θ	Dummy variable representing the (ζr) product
ω	Circular frequency
ζ	Length scaling factor of the correlation function
$\mathbb{K}$	Matching factor for tranfer function formulation
$\mathbb{T}$	Time period corresponding to shaping filter characteristics
$\mathbb{W}$	Random variable
$\overline{(\cdot)}$	Mean value of $(\cdot)$
$\langle\cdot\rangle$	Ensemble average

$(\cdot)'$ Reference to the point located by $\underset{\sim}{x}+\underset{\sim}{r}$ in the two-point velocity correlation

δ_{ij} Kronecker delta tensor

$\mathcal{L}, \mathcal{L}^{-1}$ Laplace and inverse Laplace transformations, respectively

$\mathcal{O}(\cdot)$ "On the order of $(\cdot)$"

CHAPTER 1

An Introduction to Microbursts and Wind Shears

§ 1.1   INTRODUCTION TO THE PHENOMENON

Meteorological events such as thunderstorms and unstable frontal systems have long been considered dangerous from the perspective of aviation safety. Investigations into the alarming number of recent aircraft accidents involving thunderstorms have revealed the meteorological culprit - a strong, turbulent blast of air directed toward the ground - which has come to be known as a "downburst."

The mechanism by which the downburst is created is both a complex and sometimes violent one. From the investigation of the airliner crash at JFK Airport in 1975, much was learned about the convective atmospheric dynamics which causes the downburst. It was postulated by Fujita[1] that a violent atmospheric disturbance may occur when a moist, upper air fract drops precipitation through a relatively dry layer below it. As the precipitation evaporates, the dry layer cools. Consequently, a stream of dense cold air suddenly replaces the ground-heated, low-altitude air. Furthermore, as the resulting downdraft shears through the existing horizontal flow and plunges toward the ground (cf. Figure 1), turbulence is invariably generated. The downdraft eventually impacts the ground, and spreads out both horizontally and radially thus creating even more turbulence. During the evolution of the downburst (sometimes lasting up to 15 minutes as noted in Figure 2),[2] the dimensions of the all-important, low-altitude phase may be on the order of 15-30 meters high with a radial spread of 2.5 kilometers.[3] Realization of the phenomenon's relatively

GROUND
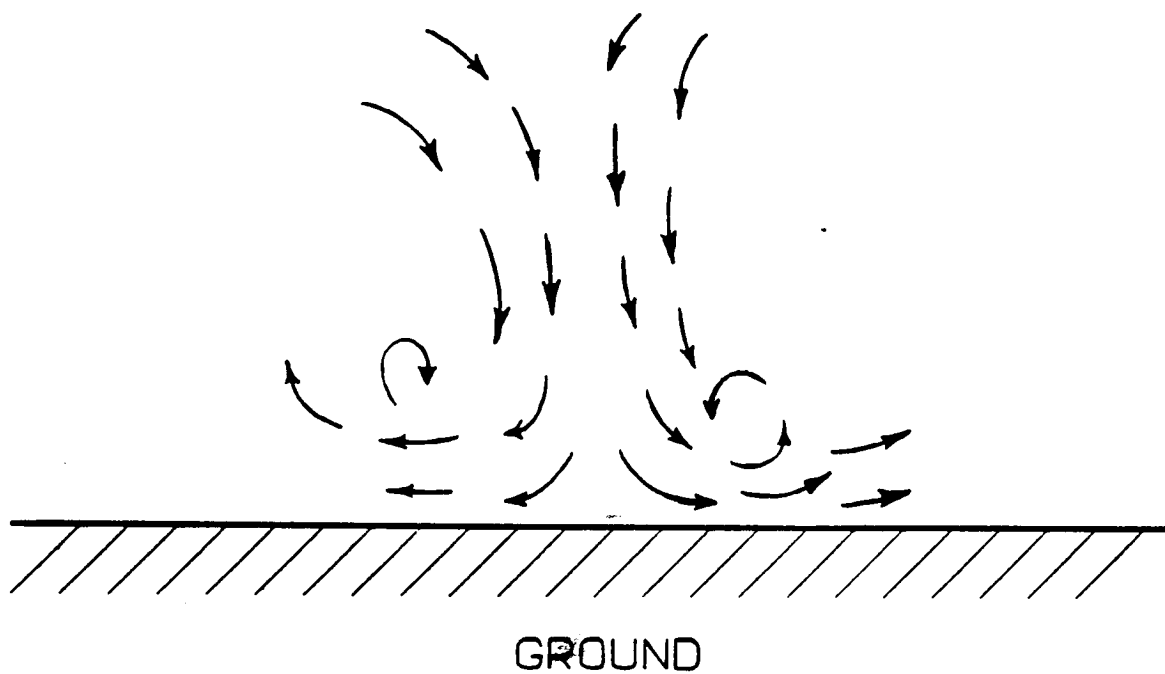
Figure 1 : Atmospheric Turbulence Generation as a
Result of the Downburst Phenomenon
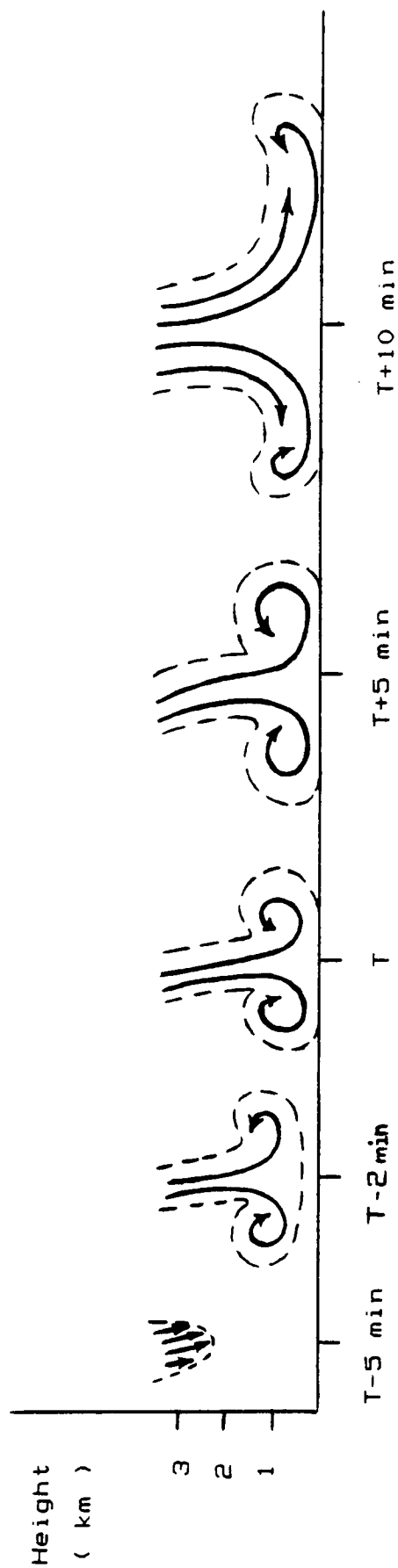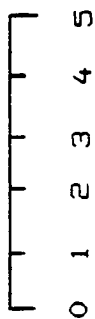
Figure 2 : Evolution of a Typical Microburst

small meteorological size serves as the motivation for the
term "microburst" to be used.

Typically, the distinguishing characteristics of the
microburst are winds which are both localized and highly
variable as can be seen from Figures 3 and 4.[4] These abrupt
changes in wind speed and/or direction over a short
atmospheric distance are referred to in the literature as
"wind shear." For the purposes of this study, wind shear
will be defined as a flow which has a spatially nonconstant,
mean velocity profile. It is obvious that flight through a
"wind shear-infected area" will tax both pilot and aircraft
since velocity gradients may drop airspeed to critically low
levels. In summary, wind shear poses an immediate threat to
flight operations at low altitudes due to its adverse
effects on aerodynamic lift.

The scenerio of microburst penetration by an aircraft
in the landing mode is shown in Figure 5. First, the
aircraft encounters a strong head wind. Although turbulence
typically accompanies the increasing airspeed, pilot
confidence is high during this phase since aircraft
performance increases with the additional aerodynamic lift.
Because the intent is to land the aircraft, the pilot
intuitively trims the aircraft through the remnants of the
downdraft. Finally, the head wind suddenly becomes a strong
tail wind. At this point, performance is seriously degraded
since the distinct head-to-tail wind swing has reduced
airspeed by as much as 50 knots.[5] Such a reduction may be
enough to lose flying speed. The result may be a fatal
crash (see Figure 6).[6]

Figure 3 : Dust Ring of a Typical Microburst
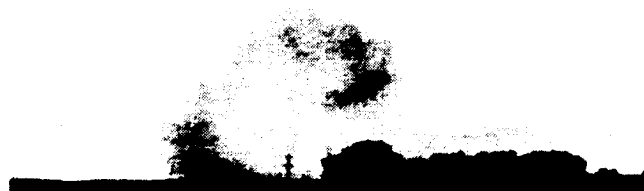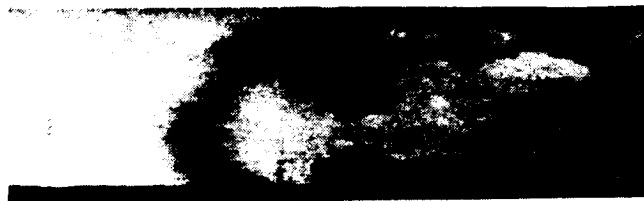
Figure 4 : Outflow Vortex Circulation in a Microburst

GROUND
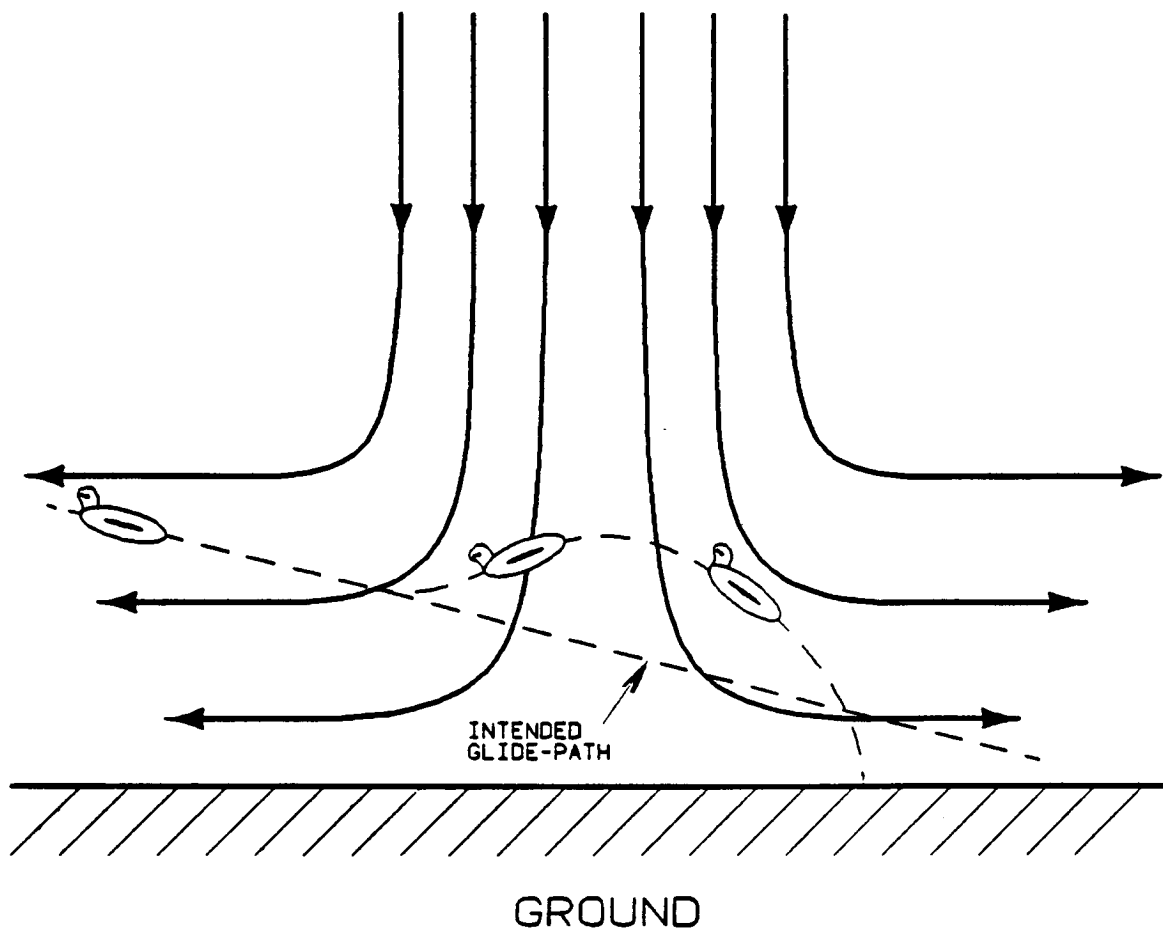
Figure 5   Typical Microburst and Aircraft Response
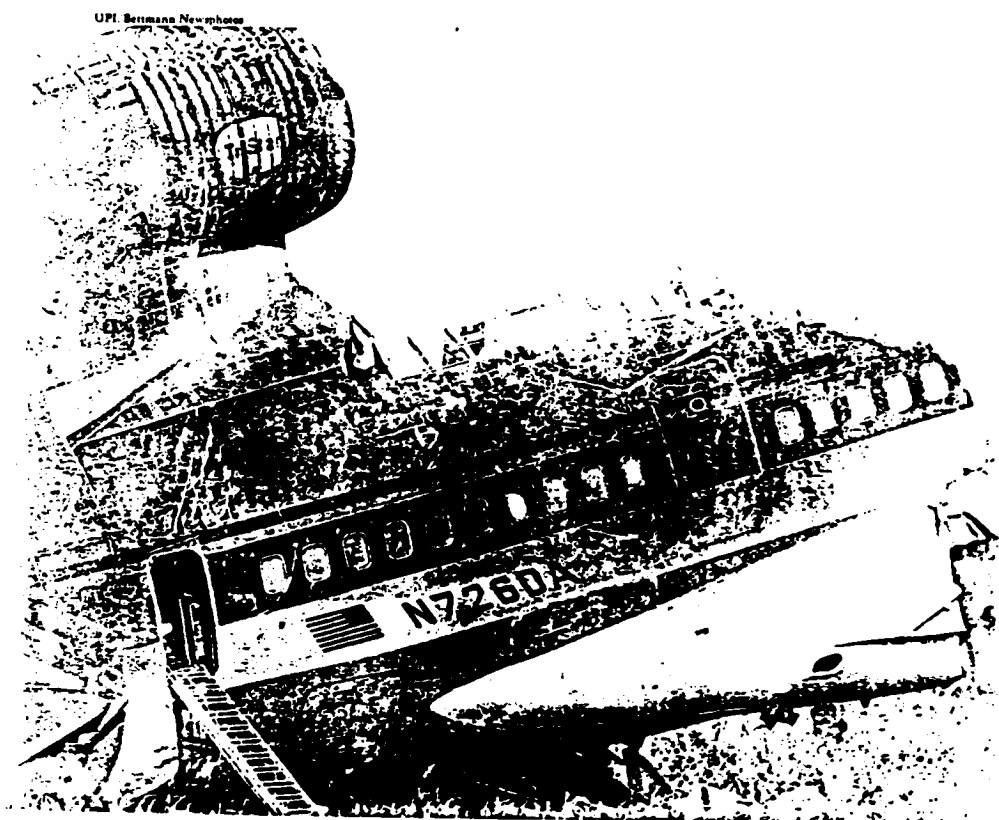
Figure 6 : 1985 Delta L-1011 Accident at Dallas-Fort Worth
          Airport (136 people killed)

In the last 10 years, 575 people have been killed in commercial aircraft accidents in the United States due to the wind shear phenomenon.[7] Likewise, wind shear-induced accidents have also been reported in Great Britain, Germany, France, Italy, Australia, and Japan. Consequently, an enhanced fundamental understanding of microbursts, wind shear, and low-level atmospheric turbulence is a high-priority research issue.

§ 1.2 RELATED RESEARCH

Flight science authorities agree that the "solution" to the wind shear "problem" is multi-faceted.[5] The related research programs of NASA and FAA primarily focus on three elements: 1) hazard characterization, 2) sensor technology, and 3) flight management and operations.

Hazard characterization is the study of the physics of the microburst phenomenon. Inherent within this phase of the research effort is analysis of aircraft aerodynamics in wind shears and heavy rain. It follows that wind shear velocity profiles, rainfall studies, and turbulence models are important contributions from this research area.

The sensor technology component of the research effort deals with the prediction and detection of potentially dangerous meteorological events. This section subdivides into airport-fixed and airborne (in situ) sensor technologies. Next Generation Radar Fields (NEXRAD) are presently being investigated by NOAA, FAA, and USAF for future use as airport radars. Technical and economical

difficulties have slowed progress in the ground-based sensor implementation. The other detection device is the *in situ*, look-ahead sensor. This onboard computer system is being devised to scan the forward atmospheric environment, evaluate a "hazard index," and annunciate a warning to the pilot in a time period adequate to ensure either avoidance or escape of the threat. Look-ahead sensor technology is beyond state-of-the-art, and is not expected to be operational until the mid-1990's.[5]

The third component of wind shear research is flight management. Simply put, this phase concentrates on informing the pilot on how to get out of the wind shear encounter subject to aircraft performance constraints.

An important element of flight management studies is flight simulation. Simulators allow pilots to experience threatening wind shears in a controlled environment with intent to better prepare them for potential real-life events. Realistic wind shear representations in flight simulators are practical and economical, and can help crews to coordinate their efforts in critical situations. Realism in the simulation of flight through hazardous atmospheric environments has improved with the introduction of lateral and vertical winds, as well as vortex[3] and turbulence influences.[8] The focus of the present work is the characterization of wind-shear turbulence. Interestingly enough, the analysis that follows may directly apply to each of the three research branches described above - a fact expanded upon in Chapter 4.

§ 1.3   PRESENT RESEARCH OBJECTIVES

There are three principle objectives of the present research:

1) to model the statistical characteristics of the turbulence associated with a low-altitude, sheared mean flow,

2) to study the effect of these characteristics on aircraft response, and

3) to consider a method of simulating the modelled turbulence.

All of these issues will herein be addressed from the perspective of power spectal density (psd) - a popular frequency domain statistic of turbulence.

CHAPTER 2

FUNDAMENTALS OF RANDOM PROCESSES

§ 2.1   Random Processes and their Classifications

Physical phenomena whose time-dependence cannot be described by deterministic mathematical relationships are known as <u>stochastic</u> or <u>random</u> <u>processes</u>. Atmospheric turbulence, with its constantly changing pressure and velocities, is an example of a random process. Consequently, random processes must be defined in probabilistic terms and statistical averages.

Stochastic processes are generally classified as either <u>stationary</u> or <u>nonstationary</u>. A stationary random process is one whose statistics are independent of time, while nonstationarity implies time-dependent statistics. *A priori* classification of random processes is often based upon the physics of the event in question. For example, the vibration environment typical of an aircraft in constant-speed, constant-altitude flight through a tame atmosphere would most likely be a stationary one; whereas, the vibration levels of booster vehicle components during the ascent the rocket would certainly be nonstationary due to the time-dependent accelerations and pressures[9] encountered. To quantitatively describe such processes, a precise and unambiguous mathematical vocabulary must first be established.

§ 2.2   Definitions for Stationary Random Processes

The definitive description of a <u>random</u> <u>variable</u> is its <u>probability</u> <u>density</u> <u>function</u> (pdf). The primary random

variables in a turbulent fluid are the (space- and)
time-dependent velocity and pressure. Clearly, if an
atmospheric experiment is repeated under identical
conditions, different values of, say, pressure would arise
each time. A graphical representation of such a random
variable data set is depicted in Figure 7. Each record is
called a sample, and the collection of time histories
necessary to totally define the random process is called an
ensemble. At a particular time, say t_1, the number of times
the entire ensemble takes on values between some { $\omega(t_1)$ }
and { $\omega(t_1) + \Delta\omega(t_1)$ } defines a pdf as $\Delta\omega \rightarrow 0$ (see Figure
8). For practical purposes, it is assumed that the pdf
formed from a large but finite number of time histories
adequately represents the random variable.

An alternative to constructing a pdf is to define
statistical averages which are also known as statistical
moments. For a fixed point in space, the shape of the
probability density function can be typically defined by its
various-order moments given as[10]

$$M_n \equiv <\omega^n> \equiv \int_{-\infty}^{\infty} \omega^n \ P(\omega) \ d\omega \qquad (2.1)$$

where M_n is the moment of order n, and $P(\omega)$ is the pdf of
the random varible ω.

The first two statistical moments of $P(\omega)$ are found to
be

- 14 -
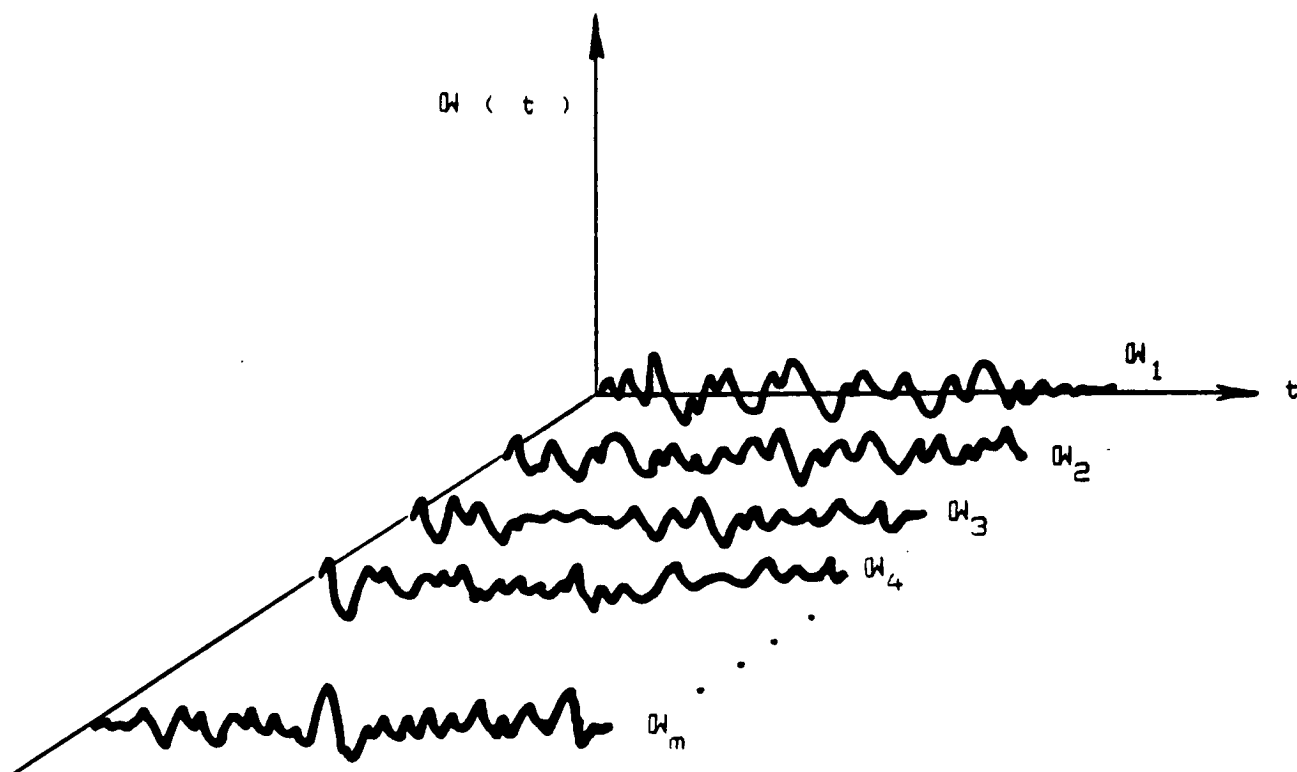
Figure 7 : Random Data Set for a Stochastic Process
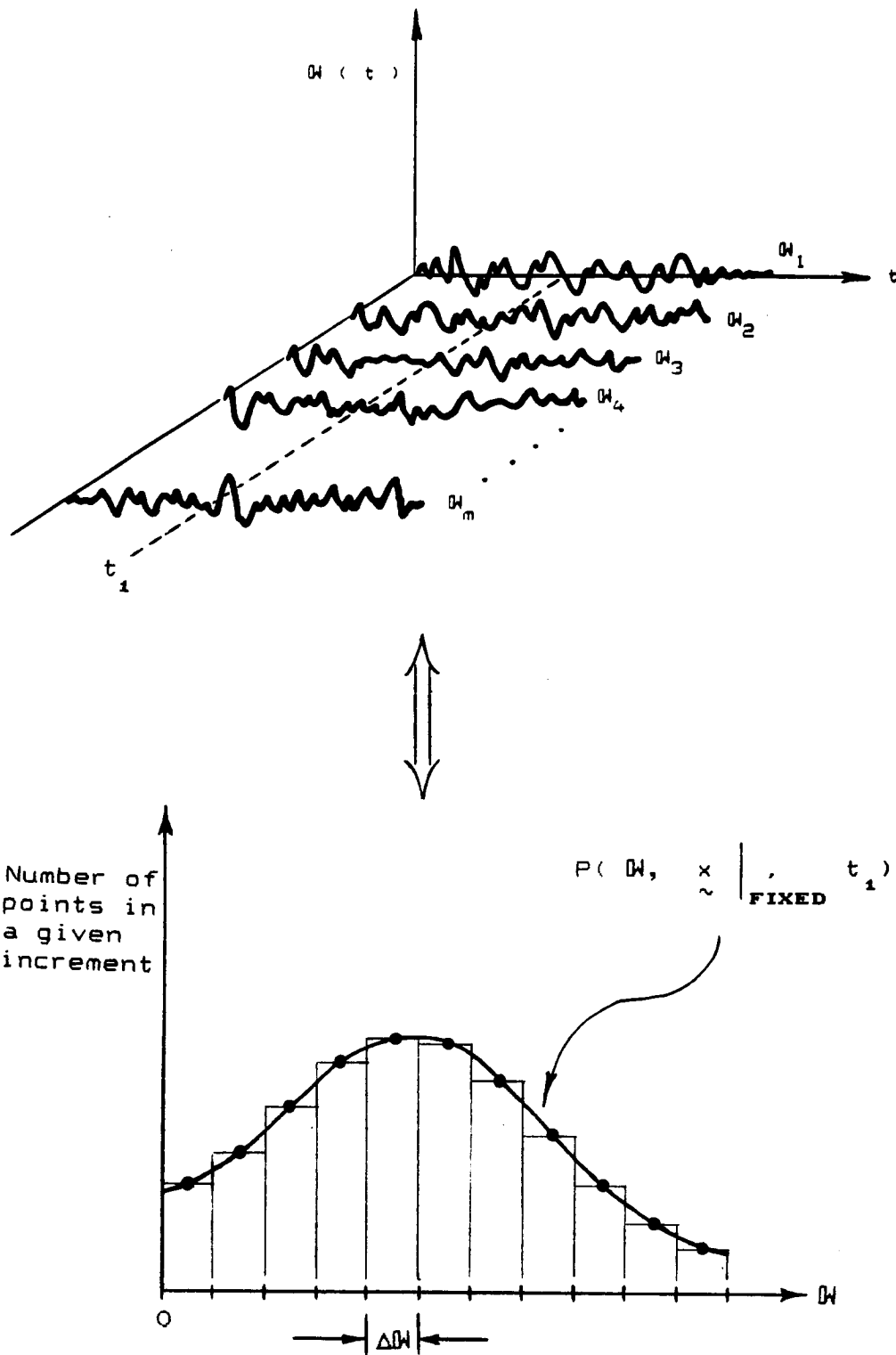
Figure 8 : Determination of a Probability
Density Function (pdf)

$$M_1 \equiv \; < \omega > \; \equiv \; \overline{\omega} \; \equiv \; \int_{-\infty}^{\infty} \omega \; P(\omega) \; d\omega \qquad . \qquad (2.2)$$

and

$$M_2 \equiv \; < \omega^2 > \; \equiv \; \overline{\omega^2} \; \equiv \; \int_{-\infty}^{\infty} \omega^2 \; P(\omega) \; d\omega \qquad . \qquad (2.3)$$

The first statistical moment, called the <u>mean</u> or <u>expected value</u>, defines the "centroid" of the pdf. The second moment is the expected value of ω^2, and is commonly referred to as the <u>mean</u> <u>squared</u> <u>value</u> of ω . Statistical moments, if taken about the mean value, are known as <u>central</u> <u>moments</u>, and are defined as follows:

$$< \; (\; \omega - \overline{\omega} \;)^n \; > \; \equiv \; \int_{-\infty}^{\infty} (\; \omega - \overline{\omega} \;)^n \; P(\omega) \; d\omega \qquad . \qquad (2.4)$$

The first central moment can be considered as an "adjusted" centroid as indicated below:

$$< \omega - \overline{\omega} > \equiv \int_{-\infty}^{\infty} (\omega - \overline{\omega}) \, P(\omega) \, d\omega$$

$$\equiv \int_{-\infty}^{\infty} \omega \, P(\omega) \, d\omega - \overline{\omega} \int_{-\infty}^{\infty} P(\omega) \, d\omega$$

$$= \overline{\omega} - \overline{\omega} = 0$$

Evaluation of the second central moment yields:

$$< (\omega - \overline{\omega})^2 > \equiv \int_{-\infty}^{\infty} (\omega - \overline{\omega})^2 \, P(\omega) \, d\omega$$

$$= \int_{-\infty}^{\infty} \omega^2 \, P(\omega) \, d\omega - 2\overline{\omega} \int_{-\infty}^{\infty} \omega \, P(\omega) \, d\omega + \overline{\omega}^2 \int_{-\infty}^{\infty} P(\omega) \, d\omega$$

$$= \overline{\omega^2} - \overline{\omega}^2 \quad .$$

The quantity $\overline{\omega^2} - \overline{\omega}^2$ is known as the <u>variance</u> or <u>intensity</u> of ω and is commonly denoted by σ^2 . The variance serves as

a measure of the spread of the data about the mean.

The next two central moments, in conjunction with the mean and the variance, give a good description of the probability density function of the random variable. The third central moment, called the skewness, is denoted s^3 . It defines the degree of asymmetry about the expected value. The kurtosis or flatness, k^4 , is the fourth central moment, and it describes the amount of information contained in the tails of the pdf. It is important to note that the higher-order central moments (e.g., skewness and kurtosis) become important when the random process significantly deviates from the standard Gaussian form.

Recall that the Gaussian probability density function is

$$P(\omega) = \frac{1}{\sigma \sqrt{2\pi}} \exp \left\{ \frac{(\omega - \overline{\omega})^2}{2 \sigma^2} \right\} \quad . \qquad (2.5)$$

Without doubt, the Gaussian probability density function is the most widely used pdf in analyses and simulations of atmospheric velocity fluctuations. Other common pdfs that are used include: the modified Gaussian, the Bessel, and the modified Bessel. Each of these forms will be considered in more detail when turbulence simulation concepts are addressed in Chapter 4. At present, it is important to note that the Gaussian pdf demands that the odd-order moments (skewness, superskewness - the fifth-order moment, etc.)

vanish. Hence, the Gaussian probability density function is necessarily symmetric about $\overline{W}$ as is shown in Figure 9. Unfortunately, real hydrodynamic turbulence typically has a skewed, non-Gaussian pdf (see Figure 10), thereby making Gaussian turbulence simulations questionable in terms of fidelity.[11] Again, this topic will be considered in Chapter 4.

If the statistical properties of the random variable do not depend on spatial position, the process is said to be homogeneous. For the purposes of this study, homogeneiety infers that the statistical representation of low-altitude turbulence is independent of both elevation and geographic location. This is most assuredly not the case.[12] The present analysis will deal primarily with inhomogeneous turbulence.

Often, an "infinite" number of time records of a single random process is not available to meet the ensemble average criteria. If a time average for a discrete number (one as a minimum) of records results in the same statistics as that from an ensemble average, the process is said to be ergodic. It should be emphasized that, in the classical sense, the assumption of ergodicity is valid only for a stationary process, and that it allows the total random process to be completely represented by a single time record. Due to experimental and econmonical limitations, the concept of ergodicity is frequently invoked in random process analyses. Consequently, the aforementioned statistical moments may then be written as follows:

P (W)

Symmetry about mean

W̄   W
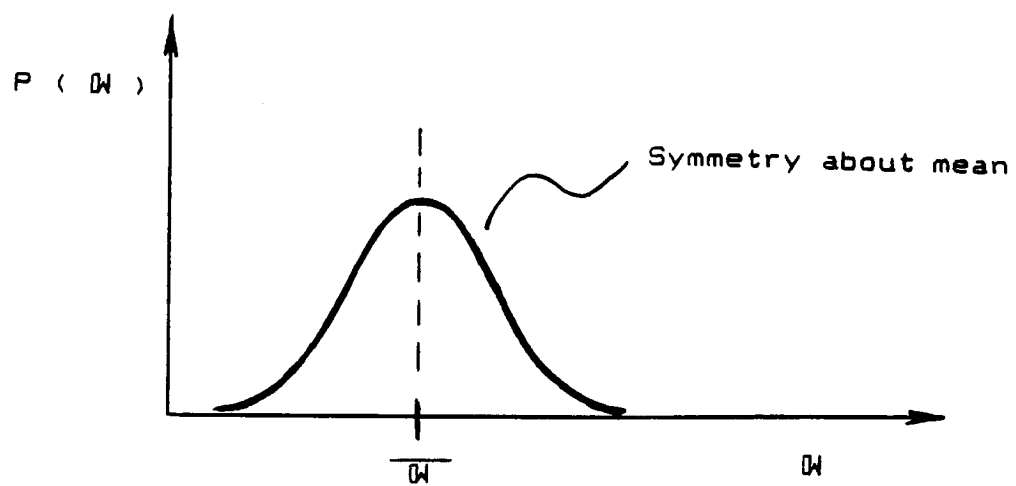
Figure 9 : Gaussian Probability Density Function (pdf)
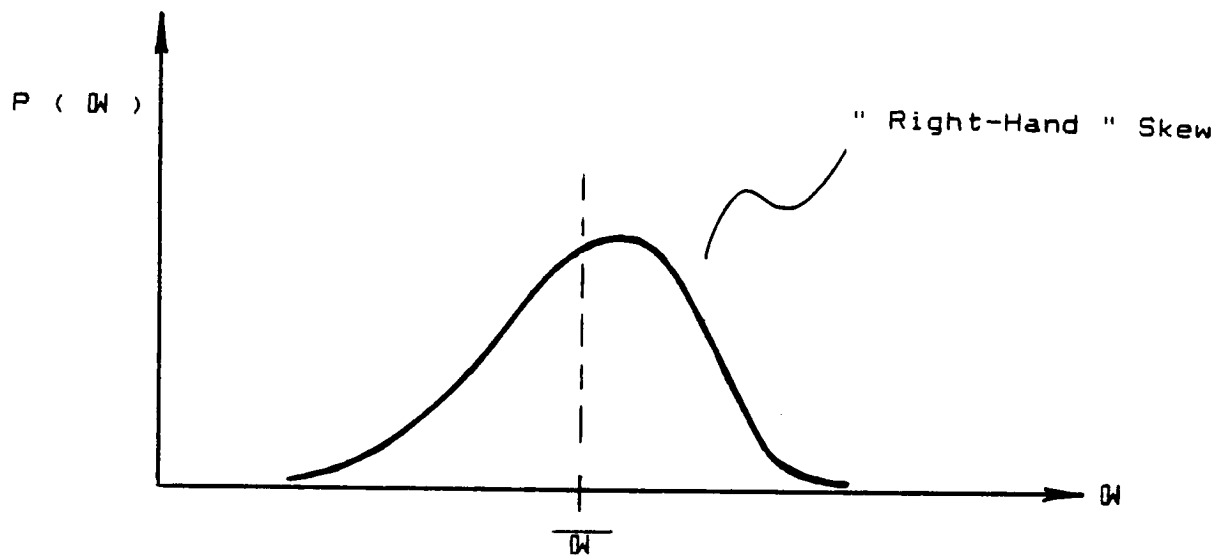
Figure 10 : Skewed Probability Density Function Typical
of Real Nonhomogeneous Turbulence

$$M_1 \equiv\ <\ \omega\ >\ \equiv\ \overline{\omega}\ =\ \lim_{T \to \infty} \frac{1}{2T} \int_{-T}^{T} \omega(\underset{\sim}{x},t)\ dt \qquad (2.6)$$

$$<\ (\ \omega\ -\overline{\omega}\ )^2\ >\ \equiv\ \sigma^2\ =\ \lim_{T \to \infty} \frac{1}{2T} \int_{-T}^{T} (\ \omega\ -\overline{\omega}\ )^2\ dt \qquad (2.7)$$

$$<\ (\ \omega\ -\overline{\omega}\ )^3\ >\ \equiv\ s^3\ =\ \lim_{T \to \infty} \frac{1}{2T} \int_{-T}^{T} (\ \omega\ -\overline{\omega}\ )^3\ dt \qquad (2.8)$$

$$<\ (\ \omega\ -\overline{\omega}\ )^4\ >\ \equiv\ k^4\ =\ \lim_{T \to \infty} \frac{1}{2T} \int_{-T}^{T} (\ \omega\ -\overline{\omega}\ )^4\ dt\ , \qquad (2.9)$$

where T is "sufficiently" large. Taking into account the practicality of a time record, Equations (2.6) - (2.9) may be rewritten as follows:

$$M_1 \equiv\ <\ \omega\ >\ \equiv\ \overline{\omega}\ =\ \lim_{T \to \infty} \frac{1}{T} \int_{0}^{T} \omega(\underset{\sim}{x},t)\ dt \qquad (2.10)$$

- 23 -

$$\sigma^2 = \lim_{T \to \infty} \frac{1}{T} \int_0^T (W - \overline{W})^2 \, dt \qquad (2.11)$$

$$s^3 = \lim_{T \to \infty} \frac{1}{T} \int_0^T (W - \overline{W})^3 \, dt \qquad (2.12)$$

$$k^4 = \lim_{T \to \infty} \frac{1}{T} \int_0^T (W - \overline{W})^4 \, dt \qquad . \qquad (2.13)$$

§ 2.3   THE AUTOCORRELATION FUNCTION

The correlation function is very useful in signal analysis. When properly interpreted, it serves as a measure of the degree of predictability of the random signal at some future time, $t+\tau$, based on the knowledge of a signal at time, t. The <u>auto</u>correlation function requires only a single signal, and is defined as[13]

$$C_{WW}(\underset{\sim}{x},\tau) \equiv < \Bar{W}(\underset{\sim}{x},t)\ \Bar{W}(\underset{\sim}{x},t{+}\tau) > = \frac{1}{T} \int_{o}^{T} \Bar{W}(\underset{\sim}{x},t)\ \Bar{W}(\underset{\sim}{x},t{+}\tau)\ dt.$$

(2.14)

The autocorrelation function may also be considered from the perspective of <u>scaling effects</u>. One scaling effect of the autocorrelation is evident since the autocorrelation function takes on the value of the variance at $\tau = 0$ (i.e., $C_{WW}(\tau = 0) = \sigma^2$) since

$$C_{WW}(\underset{\sim}{x},\tau{=}0) = \frac{1}{T} \int_{o}^{T} \Bar{W}^2(\underset{\sim}{x},t)\ dt \equiv \sigma^2(\underset{\sim}{x}) \quad .$$

Should the autocorrelation be used to analyze velocity fluctuations in a turbulent flow field, the variance (portrayed on the ordinate axis of Figure 11) would correspond to a velocity scaling effect. Note that this form of scaling is dependent on the signal itself, and is accordingly a "natural" scaling effect.

A <u>normalized correlation function</u>, defined as
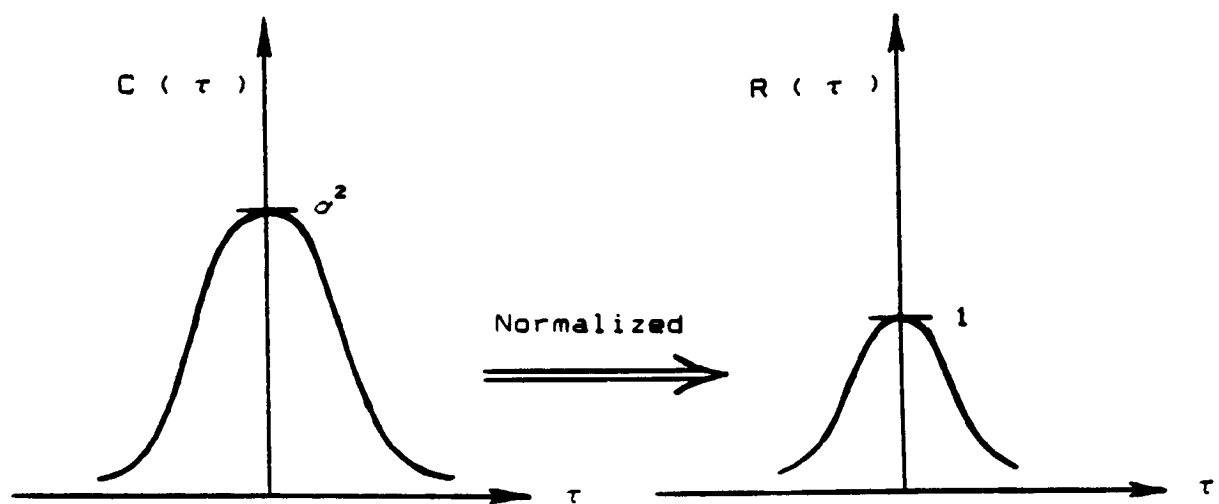
Figure 11 : Ordinate Scaling of the Autocorrelation Function

$$R(\underset{\sim}{x},\tau) \equiv \frac{C(\underset{\sim}{x},\tau)}{C(\underset{\sim}{x},\tau=0)} = \frac{C(\underset{\sim}{x},\tau)}{\sigma^2} \quad , \qquad (2.15)$$

is in essence an <u>ordinate</u> <u>scaling</u> of the autocorrelation function with $R(\underset{\sim}{x},\tau) \leq 1$ and $R(\underset{\sim}{x},\tau = 0) = 1$ as a result of the Schwartz Inequality. Abscissa scaling may be defined by

$$\Lambda(\underset{\sim}{x}) \equiv \int_0^\infty R(\underset{\sim}{x},\tau) \ d\tau \quad , \qquad (2.16)$$

where Λ is known as the <u>integral</u> <u>scale</u> (which may be graphically interpreted in Figure 12). For a turbulent velocity correlation, Λ is referred to as a <u>length</u> <u>scale</u> as a result of unit analysis of the integral of Equation (2.16). Unlike the velocity scaling effect, the length scale is quite artificial and subjective, i.e., since no absolute length scale exists in turbulence, length metrics must always be defined by the analyst in order to quantify a certain aspect of the study. Consequently, a stationary random process may then be more appropriately defined as one whose scaling effects are time invariant while nonstationarity implies time-dependent scaling effects.

- 27 -

$$\Lambda = \frac{\int_{0}^{\infty} C(\tau)\, d\tau}{C(\tau = 0)}$$
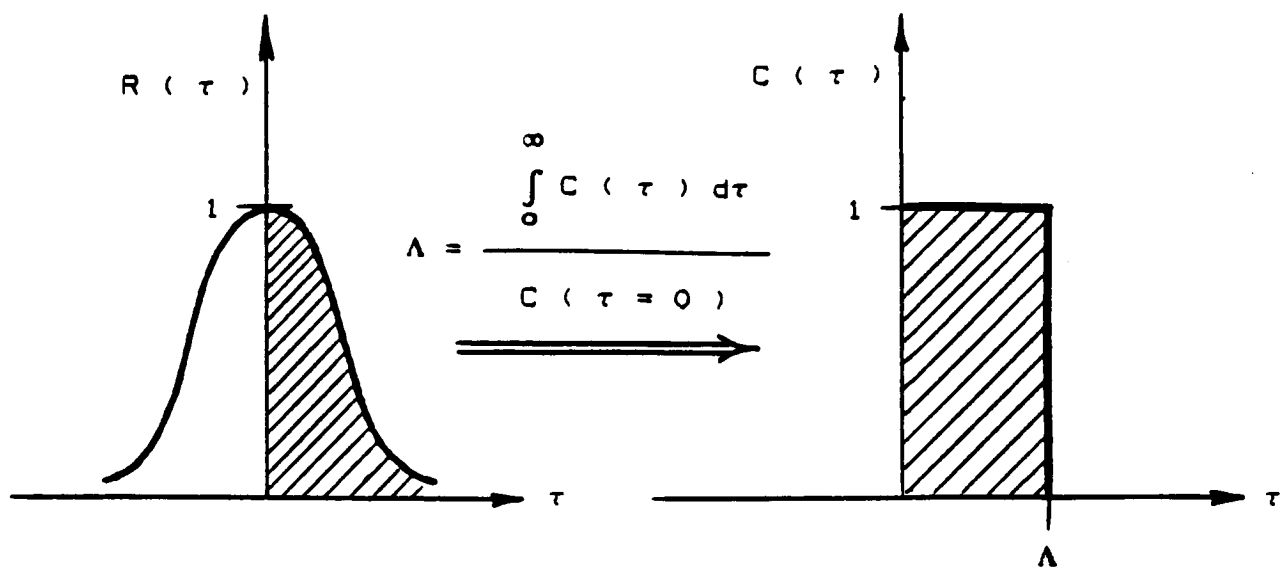
Figure 12 : Abscissa Scaling of the Autocorrelation Function

§ 2.4   Power Spectral Density

Another important tool in random process analysis is power spectral density (psd). The power spectral density function provides information on the frequency content of a random (or deterministic) process. Mathematically, the psd of a random process is the Fourier transform of an autocorrelation function - a relation known as the Wiener-Khintchine theorem for aperiodic functions with finite energy[14] Loosely stated, the information provided by the autocorrelation function in the time-lag domain is "mapped" into the frequency domain. The transform pair for an inhomogeneous random process consists of the following:

$$\Phi\,(\underset{\sim}{x},\omega) \;=\; \int_{-\infty}^{\infty} C(\underset{\sim}{x},\tau)\; e^{-\iota\omega\tau}\; d\tau \tag{2.17}$$

and

$$C(\underset{\sim}{x},\tau) \;=\; \frac{1}{2\pi} \int_{-\infty}^{\infty} \Phi\,(\underset{\sim}{x},\omega)\; e^{-\iota\omega\tau}\; d\omega \;\;\;. \tag{2.18}$$

Evaluation of Equation (2.18) at $\tau = 0$ gives

$$C(\underset{\sim}{x}, \tau = 0) = \frac{1}{2\pi} \int_{-\infty}^{\infty} \Phi(\underset{\sim}{x}, \omega) \, d\omega \quad , \qquad (2.19)$$

which is defined in electrical vernacular as the "average power" - hence, the "power" of power spectral density. To determine the total power in a frequency band $\omega_1 \leq \omega \leq \omega_2$, it follows from Equation (2.19) that

$$\text{Total Power}\Big|_{\text{Band}} = \frac{1}{2\pi} \int_{\omega_1}^{\omega_2} \Phi(\underset{\sim}{x}, \omega) \, d\omega \quad . \qquad (2.20)$$

The power spectral density has other noteworthy characteristics: it is an even-valued, real function of ω with non-negative average power,[15] and it accordingly contains no phase information.

§ 2.5   NONSTATIONARY RANDOM PROCESS THEORY

The concept of a nonstationary process is a negative and highly nondeterministic one. As stated before, a nonstationary random process is one whose statistics vary with time. Much of the previous research done on stationary processes does not strictly apply to a process with

time-varying characteristics. Nevertheless, engineers have knowingly applied stationary process theory to nonstationary signals. It is in this statement that the justification for studying nonstationarity lies. There simply exists too much data which clearly demonstrates nonstationary behavior for it to be overlooked. Consequently, the base knowledge of nonstationary random processes has been growing in recent years.

An objective of this study is to make a nonstationary random process look as much like a stationary one as possible. The autocorrelation function of Equation (2.14) for a nonstationary process now takes the time-dependent form:

$$C(t,\tau) \equiv \; < \; \Box\!\!\text{W}(t_1) \; \Box\!\!\text{W}(t_2) \; > \qquad , \qquad (2.21)$$

where $t = (t_1 + t_2)/2$ and $\tau = t_2 - t_1$. Note that the space-dependent autocorrelation becomes time-dependent when the analysis is of turbulence measured while translating through a nonhomogeneous medium (cf. Equations (2.14) and (2.21)).

As before, the autocorrelation function can be considered in terms of scaling effects. The difference here is that the nonstationary autocorrelation has time-dependent ordinate and abscissa scaling effects. Consequently, the integral scale and variance - the primary statistics in turbulence scaling - are time-variant.

The most commonly used correlation function for nonstationary random process analysis is the uniformly-modulated type,

$$C(t,\tau) = \sigma^2(t) \; R(\tau) \qquad , \qquad (2.22)$$

where $\sigma^2(t)$ is the time-varying "modulator." Implicit within this correlation form is the constraint imposed upon the integral scale - that of time-invariance.

In recent studies,[16,17] a more general form has been recommended to incorporate both variance and length time-dependent scaling effects, namely

$$C(t,\tau) = \eta \; R(\zeta\tau) \qquad , \qquad (2.23)$$

where $\eta = \eta(t) \equiv \sigma^2(t)$ and $\zeta = \zeta(t) \equiv 1/\Lambda(t)$.

The time-dependent scaling of the autocorrelation function may be better understood by considering it to be "self-preserving" with time. If the autocorrelation evolves in a self-preserving manner, its geometric shape distorts due to the scaling effects, but its algebraic form in τ is

retained (e.g., parabolas become scaled parabolas as time evolves). Figure 13 illustrates the self-preserving behavior of a time-dependent correlation function. It should be noted that the assumption of self-preservation is simply a mathematical contrivance with its related geometric analog being the affine transformation.[18,19] The application of the self-preservation assumption to the decay of atmospheric turbulence will be considered in more detail in Chapter 3.
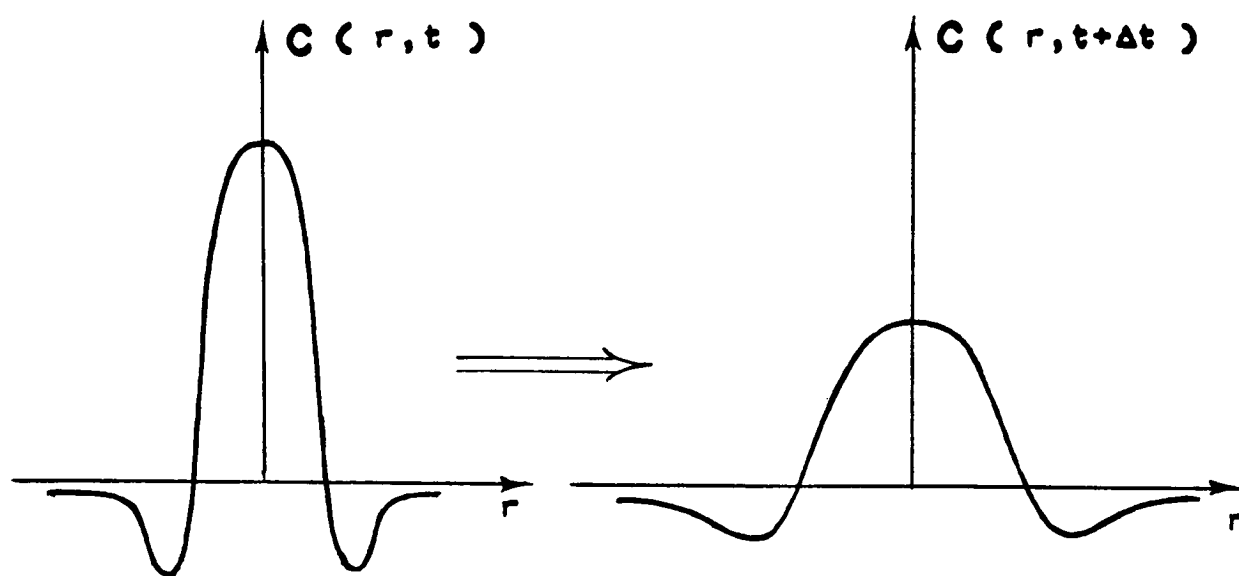
Figure 13 : Evolution of a " Self-Preserved " Correlation Function

CHAPTER 3

TURBULENCE MODELLING

§ 3.1 Turbulent Gust Environment

Random excitation of an airframe by atmospheric turbulence has long been a major concern of the aviation community. Turbulence, as defined by Hinze,[20] is "an irregular condition of flow in which various quantities (e.g. velocity and pressure) show a random variation with time and space, so that statistically distinct average values can be discerned." For the purposes of this analysis, turbulence will be defined as a random, fluctuating component which is linearly superimposed upon a deterministic mean. In general, an aircraft is exposed to the turbulent gust environment shown in Figure 14. Turbulence velocity components $u(x,t)$, $v(x,t)$, and $w(x,t)$ are known as the side, fore, and down gusts, respectively. Turbulent down gusts and their role in a wind shear will be the focus of this study; the turbulence of concern is therefore one-dimensional in nature as shown in Figure 15. The more realistic, and accordingly more complex, two-dimensional turbulence field is shown in Figure 16 for comparison.

§ 3.2 Mathematical Representations of Turbulence

In order to model the exceedingly complex nature of low-level atmospheric turbulence, the "domain" of possible mathematical representations of turbulence should be considered. The lower bound in the mathematical hierarchy is <u>isotropic turbulence</u>. Isotropy requires turbulence

- 36 -

u ($\underset{\sim}{x}$, t) : Sidewash Gusts

v ($\underset{\sim}{x}$, t) : Fore and Aft Gusts

w ($\underset{\sim}{x}$, t) : Up and Downwash Gusts
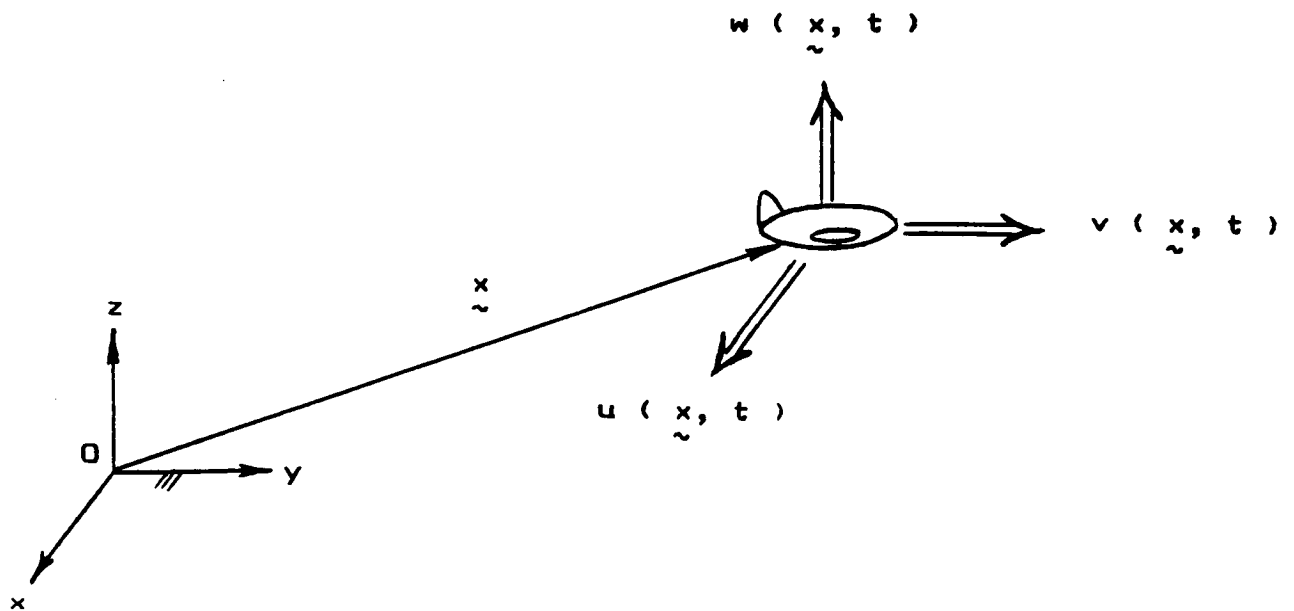
Figure 14 : Turbulent Gust Environment
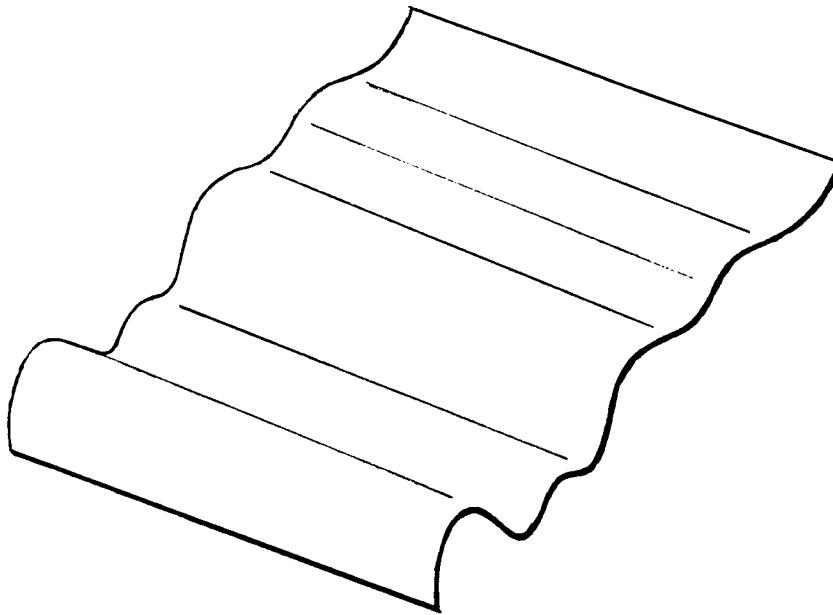
Figure 15 : One-Dimensional Turbulent Downwash Field
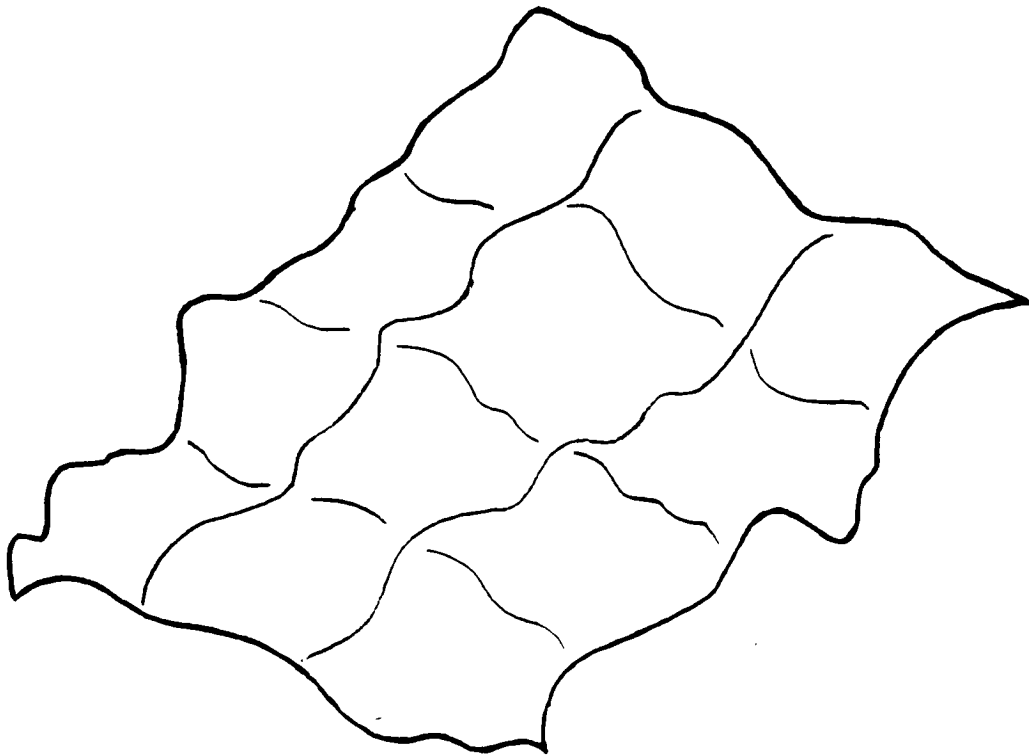
Figure 16 : Two-Dimensional Turbulent Downwash Field

quantities to be unaltered by rotation and reflection of the defining coordinate system. Isotropic turbulence therefore has statistical parameters which scale the same way in all spatial directions. This type of turbulence, although mathematically pleasing, is purely hypothetical in a global sense. Nonetheless, it, like its analog in solid mechanics (material isotropy), is of considerable value. Often, the difference between results based upon the assumption of isotropy and actual results is sufficiently small, thereby making isotropy-based assumptions acceptable for first estimations.

Anisotropic turbulence is that which does not fit the definition of isotropy. This brand of turbulence is much more difficult to mathematically represent. As shown in Figures 17(a) and 17(b), gradients in a turbulent field do not meet the criteria which define isotropy. Therefore, the turbulence associated with both microburst and low-altitude wind shear phenomena is undeniably anisotropic.

One of the simplest mathematical forms of anisotropy is axisymmetric turbulence. It is characterized by a tendency for preferred scaling in one prescribed spatial direction (known as a "preferred direction"). This same basic concept can be applied to the turbulence associated with a microburst. In this case, the anisotropy is the result of the microburst's downward blast upon the nearby ground. Consequently, the mathematical representation chosen to model the flow peculiar to a microburst - the axisymmetric type - serves as a "middle ground" of sorts with the extremes being both the intimidating complexity of full, probabilistic anisotropy and the unrealistic character of
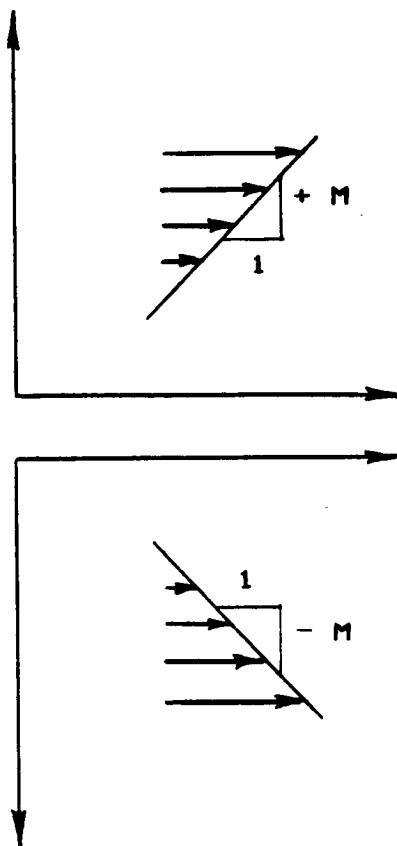
A positive-velocity gradient becomes a negative one
upon reflection about the x-axis

Figure 17 (a) : Anisotropy *via* Sign Change Upon
                  Reflection of Axes
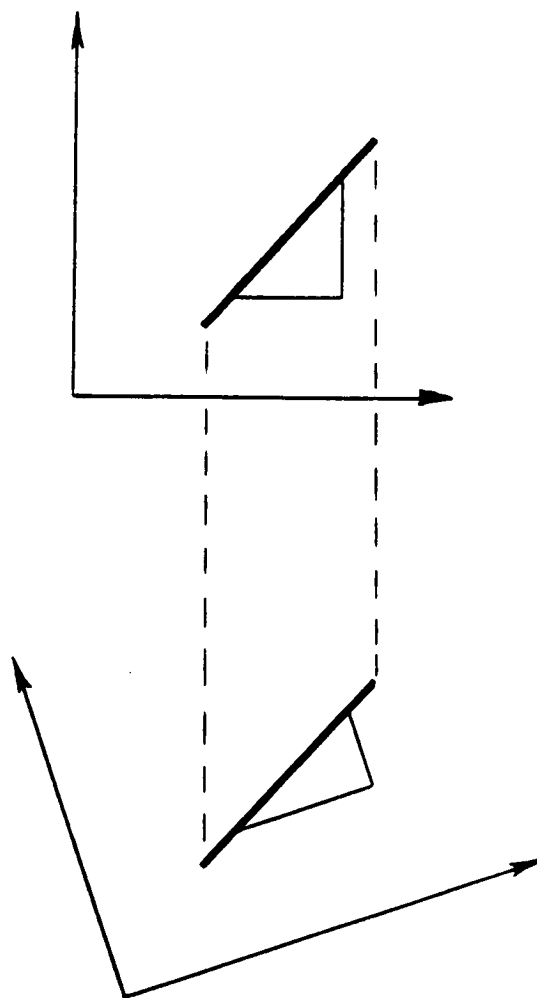
A change in the magnitude of the velocity gradient
after rotation of the defining coordinate axes

Figure 17 (b) : Anisotropy *via* Magnitude Change Upon
Rotation of Axes

isotropy.

The kinematics of both isotropic and axisymmetric turbulence has been firmly established by such researchers as H.P. Robertson,[21] and George Batchelor.[22] Recall that axisymmetric turbulence, unlike the global symmetry of isotropic turbulence, has symmetry only about a defined direction. The average value of any function of velocities and of their derivatives is _invariant_ under arbitrary rotations about an axis in the preferred direction. It also requires invariance of these functions with respect to reflections in planes through the given direction. H.P. Robertson's[21] inspired application of invariant theory to the kinematical and dynamical aspects of isotropic turbulence naturally led to a similar analysis for axisymmetric turbulence. (A complete summary of invariant theory and its role in the correlation functions may be found in Appendix A.)

§ 3.3   ANISOTROPY FOR FLIGHT SIMULATION

It follows from Appendix A that the two-point velocity correlation for axisymmetric (anisotropic) turbulence is

$$C_{ij}(\underset{\sim}{r},t) \equiv A r_i r_j + B\delta_{ij} + C\lambda_i \lambda_j + D(\lambda_i r_j + \lambda_j r_i) . \quad (3.1)$$

The functions A,B,C, and D are arbitrary scalar functions of the invariants peculiar to axisymmetry, viz.

$$A = A (\underset{\sim}{r} \cdot \underset{\sim}{r}, \ \underset{\sim}{\lambda} \cdot \underset{\sim}{r}, \ t)$$

$$B = B (\underset{\sim}{r} \cdot \underset{\sim}{r}, \ \underset{\sim}{\lambda} \cdot \underset{\sim}{r}, \ t)$$

$$(3.2)$$

$$C = C (\underset{\sim}{r} \cdot \underset{\sim}{r}, \ \underset{\sim}{\lambda} \cdot \underset{\sim}{r}, \ t)$$

$$D = D (\underset{\sim}{r} \cdot \underset{\sim}{r}, \ \underset{\sim}{\lambda} \cdot \underset{\sim}{r}, \ t) \qquad .$$

Now consider the geometry of the approach and departure phases of aircraft flight depicted in Figure 18. Typically the glide-slope path angle, α , is quite small for large aircraft, namely

$$\alpha \cong \mathcal{O} (3° - 5°) \qquad . \qquad (3.3)$$

Consequently, the invariant $\underset{\sim}{\lambda} \cdot \underset{\sim}{r}$ is an important quantity in this particular study. It is defined by

$$\underset{\sim}{\lambda} \ \Big|_{\text{BOUNDARY}} \equiv \Big\{ 0, \ 0, \ 1 \Big\} \qquad (3.4)$$

and
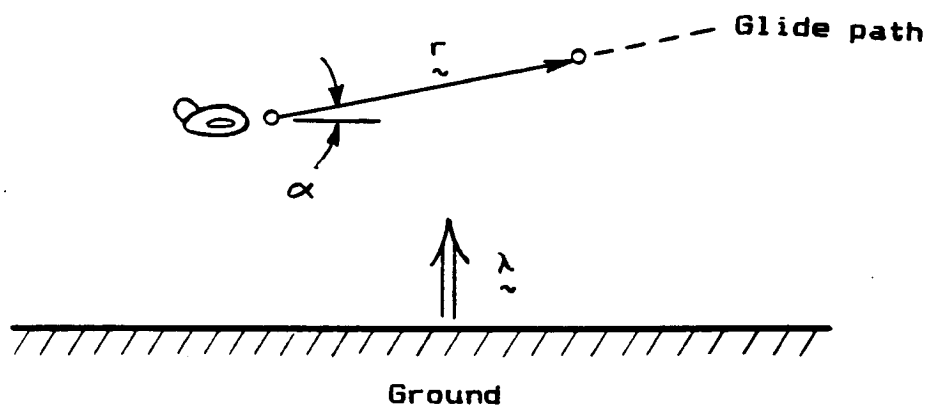
α : Glide-slope angle

λ : " Preferred " direction of flow

Figure 18 : Geometry of the Approach and Departure Phases of
Aircraft Flight Through a Low-Altitude Microburst

$$\left. \mathbf{r} \right|_{\substack{\text{GLIDE} \\ \text{PATH}}} \cong \left\{ r,\ 0,\ \pm\,\alpha\,r \right\} \,. \tag{3.5}$$

The following truncated Taylor series expansion in "$\lambda \cdot \mathbf{r}$" illustrates the relatively weak dependence of the arbitrary scalar functions on the the $\lambda \cdot \mathbf{r}$ invariant:

$$A\,(\mathbf{r}\cdot\mathbf{r},\ \lambda\cdot\mathbf{r},\ t) \cong A\,(\mathbf{r}\cdot\mathbf{r},\ 0,\ t) + \frac{\partial A}{\partial\,(\lambda\cdot\mathbf{r})}\,\lambda\cdot\mathbf{r}$$

$$B\,(\mathbf{r}\cdot\mathbf{r},\ \lambda\cdot\mathbf{r},\ t) \cong B\,(\mathbf{r}\cdot\mathbf{r},\ 0,\ t) + \frac{\partial B}{\partial\,(\lambda\cdot\mathbf{r})}\,\lambda\cdot\mathbf{r}$$

$$\tag{3.6}$$

$$C\,(\mathbf{r}\cdot\mathbf{r},\ \lambda\cdot\mathbf{r},\ t) \cong C\,(\mathbf{r}\cdot\mathbf{r},\ 0,\ t) + \frac{\partial C}{\partial\,(\lambda\cdot\mathbf{r})}\,\lambda\cdot\mathbf{r}$$

$$D\,(\mathbf{r}\cdot\mathbf{r},\ \lambda\cdot\mathbf{r},\ t) \cong D\,(\mathbf{r}\cdot\mathbf{r},\ 0,\ t) + \frac{\partial D}{\partial\,(\lambda\cdot\mathbf{r})}\,\lambda\cdot\mathbf{r}$$

and, for the small-angled glide-slope geometry of concern, the functional dependencies of Equation (3.2) become

$$A \cong A \, (\underset{\sim}{r} \cdot \underset{\sim}{r}, \; 0 \;, t)$$
$$B \cong B \, (\underset{\sim}{r} \cdot \underset{\sim}{r}, \; 0 \;, t) \qquad\qquad (3.7)$$
$$C \cong C \, (\underset{\sim}{r} \cdot \underset{\sim}{r}, \; 0 \;, t)$$
$$D \cong D \, (\underset{\sim}{r} \cdot \underset{\sim}{r}, \; 0 \;, t) \qquad .$$

Since it has been shown in Appendix A that the functional dependencies of the scalar functions A, B, and C are even in both "r" and "$\underset{\sim}{\lambda} \cdot \underset{\sim}{r}$" while D is an odd function of "$\underset{\sim}{\lambda} \cdot \underset{\sim}{r}$," it follows that D = 0 (see Figure 19). Thus, the two-point velocity correlation for anisotropic turbulence of Equation (3.1) can be written as

$$C_{ij}(\underset{\sim}{r}, t) \cong A \, r_i r_j \; + \; B \, \delta_{ij} \; + \; C \, \lambda_i \lambda_j \qquad . \qquad (3.8)$$

Now recall the geometry of the low-altitude wind shear

$$D (\underset{\sim}{\lambda} \cdot \underset{\sim}{r} , \underset{\sim}{r} \cdot \underset{\sim}{r} , t)$$

an odd function

$$\underset{\sim}{\lambda} \cdot \underset{\sim}{r}$$

O
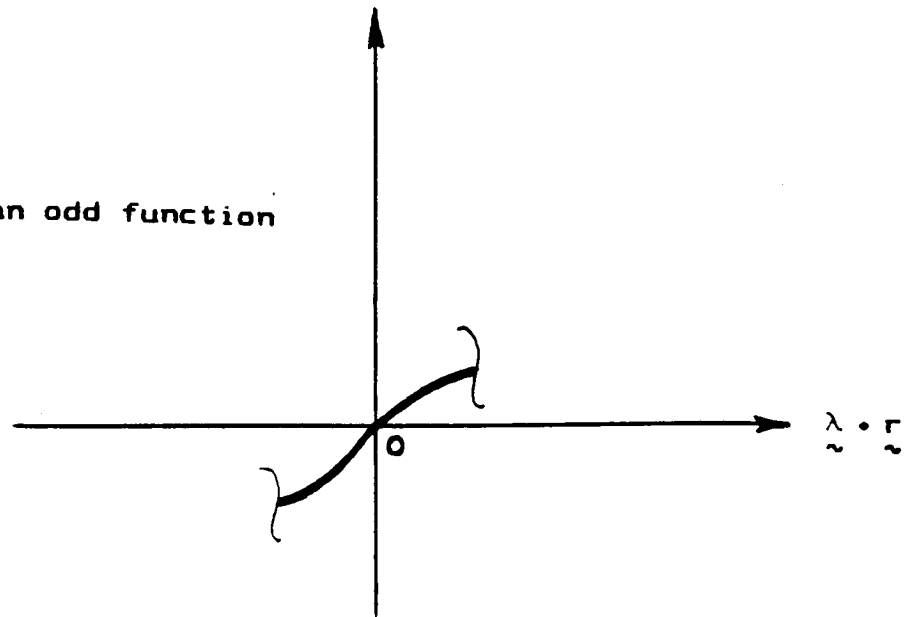
Figure 19 : Graphical Evaluation of the Arbitrary
Scalar Function, D

encounter depicted in Figure 18. Due to the small-angled descent or ascent, it follows that the aircraft senses only a "small" amount of anisotropy in a necessarily large amount present along the flight path   Hence, Equation (3.8) may be considered as

$$C_{ij} = I_{ij} + A_{ij} \qquad (3.9)$$

where

$$I_{ij} \equiv \left\{ \begin{array}{c} \text{Isotropic} \\ \text{Turbulence} \\ \text{Tensor} \end{array} \right\} \equiv A\, r_i r_j + B\, \delta_{ij} \qquad (3.10)$$

and

$$A_{ij} \equiv \left\{ \begin{array}{c} \text{Anisotropic} \\ \text{Turbulence} \\ \text{Tensor} \end{array} \right\} \equiv C\, \lambda_i \lambda_j \qquad . \qquad (3.11)$$

From the theory of isotropic turbulence,[20] the arbitrary functions "A" and "B" are found to be

$$A = \frac{\sigma^2 (f - g)}{r^2} \qquad\qquad (3.12)$$

and

$$B = \sigma^2 g \qquad , \qquad\qquad (3.13)$$

with "f" and "g" being the longitudinal and transverse correlation functions, respectively, for isotropic turbulence. (See Appendix B for the derivation of these expressions from standard grid-induced turbulence experiments.)

Now that the invariant functions have been determined for the isotropic portion of Equation (3.9), the anisotropic part can be considered. As proven in Appendix C, the divergence of the correlation tensor, C_{ij} , yields the following:[22]

$$4A \;+\; \frac{r \,\partial\, A}{\partial\, r} \;+\; \left[\frac{1}{r} \frac{\partial\, B}{\partial\, r} \;-\; \frac{\beta}{r^2} \frac{\partial\, B}{\partial\, \beta} \right] \;+$$

$$\beta \, \frac{\partial\, D}{\partial\, r} \;+\; \left[\frac{1 - \beta^2}{r} \right] \frac{\partial\, D}{\partial\, \beta} \;=\; 0 \qquad\qquad (3.14)$$

and

$$\frac{1}{r} \frac{\partial\, B}{\partial\, \beta} \;+\; \beta \, \frac{\partial\, C}{\partial\, r} \;+\; \left[\frac{1 - \beta^2}{r} \right] \frac{\partial\, C}{\partial\, \beta} \;+$$

$$r \, \frac{\partial\, D}{\partial\, r} \;+\; 4D \;=\; 0 \qquad , \qquad\qquad (3.15)$$

where β is defined from $\underset{\sim}{\lambda} \cdot \underset{\sim}{r} \equiv \beta r$. The aforementioned expressions for "A" and "B" (with D = 0) identically satisfy Equation (3.14), while (3.15) reduces to

- 51 -

$$\alpha \ \frac{\partial \ C}{\partial \ r} \ \cong \ 0 \ . \qquad\qquad (3.16)$$

An approximation for the arbitrary function "C" which satisfies Equation (3.16) is[23]

$$C \ = \ a \ |r| \ + \ b \qquad , \qquad\qquad (3.17)$$

where $\dfrac{\partial \ C}{\partial \ r} = a = \mathcal{O}(\alpha) = \mathcal{O}(\text{ small value })$. Theory demands that "a" and "b" are time-dependent parameters which define the anisotropy. Consequently, Equation (3.8) becomes

$$C_{ij} \ \cong \ \sigma^2 \left\{ \frac{f \ - \ g}{r^2} \right\} \ r_i r_j \ + \ (\ \sigma^2 g \ ) \ \delta_{ij} \ + \ \left\{ a|r| \ + \ b \right\} \lambda_i \lambda_j \ .$$

$$(3.18)$$

From Equation (3.18), the turbulence component of interest - the downwash autocorrelation - results:

- 52 -

$$C_{99} = (\alpha r)^2 A + B + C \cong B + C \qquad (3.19)$$

or

$$C_{99} \cong \sigma^2 g + a|r| + b \quad . \qquad (3.20)$$

From Equations (3.9) and (3.20), it follows that the two-point velocity correlation takes the general form

$$C_{99} = \left\{ \begin{array}{c} \text{ISOTROPIC} \\ \text{CORRELATION} \end{array} \right\} + \left\{ \begin{array}{c} \text{ANISOTROPIC} \\ \text{CORRELATION} \end{array} \right\} , \qquad (3.21)$$

where

$$\left\{ \begin{array}{c} \text{ISOTROPIC} \\ \text{CORRELATION} \end{array} \right\} = \sigma^2 g \qquad \text{and} \qquad \left\{ \begin{array}{c} \text{ANISOTROPIC} \\ \text{CORRELATION} \end{array} \right\} = a|r| + b \ .$$

$$(3.22)$$

- 53 -

The contributions of isotropy and anistropy to the total
autocorrelation function are shown in Figure 20. It is
important to note that the same autocorrelation for strictly
isotropic turbulence (cf. Equation (3.19)) is $C_{33} = \sigma^2 g$.
Evaluations of the other relevant correlations for the
"small anisotropy" turbulence model are shown in Table 1.
Since Table 1 indicates that the longitudinal and transverse
autocorrelations for "small anisotropy" are the same as
those provided by isotropic theory, the present turbulence
model may also be referred to as a "transverse isotropy"
model.
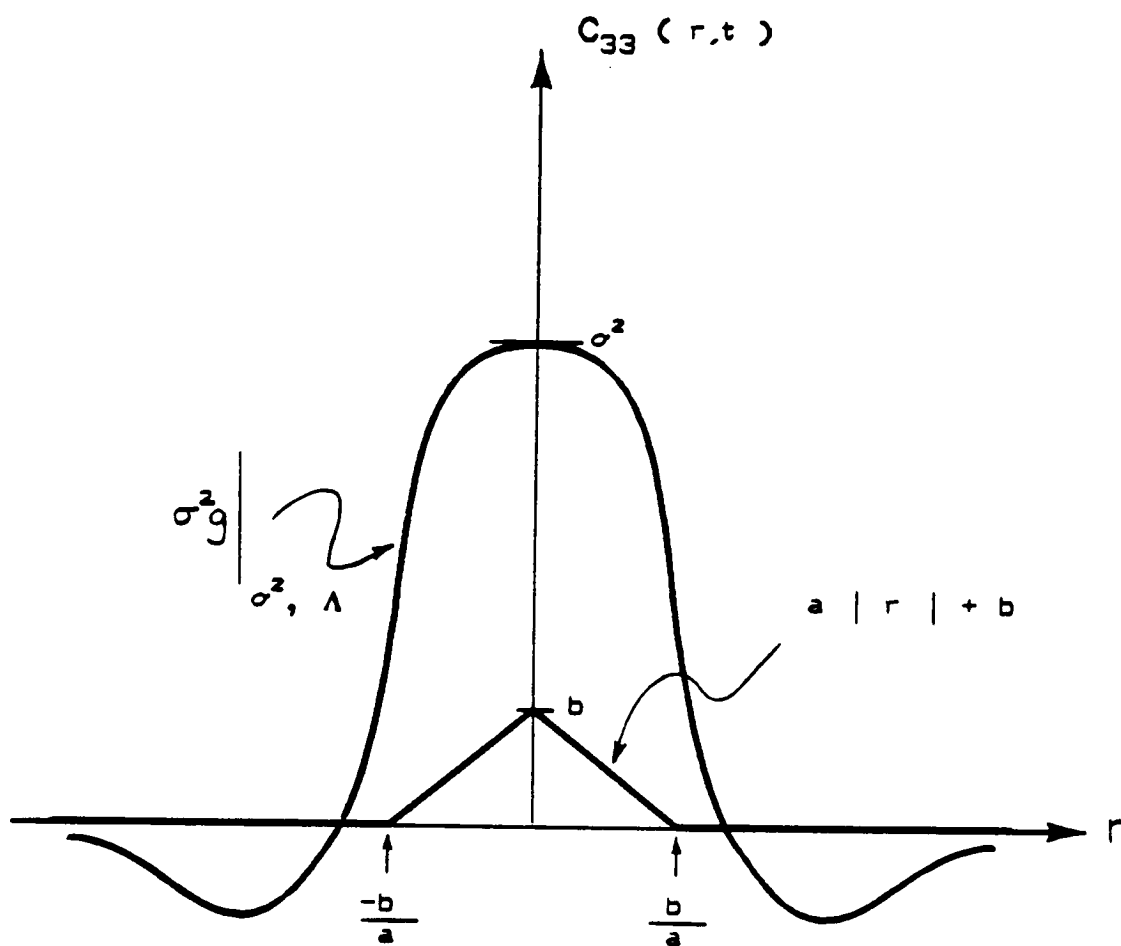
Figure 20 : Isotropic and Anisotropic Contributions to
the Downwash Autocorrelation Function

Table 1 : Important Two-point Correlation Functions for the Modelled Anisotropic Turbulence

Type of Correlation	Modelled Anisotropic Turbulence Correlation
Longitudinal - Longitudinal	$C_{11} = <uu'> \cong \sigma^2 f$
Transverse - Transverse	$C_{22} = <vv'> \cong \sigma^2 f$
Vertical - Vertical	$C_{33} = <ww'> \cong \sigma^2 g + a|r| + b$
Longitudinal - Vertical	$C_{13} = <uw'> \cong \alpha\sigma^2 (f-g)$

where $< uu' > \equiv < u(\underset{\sim}{x})\ u(\underset{\sim}{x}+\underset{\sim}{r}) >$

Knowledge of the sheared mean-wind/ turbulence interplay requires that the fluid's governing equation - the Navier-Stokes equation - be considered. The full Navier-Stokes equation is

$$\rho \, \frac{d \, U_i}{d \, t} = \rho g_i - \frac{\partial \, p}{\partial \, x_i} + \mu \, \frac{\partial^2 \, U_i}{\partial \, x_j \, \partial \, x_j} \qquad (3.23)$$

where ρ is the fluid density, p the pressure, and μ the viscosity coefficient. The Navier-Stokes equation for a steady-state, high Reynolds number, turbulent flow with body and pressure forces neglected is

$$\frac{\partial \, (U_i U_m)}{\partial \, x_m} \cong 0 \quad . \qquad (3.24)$$

The assumptions made in arriving at Equation (3.24) will now be considered.

The steady-state turbulence assumption is common one. Its genesis is the Taylor-von Kármán Hypothesis[24] whereby the turbulent gust field is considered "frozen" with respect to time variations. In other words, as the aircraft rapidly translates through the turbulent eddies, the effects of turbulence variation with time is negligible over the range of space in consideration.

Neglected viscosity is a direct result of the high Reynolds number hypothesis. Inherent within this idealization is the common assumption that large-scale interactions, which are predominantly responsible for momentum transport, are unaffected by the fluid viscosity. In terms of sources and sinks, the high Reynolds number hypothesis implies that the streamlines emanating from the source are not significantly altered by the presence of the sink - the fluid viscosity.

Ignoring pressure is acceptable in the case of isotropic turbulence since the pressure-velocity correlation is necessarily zero[21] for this type of turbulent field. This is definitely not the case in anisotropic turbulence or, for that matter, turbulence with a "small" amount of perceived anisotropy. Nevertheless, little research has been done concerning the relationship between pressure and velocity in an anisotropic turbulent field. This lack of fundamental knowledge is partly due to the difficulty in the measurement of dynamic pressure. For these reasons, pressure will not be considered in the present analysis. Furthermore, since the results which stem from this assumption will be used only as rough estimates in the turbulence simulation scheme presented later, the neglected-pressure assumption is deemed an acceptable one

for the purposes of this study. Hence, Equation (3.24) will
hereinafter serve as the governing equation for the
turbulent flow associated with low-altitude, sheared mean
winds.

The standard assumption that the total flow can be
considered as the linear combination of mean and fluctuating
components, viz.

$$U_i \cong \overline{U}_i + u_i \quad , \qquad (3.25)$$

permits the continuity equation to be written as

$$\frac{\partial \overline{U}_i}{\partial x_i} = 0 \quad \text{and} \quad \frac{\partial u_i}{\partial x_i} = 0 \quad . \qquad (3.26)$$

It is evident that the approximation made in Equation (3.25)
does not fully satisfy the nonlinear character of the
Navier-Stokes equation. Nonetheless, the assumption of a
linear combination of components has consistently been made
and will continue to be made until closed form solutions of
the full Navier-Stokes equation are found. (For additional

information on improved estimates to the component-
composition problem associated with nonlinear equations
consult Reference 25.)

Since Navier-Stokes is written for a single point in
space, a more general application of the governing equation
is necessary. For two points in a turbulent flow, denoted
P and P', the governing equation demands

$$\text{Point P :} \qquad \frac{\partial (U_i U_m)}{\partial x_m} \cong 0 \qquad\qquad (3.27)$$

and

$$\text{Point P' :} \qquad \frac{\partial (U'_j U'_m)}{\partial x'_m} \cong 0 \qquad . \qquad (3.28)$$

Subsequent substitution of Equations (3.25) and (3.26) yields

Point P :

$$\overline{U}_m \frac{\partial \overline{U}_i}{\partial x_m} + \overline{U}_m \frac{\partial u_i}{\partial x_m} + u_m \frac{\partial \overline{U}_i}{\partial x_m} + \frac{\partial (u_i u_m)}{\partial x_m} \cong 0$$

(3.29)

and

Point P' :

$$\overline{U}'_m \frac{\partial \overline{U}'_j}{\partial x'_m} + \overline{U}'_m \frac{\partial u'_j}{\partial x'_m} + u'_m \frac{\partial \overline{U}'_j}{\partial x'_m} + \frac{\partial (u'_j u'_m)}{\partial x'_m} \cong 0.$$

(3.30)

The standard two-point velocity correlation technique is invoked, and accordingly yields:

$$\bar{U}_m \langle u_j' \frac{\partial u_i'}{\partial x_m} \rangle \; + \; \left\{ \frac{\partial \bar{U}_i}{\partial x_m} \langle u_m u_j' \rangle \right\} \; + \; \frac{\partial}{\partial x_m} \langle u_i u_m u_j' \rangle \; +$$

$$\bar{U}_m' \langle u_i \frac{\partial u_j'}{\partial x_m'} \rangle \; + \; \left\{ \frac{\partial \bar{U}_j'}{\partial x_m'} \langle u_i u_m' \rangle \right\} \; + \; \frac{\partial}{\partial x_m'} \langle u_j' u_m' u_i \rangle \; \cong \; 0$$

$$(3.31)$$

- a result derived in Appendix D. The interplay between the underlying mean flow and the turbulence is evident upon inspection of the bracketted "shear terms" of Equation (3.31). Additionally, further consideration of the equation suggests that turbulence superimposed upon a sheared mean flow will have different statistical characteristics than that of turbulence superimposed upon a constant mean flow.

Simplification of Equation (3.31) can be made defining the following correlation tensors:[26]

$$C_{ij}(\underset{\sim}{r},t) \equiv \langle u_i u_j' \rangle \qquad \text{and} \qquad S_{imj}(\underset{\sim}{r},t) \equiv \langle u_i u_m u_j' \rangle \;, \qquad (3.32)$$

where the third-order tensor of Equation (3.28) is often

referred to as the "turbulence self-interaction" tensor.

Furthermore, recognize that, in Equations (3.29) and (3.30), the following conversion may be made: $\overline{U}_m \dfrac{\partial(\cdot)}{\partial x_m} = \overline{U}_m' \dfrac{\partial(\cdot)}{\partial x_m'} = \dfrac{\partial(\cdot)}{\partial t}$ — a conversion which implies that turbulence inhomogeneities are sensed as nonstationarities as the aircraft translates through the turbulence.[27,28] As shown in previous work,[8] the conversion found above also applies to an aircraft-based axis system during flight through a spatially, homogeneous sheared mean wind. Substitution of the equations of (3.32) and introducing the aforementioned conversion into Equation (3.31) eventually produces

$$\frac{\partial}{\partial t} C_{ij} + \frac{\partial \overline{U}_i}{\partial x_m} C_{mj} - 2 \frac{\partial}{\partial r_m} S_{imj} + \frac{\partial \overline{U}_j'}{\partial x_m'} C_{im} = 0 \quad . \quad (3.33)$$

(The "$\partial / \partial r_m$" of Equation (3.33) results from the fact that $\underset{\sim}{r} = \underset{\sim}{x}' - \underset{\sim}{x}$ from which $\partial/\partial x_m = -\partial/\partial r_m$ immediately follows.) Index contraction results in the more tractable expression:

- 63 -

$$\frac{\partial}{\partial t} C_{ii} + \frac{\partial \bar{U}_i}{\partial x_m} C_{mi} + \frac{\partial \bar{U}_i{}'}{\partial x_m{}'} C_{mi} - 2 \frac{\partial}{\partial r_m} S_{imi} = 0 \quad .$$

$$(3.34)$$

Recall that the velocity correlation tensor can take the general form, $C_{ij} \equiv I_{ij} + A_{ij}$, where I_{ij} and A_{ij} are the isotropic and anisotropic components, respectively. In addition, the self-interaction tensor for the formulated "small anisotropy" scenario can be shown to be identical to that for isotropic turbulence by invoking $\partial C_{ij} / \partial r_m = S_{ijm}$.[28] To prove this, C_{ij} is defined as in Equations (3.9) - (3.11), and a term-by-term analysis similar to that in Appendix C is effected. Since the aircraft senses a "small" amount of anisotropy along the glide path, Equation (3.34) essentially requires the solution of separate isotropic and anisotropic dynamical problems[28] i.e.,

$$i) \qquad \frac{\partial}{\partial t} I_{ii} - 2 \frac{\partial}{\partial r_m} S_{imi} \cong 0 \qquad\qquad (3.35)$$

$$ii) \qquad \frac{\partial}{\partial t} A_{ii} + \frac{\partial \overline{U}_i}{\partial x_m} C_{mi} + \frac{\partial \overline{U}_i{}'}{\partial x_m{}'} C_{mi} \cong 0 \; . \qquad (3.36)$$

First, the basis for a scaling comparison - the isotropic turbulence case - will be considered. Introducing the "f" and "k" functional representations for the correlation tensors,[20] viz.

$$I_{ii} = r^{-2} \frac{\partial (r^3 f)}{\partial r} \qquad (3.37)$$

and

$$S_{imi} = \sigma^3 (2r^4)^{-1} \frac{\partial (r^4 k)}{\partial r} r_m \qquad (3.38)$$

into Equation (3.35) gives a result whose first integral is the Kármán - Howarth equation for high Reynolds number isotropic turbulence,[26] i.e.,

$$\frac{\partial}{\partial t} (\sigma^2 f) - \sigma^3 \left[\frac{4\,k}{r} + \frac{\partial\,k}{\partial\,r} \right] \cong 0 \quad , \qquad (3.39)$$

where $k = k(r,t)$ is the single scalar function required to specify third-order velocity product moments (cf. Equation (3.28) of Reference 20). Since the third-order moments are not altered as a consequence of the self-preservation, it follows that $k(r,t)$ may also have such a time evolution, i.e., $k(r,t) \cong k(\zeta r) = k(r/\Lambda(t))$ as illustrated in Figure 21. Incorporation of this feature into the integration of the "modified" Kármán - Howarth equation of (3.39) results in

$$\frac{d}{dt} \left\{ \sigma^2(t)\Lambda(t) \right\} \cong \sigma^3 \int_0^\infty \left[\frac{4\,k(r/\Lambda)}{r} + \frac{\partial\,k(r/\Lambda)}{\partial\,r} \right] dr \quad ,$$

$$(3.40)$$

with $\Lambda \equiv \int_0^\infty f \, dr$. Integration of the right-hand side of Equation (3.40) over the given range is mathematically permissible since $k(r,t) \cong \mathcal{O}(r^3)$ near the origin.[20] Note
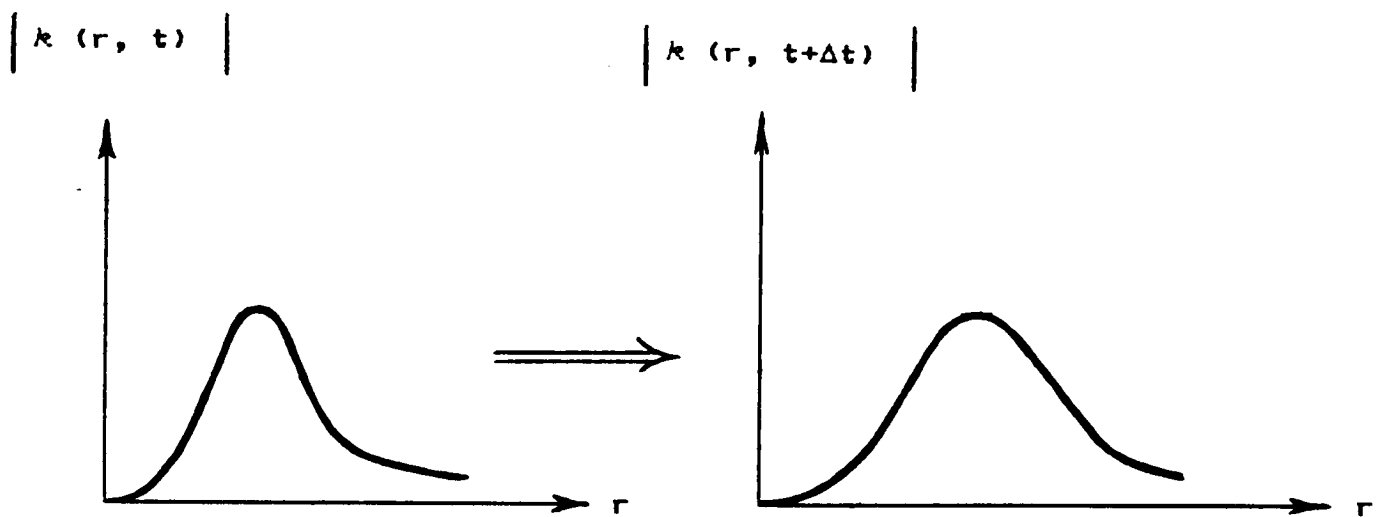
Figure 21 : " Self-Preserved " Behavior of the Single Function
Needed to Define the Turbulence Self-Interaction Tensor

that a self-preserved $k(r,t)$ provides a means for partially closing the Navier-Stokes equation.

As an important aside, the assumption of self-preserved functions will now be considered in more detail. Works of von Kármán,[29] von Kármán and Howarth,[30] von Kármán and Lin,[31] and Dryden[32] have incorporated self-preserved functions for the study of turbulent energy decay. Clearly, the assumption is a mathematical contrivance. In the present case, self preservation is a definite statement about the third-order velocity correlation function - that function which manifests due to the ensemble averaging inherent in the two-point correlation, and which opens an otherwise closed problem. In making the self-preservation claim, a distinct approach is taken in order to solve the closure problem. Exactly what is implied about the energy transfer mechanism from the self-preservation assumption is quite bold and specific: all turbulence length scales must decay at the same rate. Since the decay of turbulence may be physically interpreted as the manner in which energy is transferred between large turbulent eddies and smaller ones, self preservation intuitively seems unrealistic. In fact, experimental evidence has indicated that said assumption is only acceptable for large scale structures in the later stages of decay.[33] Consequently, care must be taken when basing conclusions upon results derived from self-preserved functions.

Further progress in solving Equation (3.40) is now made by introducing the dummy variable, $\theta \equiv r/\Lambda(t)$. In doing so, Equation (3.40) becomes

$$\frac{d}{dt} \left\{ \sigma^2(t) \Lambda(t) \right\} \cong \sigma^3 C_k \quad , \tag{3.41}$$

where

$$C_k \equiv \int_0^\infty \left[\frac{4\,k(\theta)}{\theta} + \frac{\partial\,k(\theta)}{\partial\,\theta} \right] d\theta = \text{constant} \quad . \tag{3.42}$$

Since k is a negative-valued function,[20] C_k is always a negative number - a fact invoked later. Solution of Equation (3.41) gives the time-dependence for the isotropic integral scale, namely

$$\Lambda(t) \cong \frac{C_k}{\sigma^2(t)} \int_0^t \sigma^3(t)\, dt \quad . \tag{3.43}$$

Introducing the power-law form for isotropic intensity[20] i.e., $\sigma^2(t) = t^n$ for $n = \pm 1, \pm 2, \ldots$, allows Equation (3.43) to take the form

$$\left. \Lambda(t) \right| \cong \frac{2\,C_k}{3n+2}\, t^{\frac{n+2}{2}} \qquad n = \pm 1, \pm 2, \ldots \quad . \quad (3.44)$$

$$\left. \right|_{\sigma^2(t) = t^n}$$

For the specific turbulence intensity, $\sigma^2(t) = t^{-1}$ (a common power-law approximation made in grid-induced turbulent decay studies[20]), the resulting time-dependent integral scale may be found by consulting in Table 2.

To consider the anisotropic problem, gradients must first be defined. The two steady-state, wind-shear profiles chosen for analysis are illustrated in Figures 22a and 23a, and will hereinafter be referred to as "Shear-Flow I" and "Shear-Flow II," respectively. Note that both profiles have a "head-to-tailwind swing" - a phenomenon frequently observed in microburst encounters. The mean velocity for Shear-Flow I is $\overline{U}_i = \left\{ U(z),\ 0,\ 0 \right\} \equiv \left\{ M_1 z,\ 0,\ 0 \right\}$ as shown in Figure 22b. Analysis of Shear-Flow II is restricted to the two-dimensional case with $\overline{U}_i = \left\{ U(x),\ 0,\ W(z) \right\}$ and gradients of the form $\dfrac{d\overline{U}}{dx} = \dfrac{-d\overline{W}}{dz}$

Table 2 : Integral Scales Resulting from Power-law Approximations

$\sigma^2(t)$	$\Lambda(t)$
t^n	$\dfrac{2\,C_k}{3n+2}\ t^{\frac{n+2}{2}}$
t^{-1}	$\varnothing\ (t^{1/2})$
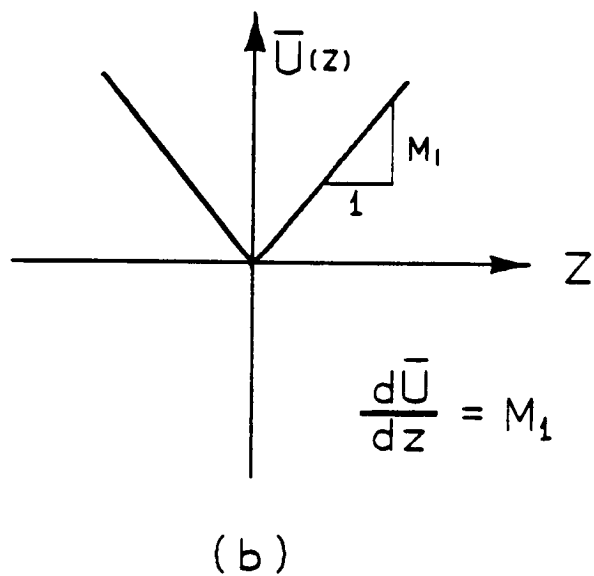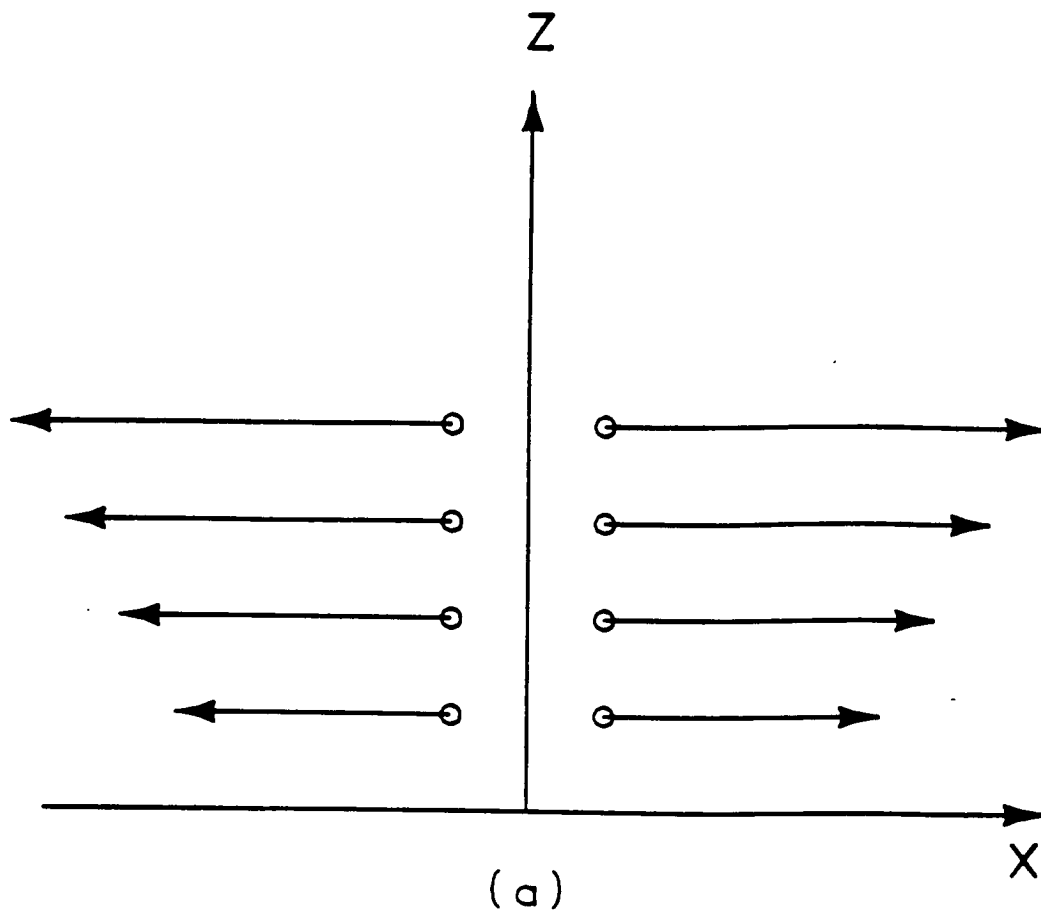
Figure 22 (a)   Sheared Mean Velocity Profile for "Shear-Flow I"

(b)   Corresponding Velocity Gradients

$$\frac{d\overline{U}}{dx} = -\frac{d\overline{W}}{dz} = M_2$$
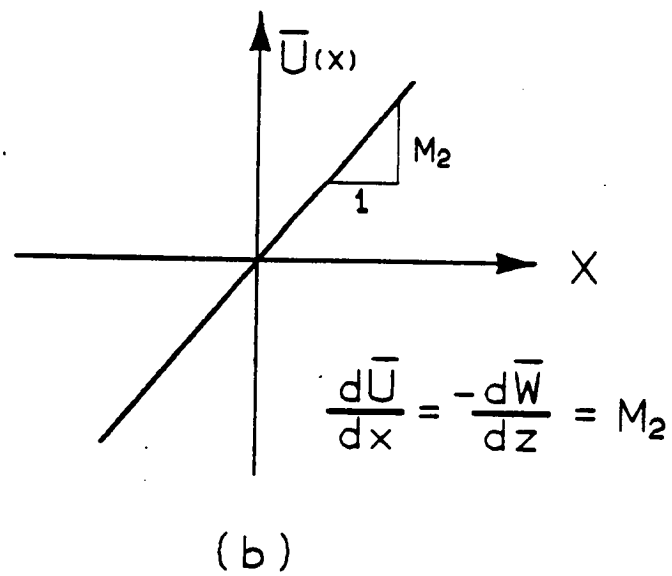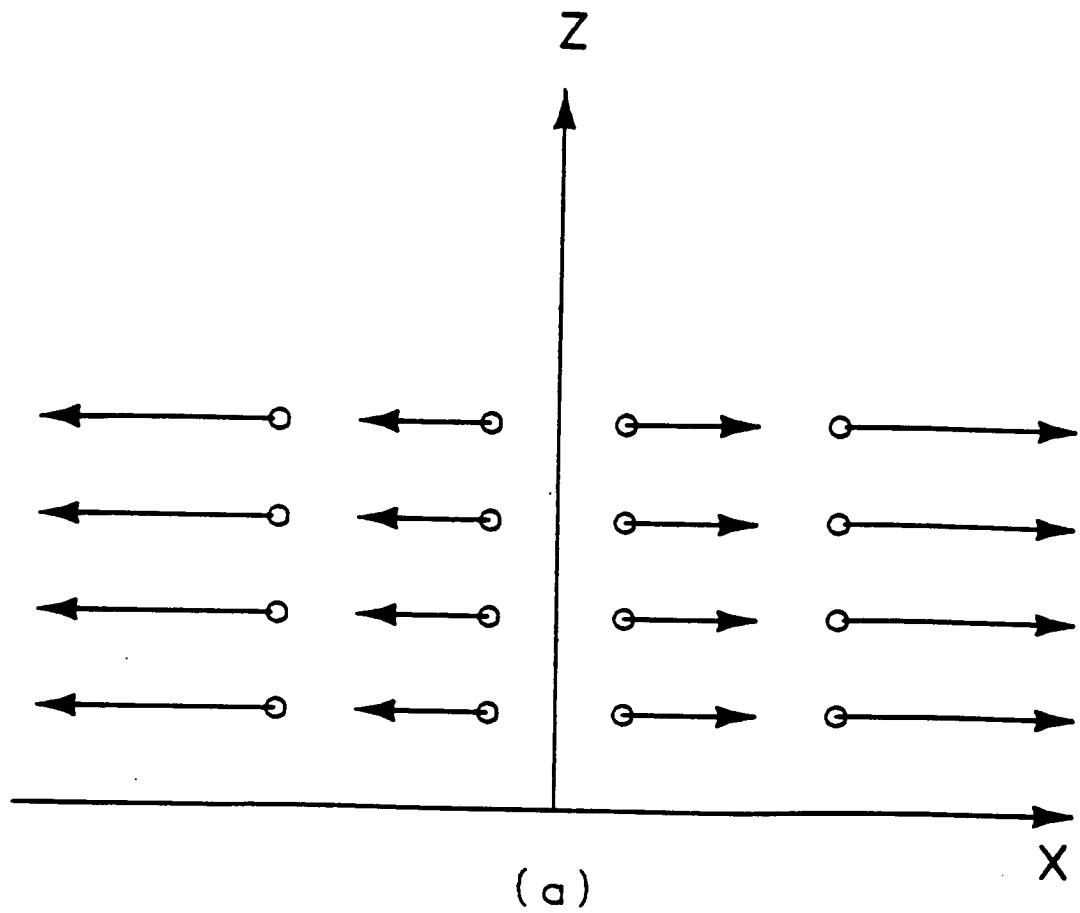
Figure 23 (a)   Sheared Mean Velocity Profile for "Shear-Flow II"

(b)   Corresponding Velocity Gradients

$= M_2$ — a consequence of mass conservation. (See Figure 23b for a graphical interpretation of Shear-Flow I). Indeed, mass conservation for the two shear flows is satisfied as shown below:

Shear-Flow I :

$$\frac{\partial U_i}{\partial x_i} = \frac{\partial U}{\partial x} + \frac{\partial V}{\partial y} + \frac{\partial W}{\partial z} = 0$$

$$= 0 + 0 + 0 = 0$$

and likewise,

Shear-Flow II :

$$\frac{\partial U_i}{\partial x_i} = \frac{\partial U}{\partial x} + \frac{\partial V}{\partial y} + \frac{\partial W}{\partial z} = 0$$

$$= M_2 + 0 + -M_2 = 0 \quad .$$

The turbulent sheared mean wind of Shear-Flow II will now be considered in detail. Incorporation of Shear-Flow II characteristics into (3.36) yields

$$\frac{\partial \left(a|r| + b \right)}{\partial t} + 2M_2 \left\{ \sigma^2 \left(f-g \right) - \left(a|r| + b \right) \right\} \cong 0 \ .$$

$$(3.45)$$

The first integral in "r" of the differential equation found immediately above yields

$$\frac{d \left(\sigma^2 \Delta \Lambda \right)}{d t} + M_2 \sigma^2 \Lambda - 2M_2 \sigma^2 \Delta \Lambda \cong 0 \ , \qquad (3.46)$$

where $\int_0^\infty \left(a|r| + b \right) dr \equiv \sigma^2 \Delta \Lambda(t)$. The solution of Equation (3.46) gives the time-decay of the change in integral scale due to anisotropy, namely

$$\Delta \Lambda \left(t \right) \Bigg|_{II} \cong \frac{- M_2 \ e^{2M_2 t}}{\sigma^2 (t)} \int_0^t e^{- 2M_2 t} \sigma^2(t) \Lambda(t) \ dt \quad . \quad (3.47)$$

- 75 -

A similar analysis[23] for Shear-Flow I has provided the following differential equation for the anisotropic contribution to the dynamical problem:

$$\frac{\partial}{\partial t} \left[a|r| + b \right] - M_1 \sigma^2 \alpha \, r \, \frac{\partial f}{\partial r} + M_1 \alpha \, r \, \sigma^2 \frac{\partial (f+2g)}{\partial r} \cong 0 \quad .$$

$$(3.48)$$

whose first integral in "r" gives

$$\frac{d}{dt} \left[\sigma^2(t) \, \Delta\Lambda(t) \right] - M_1 \, \sigma^2(t) \, \alpha \, \Lambda(t) \cong 0 \quad ; \quad (3.49)$$

the solution of which is

$$\Delta\Lambda(t) \Big|_I \cong \frac{M_1 \, \alpha}{\sigma^2(t)} \int_0^t \sigma^2(t) \, \Lambda(t) \, dt \quad . \quad (3.50)$$

As expected, the isotropic portion of the entire dynamical problem remains unaltered when considering the two individual flows (cf. Equation (3.44)). The resulting $\Delta\Lambda$'s for both shear profiles are found in Table 3 for $\sigma^2(t)=t^n$ and $\sigma^2(t)=t^{-1}$, i.e., the general and specific power-law approximations, respectively. Now, a method of "scaling" the turbulence of a low-altitude wind shear with respect to classical isotropic turbulence will be introduced to facilitate interpretation of the results provided in Tables 2 and 3.

The role played by anisotropic turbulence in a wind shear encounter will be quantified in a correlation length scale defined as $L \equiv \Lambda(t) + \Delta\Lambda(t)$. (Recall that as integral scale increases in magnitude, randomness decreases, while decreasing scale implies increased prognostication). It is clear that in order to scale with respect to isotropy only the algebraic sign of $\Delta\Lambda$ is required. Also, comparison of the decay rates of the sensed length scales of Table 3 shows that the anisotropic contribution grows or decays at a faster rate than the isotropic component of the total correlation length scale. Furthermore, inspection of Equation (3.50) indicates that, as the aircraft penetrates the headwind portion of Shear-Flow I, $\Delta\Lambda > 0$ since M_1 and α are negative in this phase of the flight (cf. Figure 22a). Consequently, the turbulence sensed by the aircraft is <u>less</u> <u>random</u> than that predicted by isotropic turbulence theory since $L = \Lambda + \Delta\Lambda > \Lambda$. Even more significant is the tailwind phase of the wind shear encounter since it provides $\Delta\Lambda < 0$ - a <u>more</u> <u>random</u> turbulence field in comparison with isotropy. A similar analysis of Equation (3.47) for Shear-Flow II yields negative $\Delta\Lambda$'s on both sides of this

- 77 -

C-2

Table 3 : Time-dependent Changes in Integral Scale Due to the
Anisotropy for Power-law Approximations for Intensity

$\sigma^2(t)$	$\Delta\Lambda(t)\big|_I$	$\Delta\Lambda(t)\big|_{II}$
t^n	$\dfrac{4\,M_1\,C_k\,\alpha}{(3n+2)(3n+4)}\;t^{\frac{n+4}{2}}$	$\dfrac{-\,4\,M_2\,C_k}{(3n+2)(3n+4)}\;t^{\frac{n+4}{2}}$
t^{-1}	$\mathcal{O}\left(t^{9/2}\right)$	$\mathcal{O}\left(t^{9/2}\right)$

wind shear, thus making it more unpredictable.[†] Table 4 summarizes the significance of wind shear on the aircraft-sensed turbulence length scale with respect to isotropy. These turbulence characteristics peculiar to low-altitude flight through turbulent wind shears, in conjunction with the loss of aerodynamic lift, must be accounted for in order to ensure enhanced realism in wind shear flight simulations.

[†]   Constants of integration have been neglected in
       obtaining Equation (3.44) and Equation (3.47).

- 79 -

Table 4 : Comparison of the Degree of Randomness of Two
Wind Shear Profiles With Respect to Isotropy

Shear - Flow I		Shear - Flow II	
Headwind side	Tailwind side	Headwind side	Tailwind side
Less Random	More Random	More Random	More Random

CHAPTER 4

POWER SPECTRAL DENSITY AND APPLICATIONS OF THE TURBULENCE MODEL

§ 4.1 PSD of Downwash Turbulence and Aircraft Response

As noted in Chapter 2, the one-dimensional power spectral density (psd) function is a common way of illustrating energy distribution versus frequency, and has been an immensely popular tool in both turbulence analyses and simulations. Mathematically, it is the one-dimensional Fourier transform of the autocorrelation function. In particular, the psd for the modelled turbulent downwash formulates as follows:

$$\Phi_{ww}(t,k) = \int_{-\infty}^{\infty} <w(x,t)w(x+r,t)> \, e^{-\iota kr} \, dr \qquad (4.1)$$

or

$$\Phi_{ww}(t,k) = \int_{-\infty}^{\infty} \left\{ \sigma^2 g + a|r| + b \right\} e^{-\iota kr} \, dr \quad , \qquad (4.2)$$

where $k = \dfrac{\omega}{V}$ is the wave number (or "spatial frequency" since its units are rad/unit length), $\iota^2 = -1$, and V is the constant forward flight speed of the aircraft. The "scaling" of the resulting psd manifests since

$$\Phi_{ww}(t, \frac{\omega}{V}) = \int_{-\infty}^{\infty} \sigma^2(t) \; R(\zeta r) \; e^{-\iota \omega r/V} \; dr \qquad . \qquad (4.3)$$

With $\zeta \equiv \Lambda(t)^{-1}$ and $\zeta r \equiv \theta$, Equation (4.3) takes the form

$$\Phi_{ww}(t, \frac{\omega \Lambda}{V}) = \sigma^2(t)\Lambda(t) \int_{-\infty}^{\infty} R(\theta) \; e^{-\iota \omega \Lambda \theta/V} \; d\theta \qquad . \qquad (4.4)$$

It is therefore clear that if the normalized correlation function, R, consists of separate isotropic and anisotropic components, so too will its Fourier transform. The isotropic contribution to the autocorrelation of Equation (4.2) is defined by the Dryden exponential formulation,[20] viz.,

$$f(r,t) \cong e^{-|r|/\Lambda(t)} \qquad .$$

Hence, if the appropriate integration limits on the anisotropic component are accounted for (cf. Figure 20), Equation (4.2) eventually integrates to

$$\Phi_{ww}(t,\varkappa) = \left\{ \sigma^2 \Lambda \, \frac{1 \; + \; 3\varkappa^2}{(1 \; + \; \varkappa^2)^2} \right\} + \left\{ 4\sigma^2 \Lambda \left[\frac{\Delta \Lambda}{\Lambda} \right] \; \frac{1 \; - \; \cos(\frac{\varkappa b}{a\Lambda})}{(\frac{\varkappa b}{a\Lambda})^2} \right\}$$

$$(4.5)$$

- a result derived in Appendix E. Equation (4.5) is the psd sensed by the aircraft as it flies through the microburst. Here $\varkappa \equiv \omega\Lambda/V$ is the non-dimensionalized wave number, σ the isotropic intensity, Λ the longitudinal correlation length (integral scale)and $\Delta\Lambda$ the change in integral scale due to the anisotropy induced by the presence of the ground. Inspection of Equation (4.5) indicates the power spectrum separates into

$$\Phi_{ww}^{(i)}(t,\varkappa) \quad \equiv \quad \sigma^2 \Lambda \; \frac{1 \; + \; 3\varkappa^2}{(1 \; + \; \varkappa^2)^2} \qquad (4.6)$$

and

$$\Phi_{ww}^{(a)}(t,\varkappa) \equiv 4\sigma^2 \Lambda \left[\frac{\Delta\Lambda}{\Lambda}\right] \frac{1 - \cos(\frac{\varkappa b}{a\Lambda})}{(\frac{\varkappa b}{a\Lambda})^2} \quad , \quad (4.7)$$

where $\Phi_{ww}^{(i)}(t,\varkappa)$ is the isotropic psd and $\Phi_{ww}^{(a)}(t,\varkappa)$ is the anisotropic psd.

Recognize that $\Phi_{ww}^{(i)}(t,\varkappa)$ is the well-known Dryden psd. Illustrated in Figure 24, the Dryden psd has long been used in both high and low-altitude flight - the reason for which Dryden's representation of isotropic turbulence is frequently described as "garden variety" turbulence. The Dryden spectrum, although slightly less realistic than the von Kármán spectrum[10] in terms of spectral characteristics, is an excellent approximation for isotropic turbulence analyses.[24] Furthermore, it is much less of a computational burden than the von Kármán for simulation purposes - a fact considered in greater detail in the following section.

Equation (4.7) is the anisotropic downwash psd corresponding to low-altitude flight through sheared turbulent winds in which a slight amount of anisotropy is sensed. This previously unquantified parameter of wind-shear turbulence will now be considered in terms of aircraft response.

The effect of anisotropic turbulence on aircraft response may be estimated from the standard input/output relationship
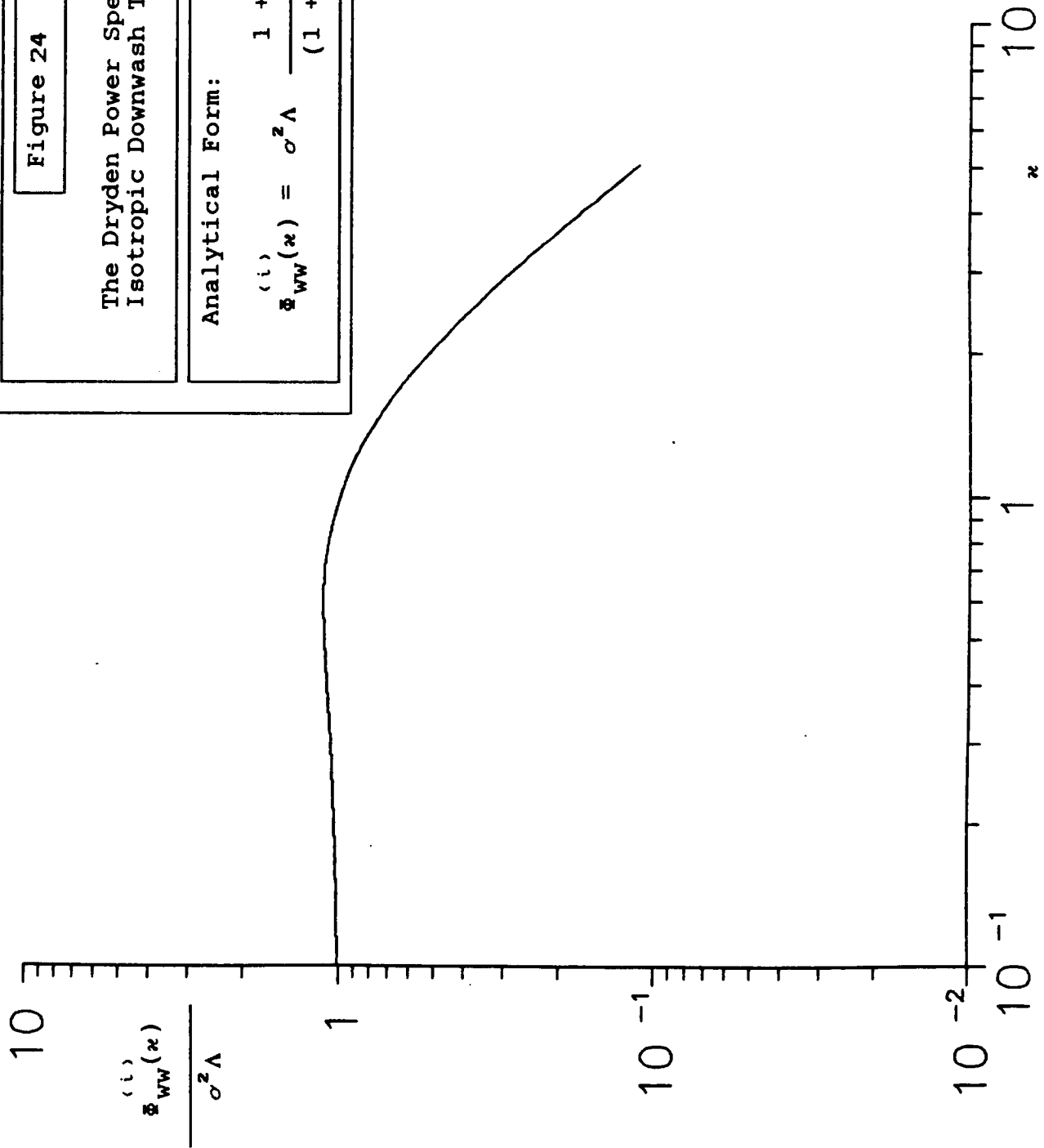
Figure 24

The Dryden Power Spectrum for
Isotropic Downwash Turbulence

Analytical Form:

$$\Phi_{ww}^{(i)}(\varkappa) = \sigma^2 \Lambda \, \frac{1 + 3\varkappa^2}{(1 + \varkappa^2)^2}$$

$$\Phi_{qq}(\varkappa) = \left| H(\varkappa) \right|^2 \Phi_{ww}(\varkappa) \qquad . \qquad (4.8)$$

Here $\Phi_{ww}(\varkappa)$ is the turbulence psd, $\Phi_{qq}(\varkappa)$ is the response psd, and $H(\varkappa)$ is the frequency response of the airframe. In a strict sense, this relation holds only if the effect of the spatial structure of the turbulence field on the response of the system is negligible. In other words, if the length scale of the turbulence, $\Lambda + \Delta\Lambda$, is large in relation to the largest dimension of the airplane, application of Equation (4.8) is justified - an acceptable assumption in the present case since $\Lambda + \Delta\Lambda \cong \mathcal{O}$ (1000 ft). The components of Equation (4.8) will now be examined.

The total input power to the aircraft from the surrounding downwash turbulence is

$$\Phi_{ww} = \overset{(i)}{\Phi_{ww}}(t,\varkappa) + \overset{(a)}{\Phi_{ww}}(t,\varkappa)$$

- a linear combination of isotropic and anisotropic psd's. Figure 25 illustrates, *via* sensitivity analysis, that the anisotropic power spectral density may play a significant role in the total input power to the aircraft received from the turbulent atmospheric environment. (It will be seen later that $b/a\Lambda = 0.5$ is a realistic value.)

- 87 -

Figure 25

Total Input Power Spectra of Turbulent Downwash for Constant $b/(a\Lambda)$ and Variable $\Delta\Lambda/\Lambda$

$$\Phi_{ww}(\varkappa) = \Phi_{ww}^{(i)}(\varkappa) + \Phi_{ww}^{(a)}(\varkappa)$$

$b/(a\Lambda) = $ constant $= 0.5$

$\Delta\Lambda/\Lambda = 0.05,\ 0.10,\ 0.15$

$\Delta\Lambda/\Lambda = 0.15$

$\Delta\Lambda/\Lambda = 0.10$

$\Delta\Lambda/\Lambda = 0.05$

Isotropic psd (Dryden)
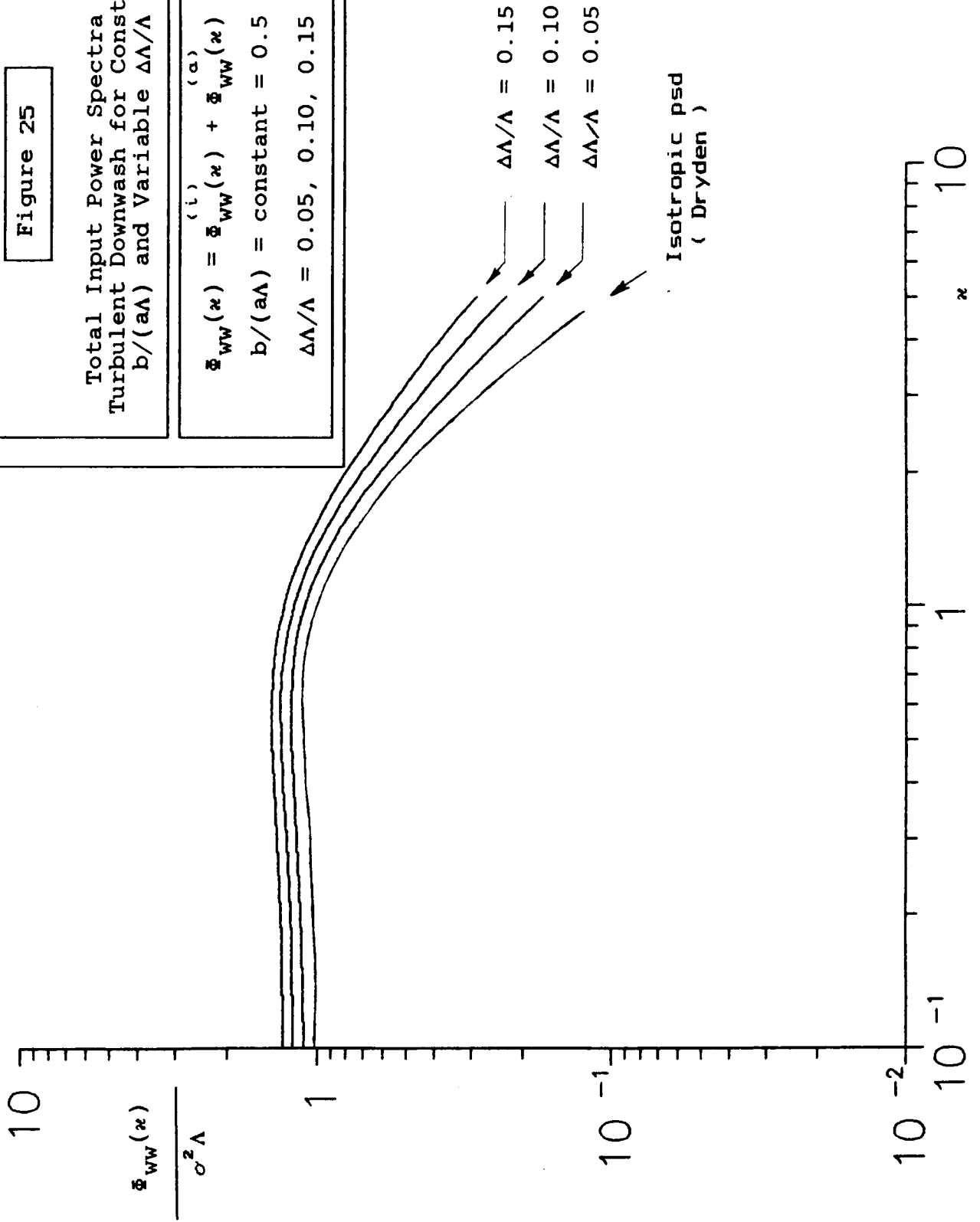
The frequency response modulus chosen for this analysis is approximated from the well-known Sears' function,[34] and is

$$\left| \; H(\nu) \; \right|^2 \cong \frac{d + \nu}{d + (\pi d + 1)\nu + 2\pi\nu^2} \quad , \qquad (4.9)$$

with $d \equiv 0.1811$, $\nu \equiv$ reduced frequency $\equiv (\omega c)/(2 V)$, and $c \equiv$ chord length. Knowing that the non-dimensionalized wave number is defined as $\varkappa \equiv (\omega \Lambda)/V$, it immediately follows that $\omega/V = \varkappa/\Lambda$. The expression for reduced frequency in terms of the non-dimensionalized wave number is therefore

$$\nu = \frac{1}{2} \left(\frac{c}{\Lambda} \right) \varkappa \quad . \qquad (4.10)$$

Subsequent substitution of Equation (4.10) into the modulus equation yields

$$\left| H(\nu) \right|^2 \cong \frac{0.1811 + 0.5(c/\Lambda)\varkappa}{0.1811 + 0.5(0.1811\pi + 1)(c/\Lambda)\varkappa \, \nu + 2\pi(0.5(c/\Lambda)\varkappa)^2}$$

(4.11)

Substitution of Equation (4.11) into (4.8) yields an approximation for the power spectrum of the random lift of the aircraft. Implementation of the FORTRAN programs of Appendix G provides an estimate of aircraft response with regard to the anisotropy-defining parameters. An important result of this method of study is illustrated in Figure 26: for $c/\Lambda = 0.01$ (e.g., chord $\cong$ 10 ft for $\Lambda \cong$ 1000 ft), aircraft response is underestimated by isotropic theory over the entire frequency range shown. Additionally, Figure 27 illustrates that the <u>degree</u> of anisotropy (i.e., $b/(a\Lambda)$ = variable) makes little difference in terms of response for $0 < \varkappa < 2$.

The preceeding analysis has highlighted the distinct advantage that the power spectral density representation has over the autocorrelation function: that of a more meaningful statement about the role that the anisotropy-defining parameters ("a" and "b") play in the estimation of the total turbulent energy in a one-dimensional, low-altitude down gust. The parameter "a" has been more well defined than "b" since

Figure 26

Comparison of { Isotropic } and
{ Isotropic + Anisotropic } Response
Psd's Due to Downwash Turbulence

Given : c/Λ = constant = 0.01

$\Delta\Lambda/\Lambda$ = constant = 0.1

$\frac{b}{a\,\Lambda}$ = 0.001

" Isotropic Response "

$\frac{\Phi_{qq}(\varkappa)}{\sigma^2\Lambda}$

$\varkappa$

Figure 27

Total Aircraft Response PSD
Due to Turbulent Downwash for
Constant $\Delta\Lambda/\Lambda$ and Variable $b/(a\Lambda)$

Given: $c/\Lambda = $ constant $= 0.01$
$\Delta\Lambda/\Lambda = $ constant $= 0.1$

$\dfrac{b}{a\,\Lambda} = 0.005$

$\dfrac{b}{a\,\Lambda} = 0.25$

$\dfrac{b}{a\,\Lambda} = 0.75$
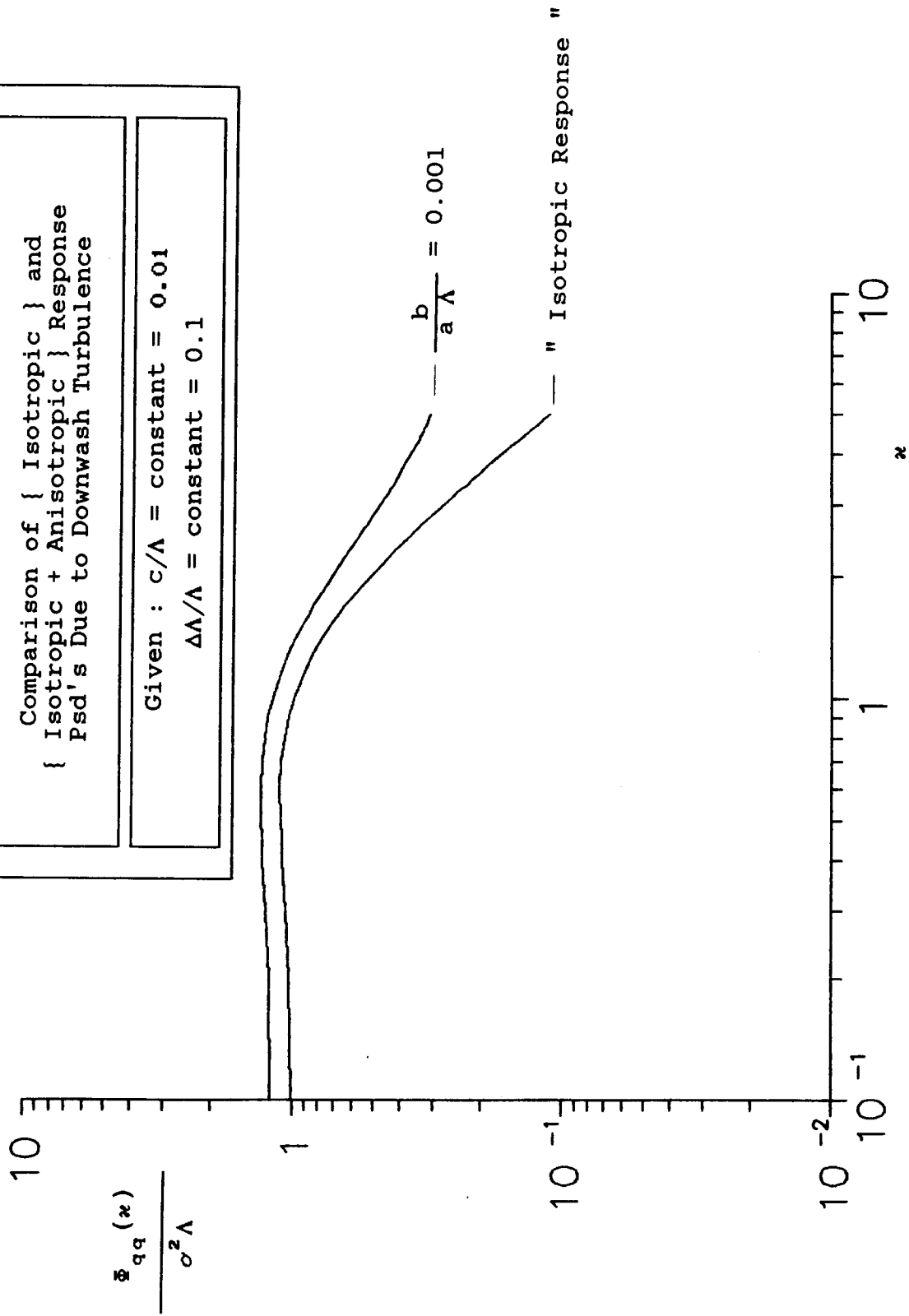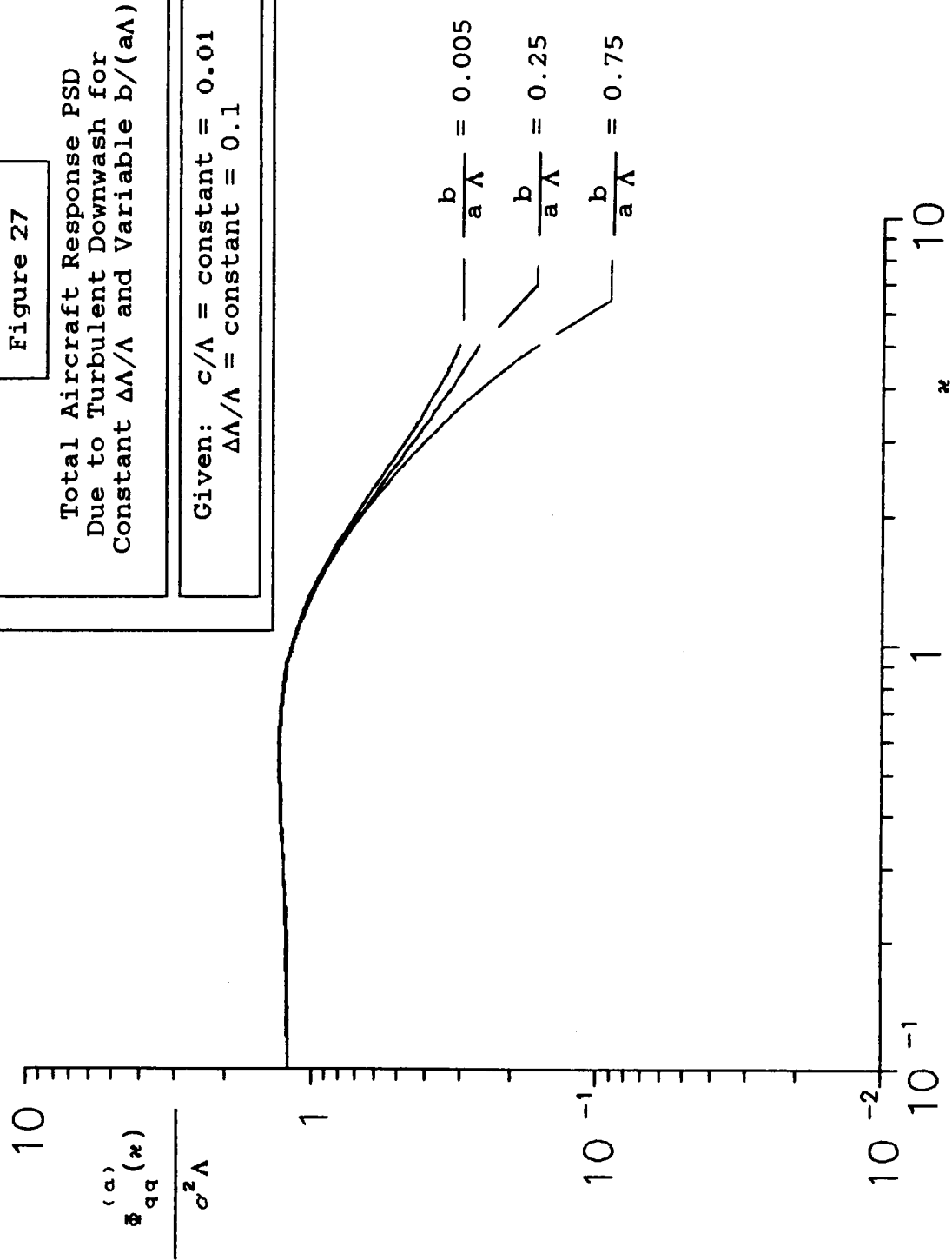
$$a \equiv \mathcal{O}(\alpha) \cong \text{constant}$$

for the scenerio in which the glide-slope path is maintained during the turbulence encounter. Consequently, "b" plays the more important role in terms of modelling the anisotropy due to the presence of the boundary. From Figure 20, "b" is related to the intensity by $\sigma^2 + b \equiv (\sigma + \Delta\sigma)^2$, where $\Delta\sigma$ is the change in intensity due to the anisotropy. This expression can be rewritten as

$$b = \sigma^2 \left\{ \frac{2\Delta\sigma}{\sigma} + \left[\frac{\Delta\sigma}{\sigma} \right]^2 \right\} \cong 2\sigma^2 \left[\frac{\Delta\sigma}{\sigma} \right] = 2\sigma\Delta\sigma \quad . \quad (4.12)$$

A more thorough evaluation of "b" will be made when turbulence simulation is addressed later.

Another way to quantify the collective effect of the anisotropy-defining parameters on the sensed power is to introduce an "energy scaling factor" defined as

$$\Delta(t, \varkappa) \equiv \frac{\Phi_{WW}^{(a)}(t, \varkappa)}{\Phi_{WW}^{(i)}(t, \varkappa)} \qquad . \qquad (4.13)$$

To analyze the scaling effect of $\Delta\Lambda/\Lambda$ in (4.13), allow $b/(a\Lambda) \cong$ constant; typical values of σ=5 ft/s, Λ=1000 ft, V=225 ft/s and a=$\mathscr{O}(\alpha)$=$\mathscr{O}(3°)$=$\mathscr{O}(0.052$ rad) are chosen, and $\Delta\sigma/\sigma$ is allowed to vary up to 0.5 (a feasible value for wind-shear turbulence severity). Incorporating Equation (4.12) gives $b/(a\Lambda)$ = $\mathscr{O}(0.5)$. Figure 28 shows that, for $\Delta\Lambda/\Lambda$ ranging from the isotropic condition, $\Delta\Lambda/\Lambda$=0, to $\Delta\Lambda/\Lambda$=0.1, the energy scaling factor is as high as 35% for $0 \leq \varkappa \leq 2$ ($0 \leq \omega \leq 0.45$ rad/s) - a frequency range which falls within that specified for the guidance and control phases of an aircraft mission involving a wind shear.[35] Hence, the energy scaling factor has been used to make an important point: <u>realistic</u> estimates of the energy transfer associated with wind-shear turbulence demand that anisotropy be accounted for in both turbulence models and related flight simulations.

§ 4.2   METHODS OF SIMULATING ATMOSPHERIC TURBULENCE   .

The role that flight simulators play in the training process of both pilots and crew is an important one. Of particular importance are the simulations involving aircraft which are particularly sensitive to atmospheric turbulence. In such cases, the turbulence may have serious implications

Energy Scaling Factor
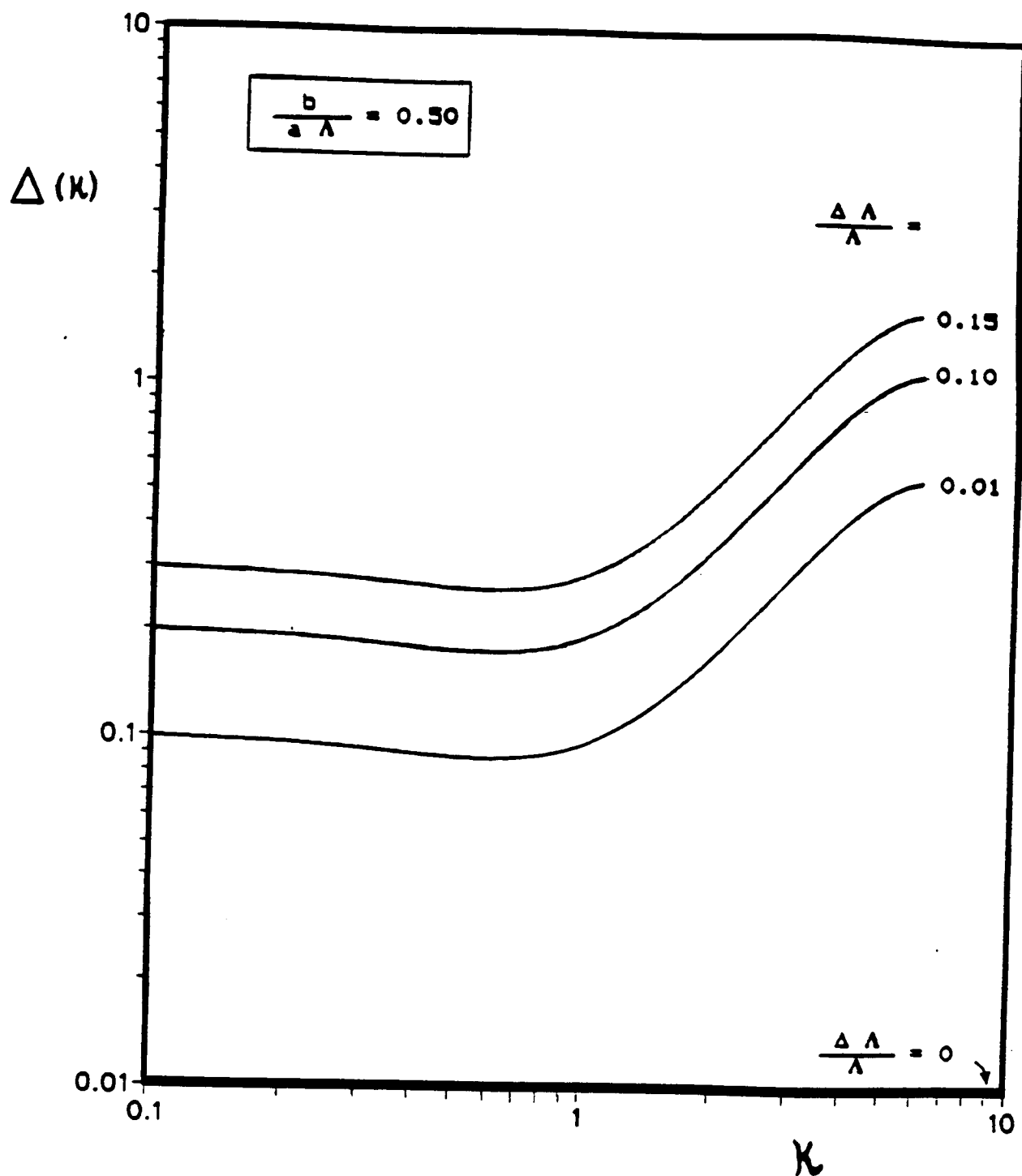
Figure 28 : Energy Scaling Factor for Constant b/(aΛ)
and Variable ΔΛ/Λ

with regard to ride quality and aircraft control.
Furthermore, the value of flight simulators is not only
practical but also economical, with studies showing that
flight simulators can be up to 10 times cheaper than actual
airborne flight training.[6] Realism in the turbulence
simulation corresponding to low-altitude flight is therefore
a research topic of great significance.

There are many phenomonological issues which must be
considered when attempting to simulate atmospheric
turbulence. One of the most important qualities is known as
"patchiness." Flight through seemingly continuous
turbulence may contain sudden interjections of turbulent
activity followed by extended calm periods. It is this
so-called "element of surprise" which characterizes the
"patchiness" of the atmospheric turbulence.[36] From a
mathematical perspective, patches of relatively intense
activity separated by extended periods of relative calm
cannot be perfectly represented by the Gaussian probability
density function. Since the Gaussian pdf proves
unsatisfactory for the probabilistic estimation of large
gusts - those gusts most important in both ride quality
and aircraft control - many simulation techniques have
been developed to account for the shortcomings of Gaussian
distributions (see Table 5[35]). A few of the basic
simulation techniques presently used will now be considered.

The most obvious method of producing realistic
turbulence for simulation is to record actual turbulence.
Unfortunately, this procedure has serious drawbacks. A
single recording of necessarily finite length may only be
useful in the simulation of a single event under similar
geometric and meteorological states for a finite period of

Table 5 : A Review of Turbulence Simulations and Models[*]

Model	Key Features
Dryden turbulence	A convenient spectral form based on an exponential autocorrelation function for the axial component.
von Karman turbulence	A spectral form for which the autocorrelation function includes a finite microscale, thus the relative proportion of spectral power at high frequencies exceeds that of the Dryden.
Ornstein-Uhlenbeck turbulence	A spectral form with first-order longitudinal and transverse components.
Etkin one dimensional turbulence power spectra	The local turbulent velocity field is approximated by a truncated Taylor series which yields uniform and gradient components. High frequency spectral components eliminated on the basis of aircraft size. Based on Dryden form, but gradient spectra are non-realizable unless simplified.
Versine gust	A discrete gust waveform.
Lappe low-altitude turbulence model	Experimentally-obtained data of vertical gust spectra, mean wind speed, and lapse rate were used to develop a low-level turbulence model. The turbulence spectra are presented for different types of terrain, height, and meteorological conditions.
Multiple point source turbulence	A two-dimensional gust field generated from two or more noise sources having prescribed correlation functions and located spanwise or lengthwise on the vehicle.
Holley-Bryson random turbulence shaping filters	A matrix differential equation formulation of uniform and gradient components including aircraft size effects. Filter equation coefficients determined from least square fit to multi-point-source-derived correlation functions.
University of Washington non-Gaussian atmospheric turbulence model	Non-Gaussian model using modified Bessel functions to simulate the patchy characteristic of real-world turbulence. Spectral properties are Dryden and include gust gradients.

[*] Refer to Reference 35 for citations

Model	Key Features
=======	==============
Delft University of Technology non-Gaussian structure of the simulated turbulent environment	Non-Gaussian model similar in form to the University of Washington model, but uses the Hilbert transform to model intermittency as well as patchiness. Includes University of Washington model features extended to approximate transverse turbulence velocities and gradients.
Royal Aeronautical Establishment model of non-Gaussian turbulence	Non-Gaussian turbulence model with a variable probability distribution function and a novel digital filtering technique to simulate intermittency. Spectral form approximately von Karman.
The Netherlands National Aerospace Laboratory model of non-Gaussian turbulence	Similar to the Royal Aeronautical Establishment model, but extended to include patchiness and gust gradient components and transverse velocities.
University of Virginia turbulence model	Models patchiness by randomizing gust variance and integral scale length of basic Dryden turbulence.
Mil Standard turbulence model	First order difference equation implementation of turbulence filters based on 8785 Dryden turbulence and refitted rolling gust intensity.
Indian Institute of Science non-stationary turbulence model	Nonstationary turbulence is obtained over finite time-windows by modulating a Gaussian process with either a deterministic or random process. The result is patchy-like turbulence similar to the University of Washington model except the time-varying statistics of the turbulence are presented for the deterministic modulating functions.
FAA wind shear models	Three-dimensional wind profiles for several weather system types including fronts, thunderstorms, and boundary layer. The profiles are available in table form.
STI wind shear model	Time and space domain models of mean wind and wind shear (ramp wave forms) are combined with MIL-F-8785C Dryden turbulence to obtain the total atmospheric disturbance. The magnitudes of the mean wind and wind shear are evaluated in terms of the aircraft's acceleration capabilities.

Model	Key Features
Sinclair frontal surface wind shear model	A generic model of frontal surface wind shear derived from a reduced-order from of Navier-Stokes equations. Relatively simple to use and can match the overall characteristics of measured wind shears.
MIL-F-8785B atmospheric disturbance model	Intensities and scale lengths are functions of altitude and use either Dryden on von Karman spectral forms or a one minus cosine discrete gust. Also spectral descriptions of rotary gusts.
MIL-F-8785C atmospheric disturbance model	Same as 8785B with the addition of a logarithmic planetary boundary layer wind, a vector shear, and a Naval carrier airwake model.
ESDU atmospheric turbulence	Rather general, but contains comprehensive descriptive data for turbulence intensity, spectra, and probability density
Boeing atmospheric disturbance model turbulence	A comprehensive model of atmospheric disturbances that includes mean wind, wind shear, and random turbulence. Turbulence is Gaussian and uses linear filters that closely approximate the von Karman spectral form. Mean wind and turbulence intensity are functions of meteorological parameters.
Wasicko carrier airwake model	Includes mean wind profile, effect of ship motion, and turbulence.
Naval ship airwake model	Includes free air turbulence filters plus steady, periodic, and random components of airwake which are functions of time and space.
Vought airwake model for DD-963 class ships	Combined random and deterministic wind components for free air and ship airwake regions. Based on wind tunnel flow measurements.
STI Wake vortex encounter model	A two-dimensional model of the flow-field due to the wake vortex of an aircraft is presented. The parameters of the flow-field model are weight, size, and speed of the vortex-generating aircraft, and distance and orientation of the vortex-encountering aircraft. Strip theory is used to model the aerodynamics of the vortex-encountering aircraft.

Model	Key Features
Cambell and Stanborne wind shear and turbulence model	Spatial model based on joint airport weather studies (JAWS) microburst data. Permits calculation of aerodynamic loads over body of aircraft.
Zhu and Etkin microburst model	Generic spatial model of microburst velocity components based on potential flow singularity distribution involving only three adjustable parameters.

time. Recording hundreds of different turbulence encounters may solve this problem but may present another - that of economics. Even if specific time records are deemed to be general enough to represent several other events, the pilot-in-training would no doubt become too familar with the characteristics of the turbulence encounter, and the versatility and flexibility demanded of both the simulator and pilot would accordingly be comprimised. Hence, such a method is unsuitable for general-utility simulations.

The most common technique used to simulate atmoshperic turbulence is the method of linearly-filtered, Gaussian white noise. In this method, a wide-band white noise signal is fed into a filter whose transfer function is such that the output spectrum matches the desired turbulence spectrum (see Figure 29). Inherent in such simulations - known as "Monte Carlo" turbulence simulations - is the flexibility absent from the aforementioned flight-recorded turbulence method. This filtering technique, while being extraordinarily easy to implement, does have a major deficiency: should the filter be linear, the output is necessarily Gaussian - a fact found to contradict experimental evidence concerning the probabilistic nature of turbulent winds.[37]

Many attempts have been made to "massage" the Gassian signal into a non-Gaussian one. One of the methods is the Modified Gaussian technique (see Table 5). In this method, it is hypothesized that the non-Gaussian patchiness may be considered as the linear combination of two components: one representing the intensity variations within the turbulence patch itself, and the other characterizing the time-dependent nature of the intensity.[38] As illustrated
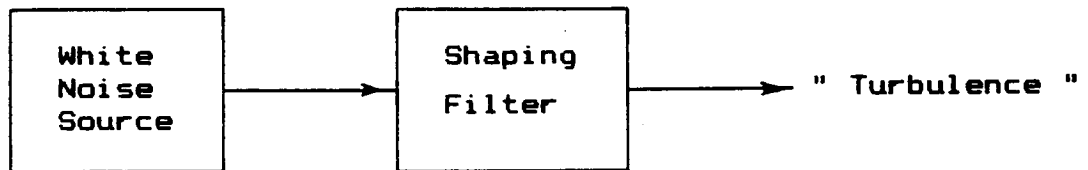
Figure 29 : Simulation of Atmospheric Turbulence *via*
Linearly-Filtered White Noise

in Figure 30, the Modified Gaussian tubulence method
involves a random variation of intensity *via* a random number
generator. The signal is passed through a distribution
modifier. The result is then fed into a matched linear
filter which outputs the simulated turbulent gust velocity.
A similar procedure may be applied for the other components
of turbulent velocity since anisotropy demands different
component values of intensity. Note that the level of the
turbulence activity corresponding to each patch is dictated
by the magnitude of the mean intensity, while the
distribution modifier provides the time-dependent
intensity.[38] In fact, the distribution modifier is patterned
after the pdf of the intensity. (Some turbulence data
suggests the a truncated Gaussian distribution adequately
represents the distribtion of the intensity.[38])

A natural extension of the Modified Gaussian Model is
the method in which an integral scale modifier is also
included. Such a turbulence simulation scheme, depicted in
Figure 31, is known as the UVA Turbulence Model.[39] (Again,
refer to Table 5 and see "University of Virginia turbulence
model.")

In summary, the need for enhanced realism in flight
simulations has given rise to many different models and
simulation techniques concerning atmospheric turbulence.
The reason so many exist is that scientists and pilots alike
find it difficult to <u>quantify</u> the "feel" of turbulence.
Some believe that nonstationarity (or nonhomogeneity)
promotes realism.[39] Other investigators have considered the
non-Gaussian characteristics of atmospheric turbulence[40] to
be the difference between simulation and reality while many
others believe that <u>one</u>-dimesional psd's will never fully

$$\sigma_i = \sigma_u, \sigma_v, \sigma_w$$

```
┌──────────────┐              ┌──────────────┐
│   Random     │              │  Intensity   │
│   Number     │─────────────▶│ Distribution │
│  Generator   │              │   Modifier   │
└──────────────┘              └──────────────┘
                                     │
                                     │ σᵢ
                                     ▼
┌──────────────┐              ┌──────────────┐        Turbulent
│    White     │              │   Shaping    │
│    Noise     │─────────────▶│              │───────▶   Gust
│   Source     │              │    Filter    │
└──────────────┘              └──────────────┘        Velocity
```
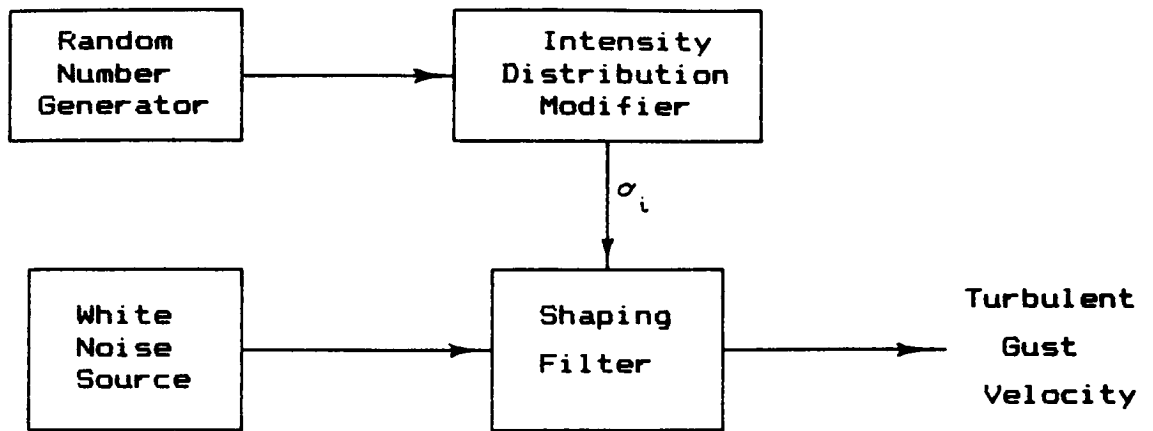
Figure 30 : Modified Gaussian Turbulence Simulation

Random
Number
Generator
(A)

Intensity
Distribution
Modifier

σ_i

White
Noise
Source

Shaping
Filter

Turbulent

Gust

Velocity

Λ_i

Random
Number
Generator
(B)

Scale
Distribution
Modifier
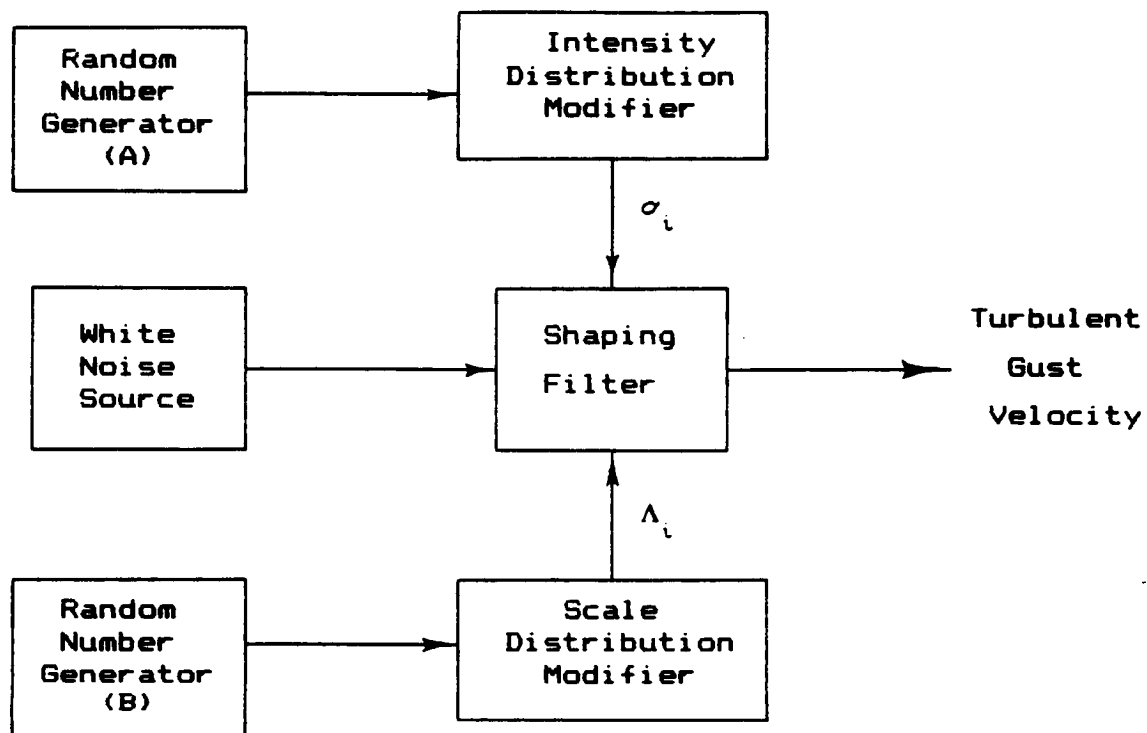
Figure 31 : UVA Gust Model Turbulence Simulation

incorporate the physical feel of true three-dimensional hydrodynamic turbulence.[41] Still others maintain that the aircraft point-mass assumption is too bold, and that spanwise gust gradients across the airfoil must be included in the rolling and yawing moments.[42] In fact, it has even been speculated that the "feel" of turbulence may be primarily due to airframe vibration[43] - a characteristic usually neglected in present flight simulators. This long list indicates that evaluation criteria for flight simulations are indeed quite subjective. For this reason, simplicity and cost effectiveness will serve as the governing factors in the following simulation considerations for the "small anisotropy" turbulence model.

§ 4.3   A Simulation Technique for the Modelled Turbulence

The task at hand is to develop a method of simulating the anisotropic turbulence modelled in Chapter 3. The technique chosen is the linear-filtering method for an output power spectrum matching that of Equation (4.5). A simple schematic of typical isotropic turbulence simulations is shown in Figure 32 in which the output of the shaping filter matches either the Dryden or von Kármán spectra. But recall that classical isotropic turbulence falls short in the estimation of the energy transfer associated with low-altitude flight. Hence, it is proposed that the present anisotropic turbulence model may be simulated as shown in Figure 33. Here, it is assumed that the white noise sources are independent, and that the matching (shaping) filters are computationally realizable - the reason for which the Dryden psd is preferred to the von Kármán psd for the isotropic portion of the simulation. In keeping with the popular methodology associated with the filtering technique, the nonstationary nature of the random process will first be suppressed, and will then later be incorporated as in the UVA simulation. The initial task is therefore to determine the transfer functions of the corresponding shaping filters.

The isotropic, Dryden shaping filter for the downwash turbulence is well known and takes the form[38]
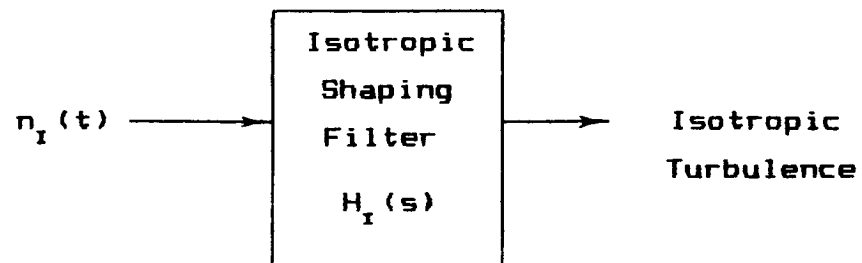
Figure 32 : Method to Simulate Isotropic Turbulence
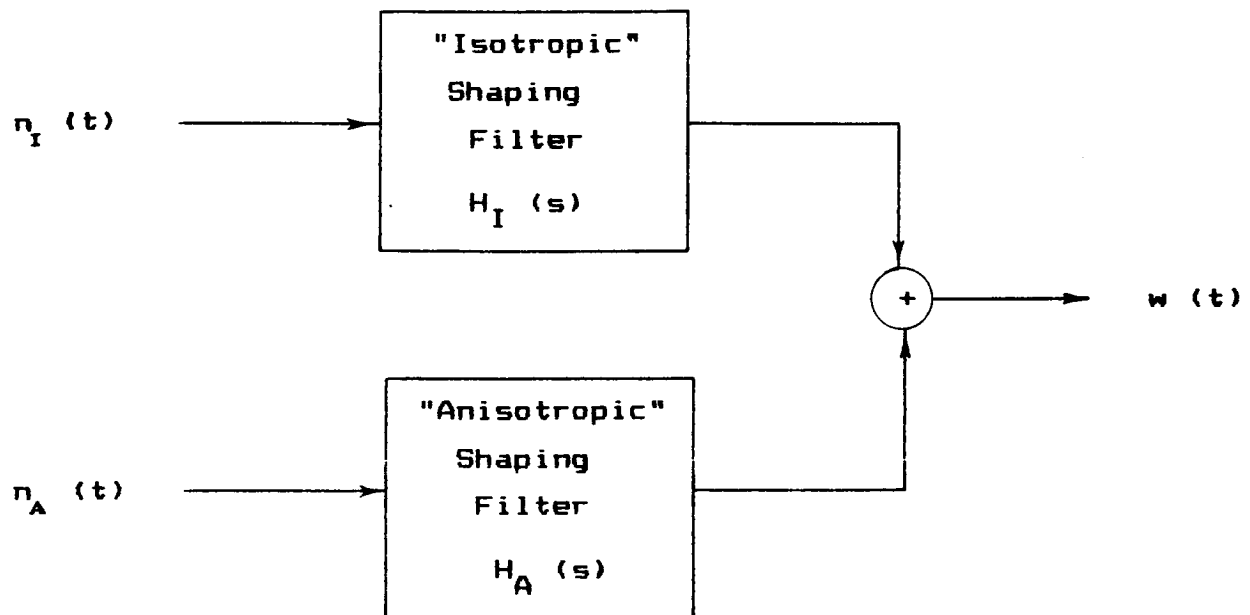
Figure 33 : Simple Simulation Scheme for the
Anisotropic Turbulence Model

$$H_I(s) = \sigma \left[\frac{3\,V}{2\pi\,\Phi_o\,\Lambda} \right]^{1/2} \frac{s + \dfrac{V}{(3)^{1/2}\Lambda}}{\left[s + \dfrac{V}{\Lambda} \right]^2} \quad , \quad (4.14)$$

where "s" is the Laplace variable, and "Φ_o" is the constant psd value of the white noise input.

Now, consider the contribution of the anisotropy. Recall that the anisotropic psd is

$$\Phi_{WW}^{(a)}(\varkappa) \equiv \left\{ 4\sigma^2\Lambda \left[\frac{\Delta\,\Lambda}{\Lambda} \right] \frac{1 - \cos(\frac{\varkappa b}{a\Lambda})}{(\frac{\varkappa b}{a\Lambda})^2} \right\} \quad . \quad (4.15)$$

Equation (4.15) may be rewritten as

$$\Phi_{WW}^{(a)}(\omega) \equiv 2\sigma^2\Delta\Lambda \left[\text{sinc}\ \frac{\omega\,b}{2\,a\,V} \right]^2 \quad . \quad (4.16)$$

With frequency matching in mind, it is noted that the sinc function may be considered as follows:

$$\text{sinc } \frac{\omega b}{2 a V} \quad \leftrightarrow \quad \text{sinc } \frac{\omega T}{2} \Bigg|_{T = \frac{b}{a V}} \qquad . \qquad (4.17)$$

Using this fact, it can be shown that the corresponding frequency response function is the zeroth-order, "catch-and-hold" filter[44] i.e.,

$$\text{sinc } \frac{\omega T}{2} \quad \leftrightarrow \quad H(s) = \underbrace{\frac{1 - e^{-sT}}{s}}_{\text{" zeroth-order filter "}} \qquad . \qquad (4.18)$$

Upon inspection of Equation (4.17), it is evident that the frequency content has been matched but the parameter $2\sigma^2 \Delta\Lambda$ has not. To do so, the input/output relationship for stationary random processes is used, viz.

- 111 -

$$\Phi^{OUT}(s) = \left[\left| H(s) \right| \left| H(-s) \right| \right]_{s=\iota\omega} \Phi^{IN}(s) . \quad (4.19)$$

In this case, Equation (4.19) becomes

$$\Phi_{WW}^{(a)}(s) = \left[\left| \mathbb{K} H(s) \right| \left| \mathbb{K} H(-s) \right| \right]_{s=\iota\omega} \Phi_0(s) , \quad (4.20)$$

where $\mathbb{K}$ is a matching factor introduced to account for the " $2\sigma^2\Delta\Lambda$ " term. Substitution of the frequency response function for the zeroth-order hold into the input/output relationship yields

$$2\sigma^2\Delta\Lambda \left[\text{sinc} \frac{\omega b}{2 a V} \right]^2 = \mathbb{K}^2 \mathbb{T}^2 \left[\text{sinc} \frac{\omega \mathbb{T}}{2} \right]^2 \Phi_0(s)$$

which simplifies to

$$K^2 = \frac{a V^2}{\Phi_o} \cong \text{constant scaling parameter .} \quad (4.21)$$

Consequently, the shaping filter for the modelled anisotropy becomes

$$H_A(s) = \left[\frac{a V^2}{\Phi_o} \right]^{1/2} \frac{1 - e^{-s(\frac{b}{a V})}}{s} . \quad (4.22)$$

In arriving at Equation (4.22), it was assumed that the parameter $b/(aV)$ varies "slowly with time" with respect to the simuland's time-domain response (see Figure 34). A similar assumption is at the very root of the UVA turbulence simulation in which the time-varying turbulence statistics $\sigma(t)$ and $\Lambda(t)$ are assumed constant over the current time period, and then updated for the next.

With the UVA method in mind, a more explicit simulation technique for the modelled downwash turbulence is

$$\frac{b}{a\ V}$$
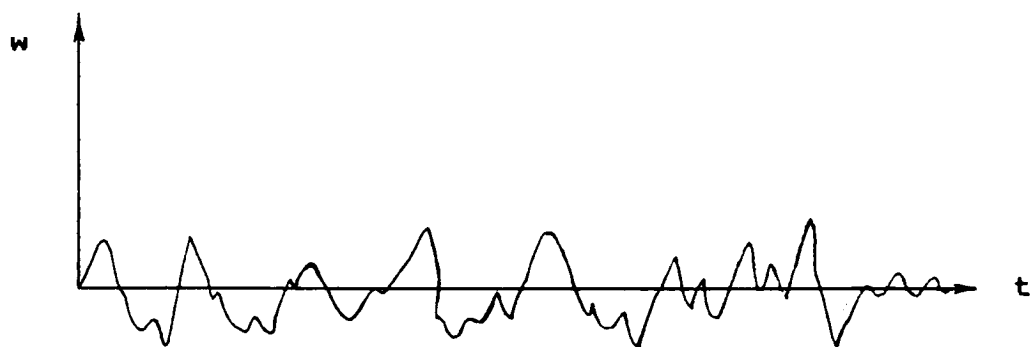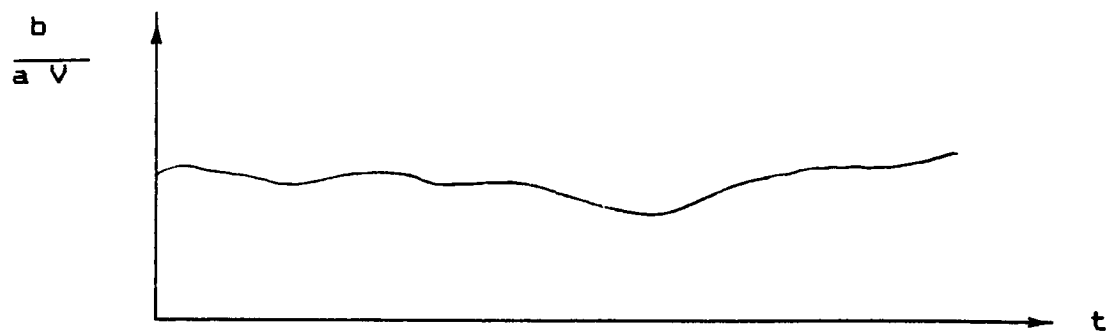
Figure 34 : Concept of a "Slow-Varying" Parameter

illustrated in Figure 35. In this scheme, however, the
independent Gaussian white noise components (n_I and n_A)
are interrelated by the intensity and length statistics.
Again, the distribution modification scheme is invoked to
account for the time-dependent turbulence statistics. In
the aforementioned figure, note that the "sensitivity
variable" for the simulation is "b" since the approximation
$a \equiv \mathcal{O}(\alpha) \cong$ constant is assumed to be an acceptable one for
simulation puposes. In order to approximate "b," Equation
(E.12) is used to give

$$b^2 = 2a\sigma^2 \Delta \Lambda \quad .$$
(4.23)

or

$$b = (2\sigma^2 \mid a \; \Delta \Lambda \mid)^{1/2}$$
(4.24)

It now becomes essential to provide a relationship between
$\Delta \Lambda$ and Λ (see Figure 35). One estimate,
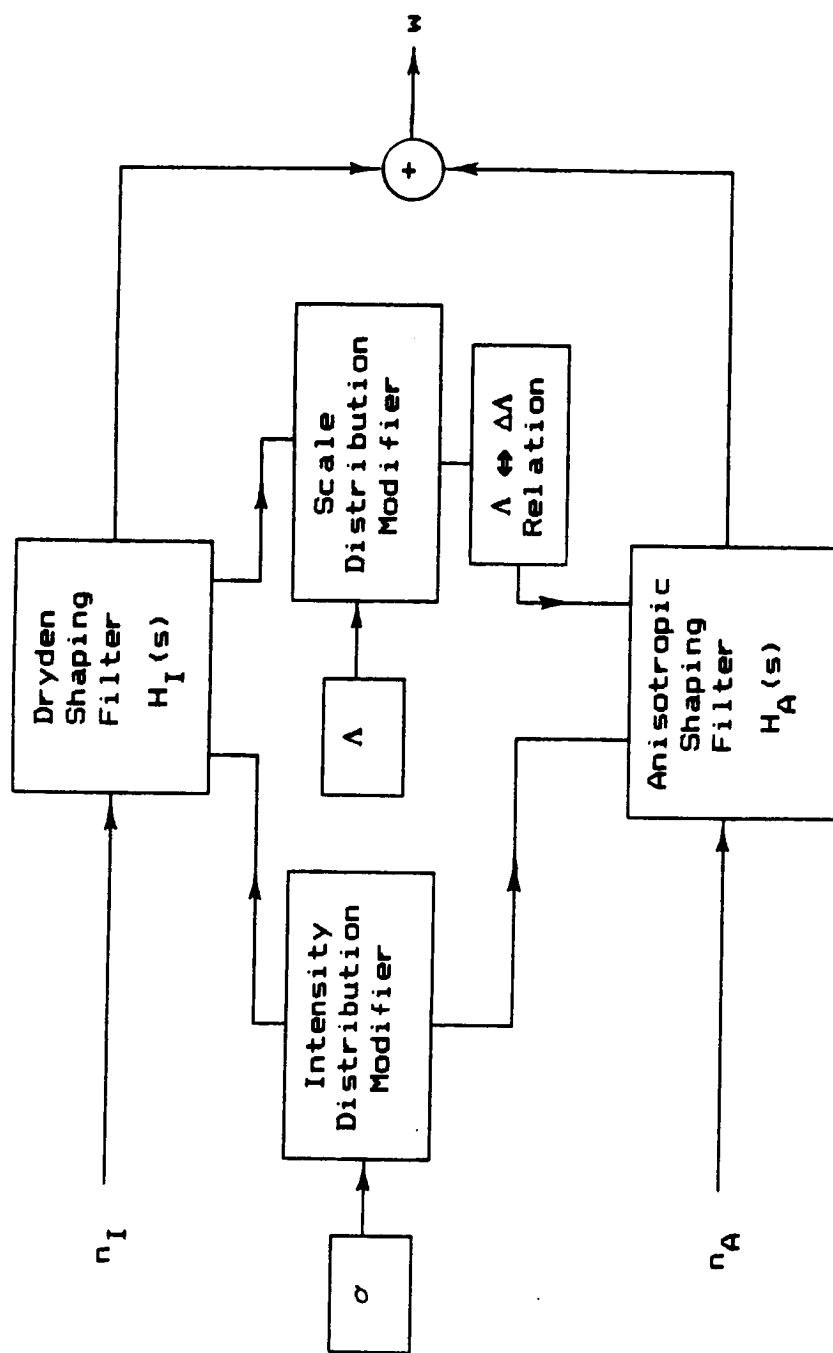
Figure 35 : Proposed Simulation Scheme for Modelled Turbulence

$$\Delta \Lambda \cong \mathcal{O} (\pm t\Lambda) \quad , \tag{4.25}$$

results from the self-similarity concepts of Chapter 3 since $\Lambda(t) \cong \mathcal{O}(t^{1/2})$ and $\Delta\Lambda(t) \cong \mathcal{O}(t^{3/2})$ for $\sigma^2 \cong \mathcal{O}(t^{-1})$. The algebraic sign on " $t\Lambda$ " in Equation (4.25) is dependent upon the side of the wind shear being simulated. If the self-similarity assumption is deemed too specific for general-purpose simulation, another approximation such as

$$\Delta \Lambda = \Psi \Lambda \tag{4.26}$$

with $\Psi \equiv$ (an accepted scaling constant) may be an appropriate starting point.

As an aside, it should be noted that if the "slow varying" assumption is accepted in the analog version of the simulation, the same must hold for the digital simulation. (One possible scheme is outlined in Figure 36.) Although digital simulation is not a goal of this study, note that one obstacle will no doubt arise - that of the initial

$$X(s) \longrightarrow \boxed{\quad H(s) \quad} \longrightarrow Y(s)$$

$$\boxed{Y(s) \; \dot{=} \; H(s) \; X(s)}$$

$$\downarrow$$

$$\boxed{\begin{array}{c} \text{Inverse Laplace Transform} \\ \textit{via} \text{ the z-transform} \end{array}}$$

$$\downarrow$$

$$\boxed{\begin{array}{c} \text{Difference Equations with} \\ \text{"Constant" Coefficients} \end{array}}$$

$$\downarrow$$

$$\boxed{\begin{array}{c} \text{Solve for Discete Time} \\ \text{Domain Representation} \end{array}}$$
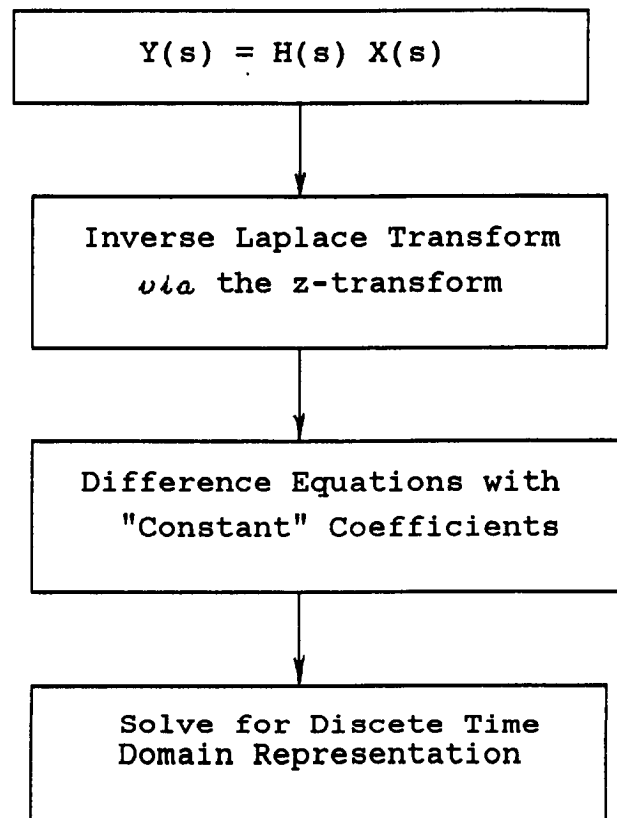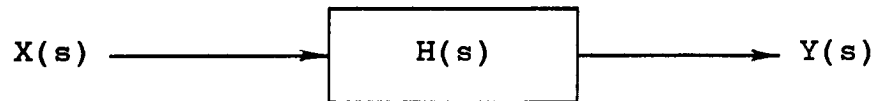
Figure 36 : Possible Digital Simulation Technique

conditions required in the z transform and the resulting transients due to non-zero initial conditions. A more pertinent concern, though, is the estimate on the elusive "b" - that single anisotropy-defining parameter which has been left unspecified by turbulence modelling theory.

§ 4.4   ESTIMATION OF "b" FROM SIMULATION CONCEPTS

At present, knowledge of the mathematical form of "b" consists of

$$b \cong 2\sigma^2 \frac{\Delta \sigma}{\sigma} \qquad . \qquad (4.27)$$

and

$$b^2 = 2a\sigma^2 \Delta\Lambda \qquad (4.28)$$

from Equations (4.12) and (E.12), respectfully. Now, consider the anisotropic turbulence input/output relationship illustrated in Figure 33. This figure clearly implies

$$w_A(s) = \left[\frac{a\,V^2}{\Phi_o} \right]^{1/2} \left[\frac{1 - e^{-hs}}{s} \right] n_A(s) \quad , \quad (4.29)$$

where $h \equiv b/(aV)$. The time-domain representation of Equation (4.29) is found *via* the inverse Laplace transform, i.e.,

$$w_A(t) = \mathcal{L}^{-1} \left\{ w_A(s) \right\} \quad . \quad (4.30)$$

The result of the transformation,

$$w_A(t) = \left[\frac{a\,V}{\Phi_o} \right]^{1/2} \int_o^{b/(aV)} n_A(t-\tau)\,d\tau \quad , \quad (4.31)$$

is derived in Appendix H. It is in the "memory effect" associated with the above definite integral from which an estimate of "b" can be made. Since two-point theory demands

that the length over which correlation exists is appriximately <u>one</u> <u>correlation</u> <u>length</u> $= \Lambda + \Delta\Lambda \equiv L$ (cf. Figure 12), Equation (4.31) accordingly implies

$$L \cong V \left(\frac{b}{a \, V} \right) \tag{4.32}$$

or

$$b \cong a L \quad . \tag{4.33}$$

Since $a = a(t) \equiv \mathcal{O}(\alpha)$, Equation (4.33) is yet another equation relating the two parameters which define "small anisotropy" in a low-altitude wind shear encounter.

§ 4.5   CONSIDERATION OF THE "HAZARD INDEX"

Other facets of the wind-shear research effort are detection and avoidance. The primary objective in the development of *in situ* detection, warning, and avoidance systems is the definition of an accepted and reliable <u>hazard</u> <u>index</u>. Such a parameter has recently been defined as[45]

$$ F \ \leq \ \frac{|\dot{U}|}{g} \ + \ \frac{|W|}{V} \ , \qquad (4.34) $$

where $\dot{U}$ is the total derivative of the horizontal wind component, and W is the vertical wind component. The inequality was derived upon consideration of the balance of mechanical energy of an aircraft translating through an accelerating, nonhomogeneous flow. Analysis has shown that the hazard index may be physically interpreted as the loss in excess thrust-to-weight ratio due to the flow characteristics of the shear.[45] Combinations of horizontal and vertical winds peculiar to a wind shear encounter likely fall outside of the index-bracketted diamond of Figure 37.[45] Such a state indicates that a threatening condition exists with respect to aircraft performance. The hazard index, commonly referred to as the "F-Factor," is made an equality by imposing a hazard threshold, F_o - a value based upon aircraft performance data.

Once a specified threshold value is exceeded, a warning is either annunciated or displayed to the pilot. The possibility of non-hazardous turbulence inducing such a threshold exceedence is incontestably of paramount concern. Horizontal and vertical turbulence models must adequately represent low-altitude encounters to ensure that the hazard alert does not become a nuisance alert.

Analysis of the turbulence-nuisance question has, up to

- 122 -

$$F \leq \frac{|\dot{u}|}{g} + \frac{|w|}{V}$$

$$\frac{|\dot{u}|}{g}$$

Accident Data

Head ⟶ Tail

$F < F_o$

Downdraft

Safe Operation

Updraft

$$\frac{|w|}{V}$$

Tail ⟶ Head
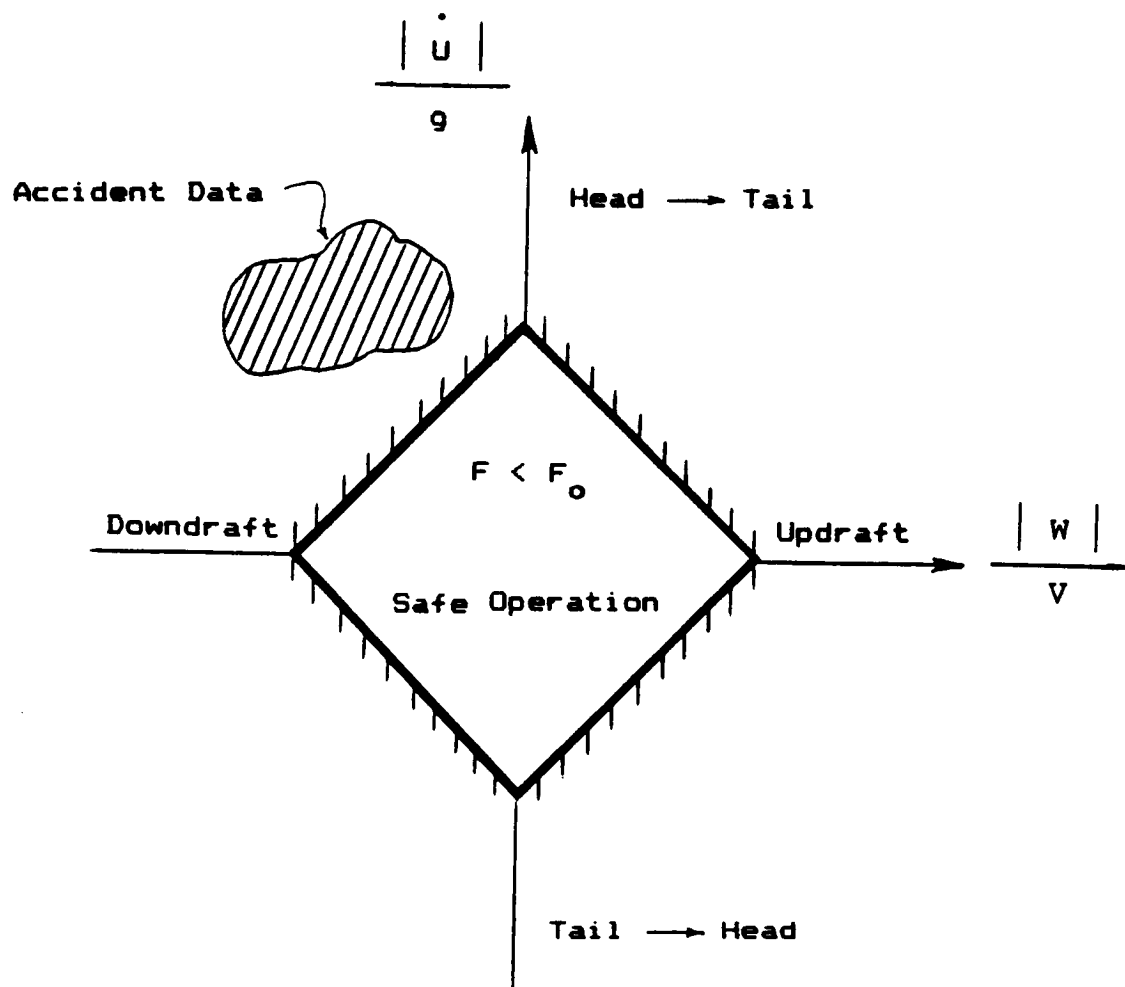
Figure 37 : The " F-Factor " as a Hazard Index

the present, only involved isotropic (Dryden)
approximations.[46] But recall that the sensitivity analysis
performed above *via* the energy scaling factor indicated that
such estimates are <u>non-conservative</u> for the environments for
which the hazard index is derived. Clearly, the turbulence
model of Chapter 3 is a prime candidate to quantify the
vertical wind component of Equation (4.34). (The
"substantial derivative" of the horizontal wind in the
F-Factor is currently being investigated,[47] and will not be
addressed here.)

The role of the turbulence model for "small
anisotropy," as it applies to Equation (4.34), may be better
exemplified by considering the variance of the F-Factor ,
viz.

$$\sigma_F^2 \;=\; \sigma^2 \Bigg|_{\dfrac{\dot{u}}{g}} \;+\; \sigma^2 \Bigg|_{\dfrac{w}{v}} \tag{4.35}$$

which may be rewitten as

$$\sigma_F^2 = \frac{1}{g} \int_{-\infty}^{\infty} \Phi_{\dot{U}} \, d\omega \; + \; \frac{1}{V} \left\{ \int_{-\infty}^{\infty} \Phi_{ww}^{(i)} \, d\omega \; + \; \int_{-\infty}^{\infty} \Phi_{ww}^{(a)} \, d\omega \right\} \quad .$$

(4.36)

Substitution of Equations (4.6) and (4.7) into (4.36), results in

$$\sigma_F^2 = \frac{1}{g} \int_{-\infty}^{\infty} \Phi_{\dot{U}} \, d\omega \; + \; \frac{\sigma_w^2}{V} \left\{ 1 + \frac{2 \, a \, \Delta\Lambda}{b} \right\} \quad . \quad (4.37)$$

Invoking Equations (4.33) and (4.28) for b^2 and $\Delta\Lambda$, resectively, yields

$$\sigma_F^2 = \frac{1}{g} \int_{-\infty}^{\infty} \Phi_{\dot{U}} \, d\omega \; + \; \left\{ \frac{\sigma_w^2}{V} + \frac{a}{V} \, L \right\} \quad . \quad (4.38)$$

Since the nature of σ_w is well documented in the literature,[36,38] Equation (4.38) is an important one since both "a" and "V" are well defined by the present turbulence model. Consequently, the bracketted term of Equation (4.38) is that portion of the total intensity of the F-Factor corresponding to the modelled anisotropy. Substitution of typical values, viz. $\sigma^2 = 15$ ft/s, $a \cong 0.052$ ft/s^2, and V = 225 ft/s provides

$$\sigma_F^2 = \left\{ \frac{1}{g} \int_{-\infty}^{\infty} \Phi_{\dot{U}} \, d\omega \right\} + (1 + 0.00023 \, L) \qquad . \qquad (4.39)$$

As is usually the case in turbulence modelling, the length scale (e.g., "L") is unspecified. Since a perfectly acceptable value of L is 1000 ft, the "0.00023 L" term is significant in comparison to unity in the turbulence model's contribution to Equation (4.39).

Clearly, these results indicate that anisotropy must be accounted for in the turbulence model used in the evaulation of a hazard index. It is important to note that Equation (4.38) demands that, if the aircraft flies along a horizontal path, the anisotropic turbulence model contributes no more than that due to isotropy alone - a fact which is in agreement with the "small anisotropy" turbulence theory. At present, it is not known how significant the vertical wind component is in comparison to

the horizontal (cf. Equations (4.34) and (4.35)), but it has become evident upon inspection of Equation (4.39) that a thumb rule for length scale with altitude is needed for *in situ* hazard index estimation. Such rules of thumb are commonly used for estimating σ and Λ (or "L") in flight simulations.[38] Once this "rule" is obtained and an acceptable performance-sensitive value for the variance of the F-Factor is imposed (presently specified 0.12 for large commercial aircraft),[46] a major step toward the minimization of nuisance alerts will have been made.

CHAPTER 5

CONCLUDING REMARKS AND RECOMMENDATIONS

§ 5.1   Conclusions

Chapter 1 introduced the potential dangers of wind shears and their corresponding turbulence, and it defined the principle objectives of the present study: 1) to model the statistical characteristics of the turbulence perceived by an aircraft translating through low-altitude, sheared mean winds, 2) to study the effect of these characteristics on aircraft response, and 3) to consider a method of simulating the modelled turbulence. From the basic premise that near-ground, wind-shear turbulence is anisotropic, the "small anisotropy" turbulence model of Chapter 3 was developed. The downwash autocorrelation function immediately followed. The anisotropic autocorrelation function was then converted into a power spectrum - a popular frequency domain statisic used in the simulation of atmospheric turbulence. Use of the power spectral density approach highlighted the fact that realistic estimates of the energy transfer associated with wind-shear turbulence demand that anisotropy must be accounted for in both turbulence models and related flight simulations. Chapter 4 then illustrated the relative ease in which the turbulence model could be simulated. Furthermore, a state-of-the-art application of the above turbulence model in wind-shear detection was introduced *via* the "F-Factor." Consequently, the goals defined at the onset of the present research effort were met and possibly surpassed.

§ 5.2   RECOMMENDATIONS FOR FURTHER WORK

The preceeding work has resulted in many questions which may be considered in follow-up studies:

- How well does the autocorrelation function for "small anisotropy" compare with that actually perceived by an aircraft flying through low-altitude, sheared winds?

- Exactly how should the analog simulation technique of Chapter 4 be effected digitally? Additionally, how well will the digitally reconstructed power spectral density compare with that produced from actual flight recordings?

- Is the "slow-varying parameter" method used to account for time (space) dependent turbulence statistics acceptable? Moreover, since b/(aV) was assumed slow varying and "b" was recognized as the more sensitive time-dependent term, could the self-similarity based result,

$$\frac{d\,b}{d\,t} \cong \frac{d}{d\,t}\left\{ a\,L \right\} = \frac{d}{d\,t}\left\{ a\left[\emptyset\,(\,t^{1/2}\,) + \emptyset\,(\,t^{3/2}\,) \right] \right\}$$

$$= a\left\{ \emptyset\,(\,\frac{1}{2}\,t^{-1/2} + \frac{3}{2}\,t^{1/2}\,) \right\}$$

serve as a criterion from which "b" could be adjusted for more realistic time-dependent simulations?

It therefore becomes clear that the validity of the assumptions made in both the turbulence model and the proposed simulation technique can only be addressed fully when in-flight recordings of the downwash turbulence during a wind-shear encounter are made.[†] It is in this rather blunt statement that the motivation for "best approximations" becomes apparent. Existing high-altitude wind shear data should first be considered. It is hoped that one possible "approximation" will ultimately consist of incorporating the aforementioned turbulence model into real simulations. Here the pilots may provide comments on the realism of the simulated turbulence that no theoretical analysis could reveal.

[†] Reference 48 may provide insight on both this data and the "rule of thumb" relating integral scale and altitude called for in Section 4.5.

REFERENCES

[1]Fujita, T.T., "Spearhead Echo and Downburst Near the Approach End of a John F. Kennedy Airport Runway, New York City," SMRP Research Paper 137, March 1976.

[2]Targ, R., "Wind Shear Avoidance With an Airborne Laser," from "Industrial Review of Forward Looking Sensor Technology for Detection of Wind Shear," Confererence at NASA-Langley Research Center, February 1987, pp. 119-162.

[3]Zhu, Shangxiang and Bernard Etkin, "Model of the Wind Field in a Downburst," *Journal of Aircraft*, July 1985, pp. 595-601.

[4]McCarthy, John, "Introduction to the JAWS Program," from "Wind Shear/Turbulence Inputs to Flight Simulation and Systems Certification." eds. Roland L. Bowles and Walter Frost, NASA Conference Publication 2474, 1987, pp. 13-27.

[5]"FAA Funding Detection Technology Research," *Aviation Week and Space Technology*, September 22, 1986, pp. 54-59.

[6]Chiles, J.R., "When Pilots' Worst Nightmares Come True - In Simulators," *Smithsonian*, pp. 78-87.

[7]"FAA Funding Detection Technology Research ("FAA Advisory Circulars Define Shear as Wind, Speed Shift")," *Aviation Week and Space Technology*, September 22, 1986, p. 55

[8]Treviño, G., "Turbulence for Flight Simulation," *Journal of Aircraft*, Vol. 23, April 1986, pp. 348-349.

[9]Piersol, A.G., "Power Spectra Measurements for Spacecraft Vibration Data," *Journal of Spacecraft and Rockets*, Vol. 4, December 1967, pp. 1613-1617.

[10]Gerlach, O.H., et. al., "Progress in the Mathematical Modeling of Flight in Turbulence," NATA-AGARD CP-140, November 1973, pp. 5.1-5.38.

[11]Treviño, G., "Comment on 'Monte Carlo Turbulence Simulation Using Rational Approximations to von Kármán Spectra,'" *AIAA Journal*, Vol. 24, November 1986, p. 1885.

[12]Reid, Lloyd D., "Correlation Model for Turbulence Along the Glide Path," *Journal of Aircraft*, Vol. 15, January 1978, pp. 13-20.

[13]Bendat, J.S. and A.G. Piersol, <u>Random</u> <u>Data: Analysis and Measurement Procedures</u>, Second edition (Revised and Expanded), John Wiley & Sons, Inc., New York, 1986.

[14]Maisel, Louis, <u>Probability, Statistics, and Random Processes</u>, Simon & Schuster, New York, 1971.

[15]Papoulis, A., <u>Probability, Random Variables, and Stochastic Processes</u>, McGraw-Hill, New York, 1965.

[16]Treviño, G., "Time-Invariant Structure of Nonstationary Atmospheric Turbulence," *Journal of Aircraft*, Vol. 22, September 1985, pp. 827-828.

[17]Treviño, G., "Time-Averaged Correlations for Self-Similar Nonstationary Data," *Journal of Sound and Vibration*, Vol. 114, 1987, pp. 593-594.

[18]Treviño, G., "Topological Invariance in Stochastic Analysis," Proceedings in the Fourth International Conference on Mathematical Modelling, X. R. Avuly, ed., New York, Pegamon Press, 1984, pp.

[19]Treviño, G., "Analysis of Nonstationary Processes by Affine Transformations," *Journal of Sound and Vibration*, Vol. 99, pp. 576-578.

[20]Hinze, J.O., Turbulence, Second edition, McGraw-Hill, 1975.

[21]Robertson, H.P., "Invariant Theory of Isotropic Turbulence," *Proceedings of the Cambridge Philosophical Society*, Vol. 36, 1940, pp. 209-233.

[22]Batchelor, G.K., "Theory of Axisymmetric Turbulence," *Proceedings of the Royal Society (Series A)*, Vol. 186, 1946, pp. 480-502.

[23]Treviño, G., "Airplane Flight Through Wind-Shear Turbulence," *Journal of Aircraft*, Vol. 23, September 1986, pp. 733-735.

[24]Gaonkar, G.H., "Review of Nonstationary Gust-Responses of Flight Vehicles," from AIAA/ASME/ASCE/AHS 21st Structures, Structural Dynamics ans Materials Conference, AIAA 80-0703, May 1980, pp. 938-956.

[25]Hussain, A.K.M.F., "Coherent Structures - Reality or Myth," *Physics of Fluids*, Vol. 26, October 1983, pp. 2816-2850.

[26]Batchelor, G.K., <u>Theory of Homogeneous Turbulence</u>, Cambridge University Press, Cambridge, U.K., 1967.

[27]Comte-Bellot, Genevieve and Stanley Corrsin, "The Use of a Contraction to Improve the Isotropy of Grid-Generated Turbulence," *Journal of Fluid Mechanics*, Vol. 25, 1966, pp. 657-682.

[28]Treviño, G., "Turbulence Structure in Microburst Phenomena," *Journal of Aircraft*, Vol. 24, April 1987, pp. 283-285.

[29]Kármán, Theodore von, "On the Statistical Theory of Isotropic Turbulence," *Proceedings of the National Academy of Sciences*, Wash., Vol. 23, p. 98.

[30]Kármán, Theodore von and Leslie Howarth, "On the Statistical Theory of Isotropic Turbulence," *Proceedings of the Royal Society (Series A)*, Vol. 164, 1937, pp. 192-215.

[31]Kármán, Theodore von and C.C. Lin, "On the Concept of Similarity in the Theory of Isotropic Turbulence," *Rev Mod Phys.*, Vol. 21, 1949, p. 516.

[32]Dryden, Hugh L., "Isotropic Turbulence in Theory and Experiment," *T von Kármán Anniversary Volume*, 1941, p. 85.

[33]Batchelor, G.K., <u>Theory of Homogeneous Turbulence</u>, Cambridge University Press, Cambridge, U.K., 1967.

[34]Fung, Y.C., <u>Theory of Aeroelasticity</u>, Dover Publications, Inc., New York, 1969.

[35]Moorhouse, David J. and Robert K. Heffley, "The Status of Military Specifications with Regard to Atmospheric Turbulence," from "Atmospheric Turbulence Relative to Aviation, Missile, and Space Programs, eds. Dennis W. Camp and Walter Frost, NASA Conference Publication 2468, 1986, pp. 181-198.

[36]Houbolt, John C., "Atmospheric Turbulence," *AIAA Journal*, Vol. 11, April 1973, pp. 421-437.

[37]Etkin, Bernard, "Turbulent Wind and Its Effect on Flight," *Journal of Aircraft*, Vol. 18, May 1981, pp. 327-345.

[38]Jacobson, Ira D. and Dinesh S. Joshi, "Investigation of the Influence of Simulated Turbulence Handling Qualities," *Journal of Aircraft*, Vol. 14, March 1977, pp. 272-275.

[39]Frost, Walter and Trevor H. Moulden, Handbook of Turbulence, Vol. 1, Plenum Press, New York, 1977.

[40]Reeves, P.M., *et al*, "Development and Application of a Non-Gaussian Turbulence Model for Use in Flight Simulators," NASA CR-2451, 1974, 147 p.

[41]Frost, Walter, "Turbulence Models," from "Wind Shear/Turbulence Inputs to Flight Simulation and Systems Certification." eds. Roland L. Bowles and Walter Frost, NASA Conference Publication 2474, 1987, pp. 125-149.

[42]Houbolt, John C., "Example on How to Model and Simulate Turbulence for Flight Simulators," from "Wind Shear/Turbulence Inputs to Flight Simulation and Systems Certification." eds. Roland L. Bowles and Walter Frost, NASA Conference Publication 2474, 1987, pp. 159-178.

[43]Campbell, C.W., "Monte Carlo Tubulence Simulation Using Rational Approximations to von Kármán Spectra," *AIAA Journal*, Vol. 24, Jan. 1986, pp. 62-66.

[44]Smith, Jon M., <u>Mathematical</u> <u>Modelling</u> <u>and</u> <u>Digital</u> <u>Simulation</u> <u>for</u> <u>Engineers</u> <u>and</u> <u>Scientists</u>, John Wiley & Sons, Inc. , New York, 1977.

[45]Bowles, Roland L., "Wind Shear Detection, Warning and Flight Guidance," from "Industrial Review of Forward Looking Sensor Technology for Detection of Wind Shear," Confererence at NASA-Langley Research Center, February 1987, pp. 53-84.

[46]Bowles, Roland L., NASA-Langley Research Center, Personal Communication, July 1987.

[47]Treviño, G., "Turbulence Parameters for Wind Shear Applications," Current NASA-Langley research contract.

[48]Chang, Ho-Pen and Walter Frost, "Development of a Microburst Turbulence Model for the JAWS Wind Shear Data," Draft Final Report Subcontract S3011 to National Center for Atmoshperic Research from FWG Associates, Inc. , Jan. 1986.

APPENDIX A   KINEMATICS OF AXISYMMETRIC TURBULENCE
VIA INVARIANTS

Kinematics, in the study of turbulence, consists of setting up velocity correlations at two (or more) arbitrary points in the turbulent fluid. The fundamental problem is: what is the correlation between the component of the velocity $\underset{\sim}{u}$ in an arbitrary direction at point P and that of $\underset{\sim}{u}'$ in an arbitrary direction at point P'? The arbitrary directions are defined by their respective direction cosines a_i and b_i. Isotropy demands that, for an arbitrary translation or rotation of the configuration governed by P, P', a_i, and b_i (cf. Figure A1 and consider the geometry as a rigid body), the velocity correlation must remain unchanged. At most, the correlation can depend on the position of the points, $r_i = x_i' - x_i$, the components of the direction cosines, a_i and b_i , and time , t . Theodore von Kármán and Leslie Howarth[A1] proved that such a correlation obeys the transformation laws of a second-order tensor and may be expressed as

$$\overline{u_i u_j{}'} = <u_i(\underset{\sim}{x},t)\, u_j(\underset{\sim}{x}+\underset{\sim}{r},t)> \equiv C_{ij} \qquad . \qquad (A.1)$$
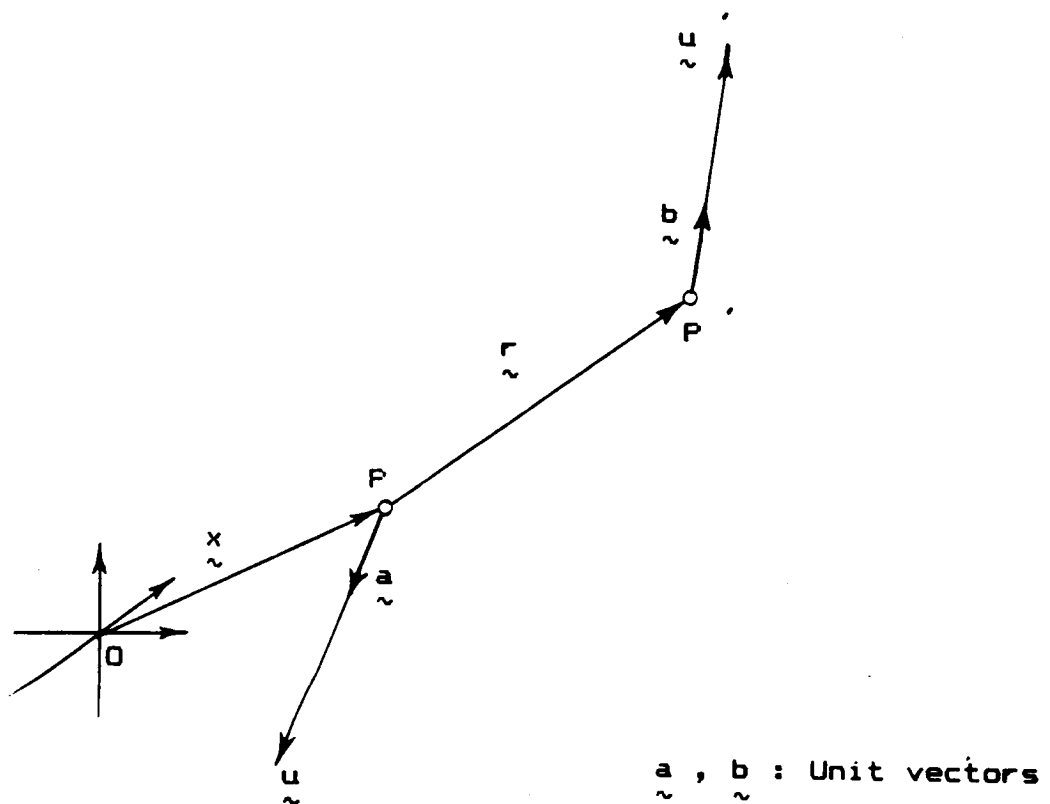
Figure A1 : Defining Geometry of a Two-Point Velocity
Correlation in a Turbulent Flow

The overscript bar indicates a time average. With isotropy
(and therefore homogeneity) in mind, the correlation
tensor may be written as

$$
C_{ij} = \begin{bmatrix} \overline{u\,u'} & \overline{u\,v'} & \overline{u\,w'} \\ \overline{v\,u'} & \overline{v\,v'} & \overline{v\,w'} \\ \overline{w\,u'} & \overline{w\,v'} & \overline{w\,w'} \end{bmatrix} \equiv \sigma^2 R_{ij} \ , \qquad (A.2)
$$

where R_{ij} is known as the <u>fundamental correlation
coefficient.</u> Thus, von Kármán and Howarth showed that the
two-point velocity correlation for arbitrary rotations about
the x_i coordinates in an isotropic turbulence field results
in a second-order tensor.

H. P. Robertson[A2] approached the same kinematical
problem from the perspective of invariant theory. In terms
of invariants, the kinematical problem for homogeneous,
isotropic turbulence becomes: determine the most general
function $R(\underset{\sim}{r}, \underset{\sim}{a}, \underset{\sim}{b}) = R_{ij}\, a_i b_j$ which is a invariant under
arbitrary and permissible rotations of the geometry-defining
vector set $\left\{ \underset{\sim}{r}, \ \underset{\sim}{a}, \ \text{and} \ \underset{\sim}{b} \right\}$. For axisymmetric turbulence,
the preferred direction, with an orientation defined by $\underset{\sim}{\lambda}$,
must be accounted for in the geometric invariance.

Consequently, the general function must be expanded to $R(\underset{\sim}{r}, \underset{\sim}{a}, \underset{\sim}{b}, \underset{\sim}{\lambda})$, and must depend only upon the fundamental invariants. For the case of axisymmetric turbulence, the fundamental invariants are all the possible scalar products formed by any two of the vectors $\underset{\sim}{r}$, $\underset{\sim}{a}$, $\underset{\sim}{b}$, and $\underset{\sim}{\lambda}$. To illustrate, first consider the <u>linear isotropic form</u>:

$$\mathscr{L} (\underset{\sim}{r}, \underset{\sim}{a}) \equiv L_i \, a_i \quad , \qquad\qquad (A.3)$$

where $\mathscr{L}$ is a linear, first-order correlation function which can depend at most on the invariants $\underset{\sim}{r} \cdot \underset{\sim}{r} = r^2$, $\underset{\sim}{a} \cdot \underset{\sim}{a} = 1$, and $\underset{\sim}{r} \cdot \underset{\sim}{a} = r_i a_i$. To be linear and homogeneous in its a_i components, the linear isotropic function generalizes to

$$\mathscr{L} (\underset{\sim}{r}, \underset{\sim}{a}) \equiv L(r^2) \, r_i a_i \quad . \qquad\qquad (A.4)$$

From (A.3), Equation (A.4) implies

$$L_i = L(r^2) \, r_i \quad . \qquad\qquad (A.5)$$

Note that the arbitrary function, L , defines the linear
first-order isotropic form, and is an even function of "r."

Now, consider the <u>linear axisymmetric form</u>. The
governing general expression is

$$\mathscr{L}\ (\underset{\sim}{r},\underset{\sim}{a},\underset{\sim}{\lambda})\ \equiv\ L_i\ a_i \quad . \tag{A.6}$$

A general algebraic form for L_i is sought with $\mathscr{L}$ depending,
at most, on the following invariants:

$$\underset{\sim}{r}\cdot\underset{\sim}{r} = r^2, \quad \underset{\sim}{a}\cdot\underset{\sim}{a} = 1, \quad \underset{\sim}{\lambda}\cdot\underset{\sim}{\lambda} = 1, \quad \underset{\sim}{r}\cdot\underset{\sim}{a} \equiv r_i a_i, \quad \underset{\sim}{r}\cdot\underset{\sim}{\lambda} \equiv r_i\lambda_i, \quad \underset{\sim}{a}\cdot\underset{\sim}{\lambda} \equiv 1$$

while being linear and homogeneous in a_i. Thus, Equation
(A.6) rewrites as

$$\mathscr{L}\ (\underset{\sim}{r},\underset{\sim}{a},\underset{\sim}{\lambda})\ =\ M\ (r^2,\ r_i\lambda_i)\ (\underset{\sim}{r}\cdot\underset{\sim}{a})\ +\ N\ (r^2,\ r_i\lambda_i)\ (\underset{\sim}{\lambda}\cdot\underset{\sim}{a})$$

$$\tag{A.7}$$

- A5 -

which requires

$$L_i = M(r^2, r_i\lambda_i)\, r_i + N(r^2, r_i\lambda_i)\, \lambda_i \qquad . \qquad (A.8)$$

Here "M" and "N" are arbitrary scalar functions governing the linear, axisymmetric form, $\mathcal{L}(\underset{\sim}{r}, \underset{\sim}{a}, \underset{\sim}{\lambda})$. With this and Equation (A.1) in mind, the <u>axisymmetric</u> <u>bilinear</u> <u>form</u> can be considered as

$$\mathcal{B}(\underset{\sim}{r}, \underset{\sim}{a}, \underset{\sim}{b}, \underset{\sim}{\lambda}) \equiv C_{ij}\, a_i b_j \qquad . \qquad (A.9)$$

Equation (A.9) may be interpretted as

$$
C(\underset{\sim}{r},\underset{\sim}{a},\underset{\sim}{b},\underset{\sim}{\lambda}) = \begin{bmatrix} a_1 & a_2 & a_3 \end{bmatrix} \begin{bmatrix} C_{11} & C_{12} & C_{13} \\ C_{21} & C_{22} & C_{23} \\ C_{31} & C_{32} & C_{33} \end{bmatrix} \begin{Bmatrix} b_1 \\ b_2 \\ b_3 \end{Bmatrix} \; .
$$

$$(A.10)$$

Invariant theory demands the general form of C_{ij} depends at most on the following invariants:

$$
\underset{\sim}{r} \cdot \underset{\sim}{r} = r^2, \quad \underset{\sim}{a} \cdot \underset{\sim}{a} = 1, \quad \underset{\sim}{b} \cdot \underset{\sim}{b} = 1, \quad \underset{\sim}{\lambda} \cdot \underset{\sim}{\lambda} = 1, \quad \underset{\sim}{r} \cdot \underset{\sim}{a} \equiv r_i a_i,
$$

$$
\underset{\sim}{r} \cdot \underset{\sim}{b} = r_i b_i, \quad \underset{\sim}{r} \cdot \underset{\sim}{\lambda} \equiv \beta r, \quad \underset{\sim}{a} \cdot \underset{\sim}{\lambda} \equiv 1, \quad \underset{\sim}{a} \cdot \underset{\sim}{b} = 1, \quad \text{and} \quad \underset{\sim}{b} \cdot \underset{\sim}{\lambda} = b_i \lambda_i \quad ,
$$

and that C_{ij} is homogeneous in $a_i b_j$. The most general invariant expression for $\mathcal{E}(\underset{\sim}{r},\underset{\sim}{a},\underset{\sim}{b},\underset{\sim}{\lambda})$ is therefore

$$\mathcal{B}(\underset{\sim}{r},\underset{\sim}{a},\underset{\sim}{b},\underset{\sim}{\lambda}) = A(r_r^2 \; \beta r) \; (\underset{\sim}{r}\cdot\underset{\sim}{a})(\underset{\sim}{r}\cdot\underset{\sim}{b}) + B(r_r^2 \; \beta r) \; (\underset{\sim}{a}\cdot\underset{\sim}{b}) +$$

$$C(r_r^2 \; \beta r) \; (\underset{\sim}{a}\cdot\underset{\sim}{\lambda}) \; (\underset{\sim}{b}\cdot\underset{\sim}{\lambda}) +$$

$$D(r_r^2 \; \beta r) \; (\underset{\sim}{r}\cdot\underset{\sim}{b}) \; (\underset{\sim}{b}\cdot\underset{\sim}{\lambda}) +$$

$$E(r_r^2 \; \beta r) \; (\underset{\sim}{r}\cdot\underset{\sim}{a}) \; (\underset{\sim}{b}\cdot\underset{\sim}{\lambda}) \; . \quad \quad (A.11)$$

Since $\mathcal{B}(\underset{\sim}{r},\underset{\sim}{a},\underset{\sim}{b},\underset{\sim}{\lambda}) = C_{ij} \; a_i b_j$, Equation (A.11) requires

$$C_{ij} \; a_i b_j = A(r_r^2 \; \beta r) \; r_i r_j a_i b_j + B(r_r^2 \; \beta r) \; \delta_{ij} \; a_i b_j +$$

$$C(r_r^2 \; \beta r) \; \lambda_i \lambda_j \; a_i b_j +$$

$$D(r_r^2 \; \beta r) \; \lambda_i r_j \; a_i b_j +$$

$$E(r_r^2 \; \beta r) \; \lambda_j r_i \; a_i b_j \; , \quad \quad (A.12)$$

where δ_{ij} is the Kronecker delta tensor. From Equation
(A.12), the resulting second-order axisymmetric tensor is

$$C_{ij} = \left\{ A\, r_i r_j + B\, \delta_{ij} \right\} + \left\{ C\, \lambda_i \lambda_j + D\, \lambda_i r_j + E\, \lambda_j r_i \right\} \; .$$

(A.13)

This expression for the C_{ij} can now be used to evaluate the specific tensor entries of Equation (A.10) by substituting specific i,j values.

It is now noted that $\mathcal{E}(\underset{\sim}{r}, \cdots) = \mathcal{E}(-\underset{\sim}{r}, \cdots)$ by inspection of Figure A2. The upshot is that arbitrary functions A, B, and C are even functions of r^2 and $(\beta r)^2$, or

$$D(-r) = -E(r) \quad \text{and} \quad E(-r) = -D(r) \qquad (A.14)$$

— a fact which implies "D" and "E" are identical and odd functions of βr.[A3] It immediately follows that Equation (A.13) can be rewritten as

- A9 -
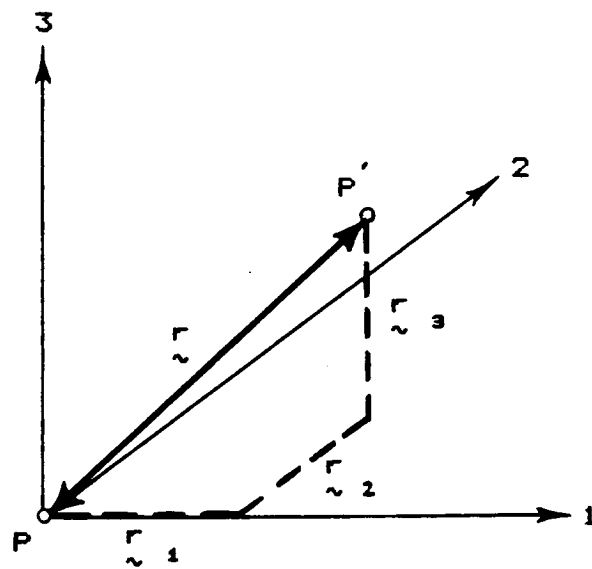
Figure A2 : Geometric Argument that the Correlation Between
P and P′ is the Same As that Between P′ and P

$$C_{ij} = \left\{ A\, r_i r_j + B\, \delta_{ij} \right\} + \left\{ C\, \lambda_i \lambda_j + D\, (\, \lambda_i r_j + \lambda_j r_i \,) \right\} .$$

$$(A.15)$$

A1 Kármán, Theodore von and Leslie Howarth, "On the Statistical Theory of Isotropic Turbulence," *Proceedings of the Royal Society (Series A)*, Vol. 164, 1937, pp. 192-215.

A2 Robertson, H.P., "Invariant Theory of Isotropic Turbulence," *Proceedings of the Cambridge Philosophical Society*, Vol. 36, 1940, pp. 209-233.

A3 Batchelor, G.K., "Theory of Axisymmetric Turbulence," *Proceedings of the Royal Society (Series A)*, Vol. 186, 1946, pp. 480-502.

APPENDIX B   EVALUATION OF THE ARBITRARY FUNCTIONS
FOR ISOTROPIC TURBULENCE

Recall that the tensor defining the correlation between two points in an isotropic turbulence field is given by

$$C_{ij}(\underset{\sim}{r},t) \equiv < u_i(\underset{\sim}{x},t)\, u_j(\underset{\sim}{x}+\underset{\sim}{r},t) > \quad . \qquad (B.1)$$

From invariant theory, Equation (B.1) may also be written as

$$C_{ij}(\underset{\sim}{r},t) = A\, r_i r_j + B\, \delta_{ij} \quad , \qquad (B.2)$$

where "A" and "B" are arbitrary scalar functions.

The standard method by which isotropic turbulence is generated in a laboratory environment is shown in Figure B1. Intuition and experimental evidence indicate that turbulent velocity measurements taken along the centerline most likely approximate the characteristics of isotropic turbulence.
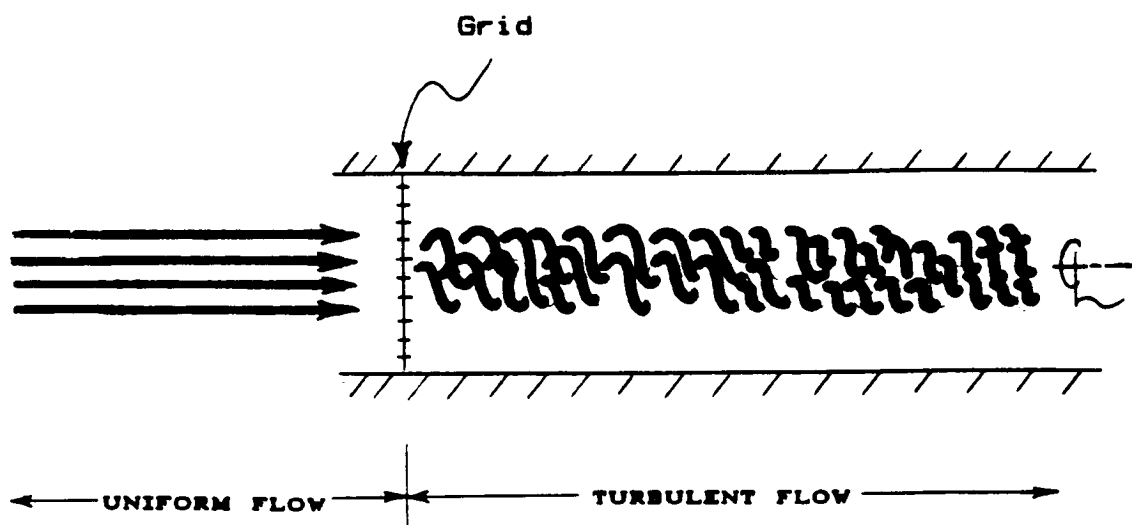
Figure B1 : Method Used to Produce Turbulence in a Wind Tunnel

Consequently, for the measurement geometry of Figure B2, component correlation functions evaluated from Equation (B.1) take the form

$$C_{uu}(\underset{\sim}{r}, t) \; = \; C_{11}(\underset{\sim}{r}, t) \; = \; A \; r^2 + B \qquad\qquad (B.3)$$

$$C_{vv}(\underset{\sim}{r}, t) \; = \; C_{22}(\underset{\sim}{r}, t) \; = \; 0 \; + \; B \qquad\qquad (B.4)$$

and

$$C_{ww}(\underset{\sim}{r}, t) \; = \; C_{33}(\underset{\sim}{r}, t) \; = \; 0 \; + \; B \qquad . \qquad (B.5)$$

Introducing definitions for the single longitudinal correlation and the two transverse correlations into Equations (B.3), (B.4), and (B.5) provides

$$A \; r^2 + B \; \equiv \; \sigma^2 f \qquad\qquad (B.6)$$

$$B \; \equiv \; \sigma^2 g \qquad\qquad (B.7)$$

$$B \; \equiv \; \sigma^2 g \qquad , \qquad (B.8)$$

- B3 -
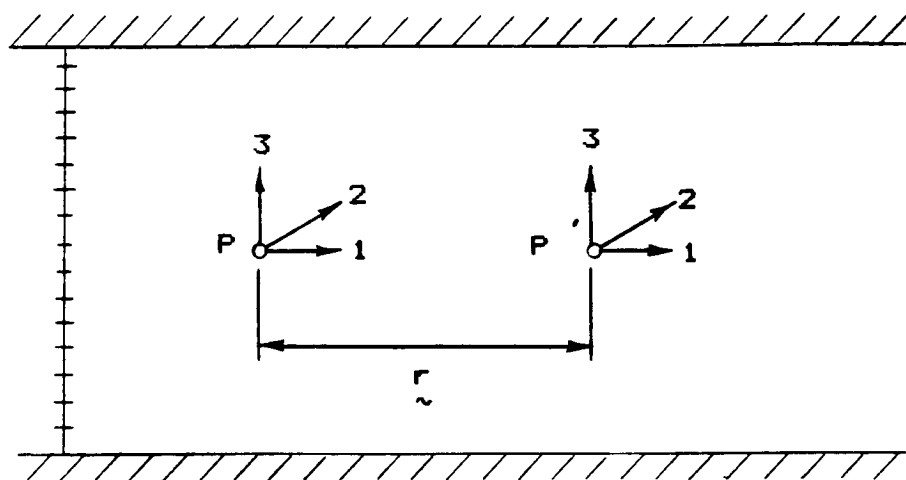
Figure B2 : Conventions for Evaluation of Turbulence
Correlation Functions

where "f" is the longitudinal correlation function for isotropic turbulence, and "g" the transverse correlation function.

Algebraic manipulation of Equations (B.6) and (B.7) yields the desired scalar equations for "A" and "B," viz.

$$A = \sigma^2 \left\{ \frac{f - g}{r^2} \right\} \quad \text{and} \quad B = \sigma^2 g \quad . \quad \text{(B.9)}$$

APPENDIX C DERIVATION OF THE DIVERGENCE OF C_{ij}

Recall that the second-order tensor for axisymmetric turbulence is written as follows :

$$C_{ij} = Ar_i r_j + B\delta_{ij} + C\lambda_i \lambda_j + D\lambda_i r_j + E\lambda_j r_i \quad . \tag{C.1}$$

Since D = E for correlation tensors with indicial symmetry, the divergence of Equation (C.1) with respect to r_j becomes

$$\frac{\partial\, C_{ij}}{\partial\, r_j} = \frac{\partial}{\partial\, r_j} \left\{ Ar_i r_j + B\delta_{ij} + C\lambda_i \lambda_j + D(\lambda_i r_j + \lambda_j r_i) \right\} \quad .$$

$$\tag{C.2}$$

The invariants which constitute the functional dependence of the arbitrary scalar functions A through D are defined as

$$\underset{\sim}{r} \cdot \underset{\sim}{r} = r_i r_i = r^2 \qquad \text{and} \qquad \underset{\sim}{r} \cdot \underset{\sim}{\lambda} = r_i \lambda_i \equiv \beta r \qquad . \quad \text{(C.3)}$$

Also of use in the evaluation of Equation (C.2) is

$$\frac{\partial}{\partial r_i} = \left(\frac{\partial r}{\partial r_i} \right) \frac{\partial}{\partial r} + \left(\frac{\partial \beta}{\partial r_i} \right) \frac{\partial}{\partial \beta} \qquad \text{(C.4)}$$

since

$$\frac{\partial \beta}{\partial r_i} = \frac{\partial \text{ (constant)}}{\partial r_i} = 0 \qquad . \qquad \text{(C.5)}$$

Equation (C.4) may be further expanded to

$$\frac{\partial}{\partial r_i} = \left(\frac{r_i}{r} \right) \frac{\partial}{\partial r} + \left(\frac{\lambda_i}{r} - \frac{\beta r_i}{r^2} \right) \frac{\partial}{\partial \beta} \qquad \text{(C.6)}$$

since

$$\frac{\partial r}{\partial r_i} = \frac{\partial (r_n r_n)^{1/2}}{\partial (r_n r_n)}$$

$$= \frac{1}{2} (r_n r_n)^{-1/2} \left[\frac{\partial r_n}{\partial r_i} r_n + r_n \frac{\partial r_n}{\partial r_i} \right]$$

$$= \frac{1}{2} (r_n r_n)^{-1/2} \left[\delta_{ni} r_n + r_n \delta_{ni} \right]$$

or

$$\frac{\partial r}{\partial r_i} = \frac{r_i}{r} \quad , \tag{C.7}$$

and, since $\partial \beta / \partial r_i = 0$,

$$\frac{\lambda_i}{r} = \frac{\beta r_i}{r^2} \quad . \tag{C.8}$$

- C3 -

Now, Equation(C.2) will be considered in separate components.

The "A" part of Equation (C.2):

$$\frac{\partial}{\partial r_j} (A r_i r_j) = \frac{\partial A}{\partial r_j} r_i r_j + A \frac{\partial r_i}{\partial r_j} r_j + A r_i \frac{\partial r_j}{\partial r_j}$$

$$= \frac{\partial A}{\partial r_j} r_i r_j + A \delta_{ij} r_j + A r_i \delta_{jj}$$

$$= \left\{ \left(\frac{r_j}{r} \frac{\partial A}{\partial r} \right) + \left(\frac{\lambda_j}{r} - \frac{\beta r_j}{r^2} \right) \frac{\partial A}{\partial \beta} \right\} r_i r_j$$

$$+ 4 A r_i$$

$$= \left\{ \frac{r_j r_j}{r} \frac{\partial A}{\partial r} + \left(\frac{\lambda_j r_j}{r} - \frac{\beta r_j r_j}{r^2} \right) \frac{\partial A}{\partial \beta} \right\} r_i$$

$$+ 4 A r_i$$

$$= \left\{ r \frac{\partial A}{\partial r} + \left(\beta - \beta \right) \frac{\partial A}{\partial \beta} + 4 A \right\} r_i$$

- C4 -

or

$$\frac{\partial}{\partial r_j} \left(A r_i r_j \right) = \left\{ r \frac{\partial A}{\partial r} + 4 A \right\} r_i \quad . \qquad (C.9)$$

The "B" part of Equation (C.2):

$$\frac{\partial}{\partial r_j} \left(B \delta_{ij} \right) = \delta_{ij} \left[\frac{\partial B}{\partial r_j} \right]$$

$$= \left\{ \frac{r_j}{r} \frac{\partial B}{\partial r} + \left(\frac{\lambda_j}{r} - \frac{\beta r_j}{r^2} \right) \frac{\partial B}{\partial \beta} \right\} \delta_{ij}$$

$$= \left\{ \frac{r_j}{r} \delta_{ij} \frac{\partial B}{\partial r} + \frac{\lambda_j}{r} \delta_{ij} - \frac{\beta r_j \delta_{ij}}{r^2} \right\} \frac{\partial B}{\partial \beta}$$

or

$$\frac{\partial}{\partial r_j} \left(B \, \delta_{ij} \right) = \left\{ \frac{1}{r} \frac{\partial B}{\partial r} - \frac{\beta}{r^2} \frac{\partial B}{\partial \beta} \right\} r_i +$$

$$\left\{ \frac{1}{r} \frac{\partial B}{\partial \beta} \right\} \lambda_i \quad . \quad \text{(C.10)}$$

The "C" part of Equation (C.2):

$$\frac{\partial}{\partial r_j} (C \lambda_i \lambda_j) = \frac{\partial C}{\partial r_j} \lambda_i \lambda_j + C \frac{\partial \lambda_i}{\partial r_j} \lambda_j + C \lambda_i \frac{\partial \lambda_j}{\partial r_j}$$

$$= \frac{\partial C}{\partial r_j} \lambda_i \lambda_j$$

$$= \left\{ \frac{r_j}{r} \frac{\partial C}{\partial r} + \left(\frac{\lambda_j}{r} - \frac{\beta r_j}{r^2} \right) \frac{\partial C}{\partial \beta} \right\} \lambda_i \lambda_j$$

$$= \left\{ \frac{r_j \lambda_j}{r} \frac{\partial C}{\partial r} + \left(\frac{\lambda_j \lambda_j}{r} - \frac{\beta r_j \lambda_j}{r^2} \right) \frac{\partial C}{\partial \beta} \right\} \lambda_i$$

$$= \left\{ \frac{\beta r}{r} \frac{\partial C}{\partial r} + \left(\frac{1}{r} - \frac{\beta^2 r}{r^2} \right) \frac{\partial C}{\partial \beta} \right\} \lambda_i$$

or

$$\frac{\partial}{\partial r_j} (C \lambda_i \lambda_j) = \left\{ \beta \frac{\partial C}{\partial r} + \left(\frac{1 - \beta^2}{r} \right) \frac{\partial C}{\partial \beta} \right\} \lambda_i \quad .$$

(C.11)

- C7 -

The "D" part of Equation (C.2):

$$\frac{\partial \left(D\lambda_i r_j + D\lambda_j r_i \right)}{\partial r_j} =$$

$$= \left\{ \frac{\partial D}{\partial r_j} \lambda_i r_j + D \frac{\partial \lambda_i}{\partial r_j} r_j + D\lambda_i \frac{\partial r_j}{\partial r_j} \right\}$$

$$+ \left\{ \frac{\partial D}{\partial r_j} \lambda_j r_i + D \frac{\partial \lambda_j}{\partial r_j} r_i + D\lambda_j \frac{\partial r_i}{\partial r_j} \right\}$$

$$= \left\{ \frac{\partial D}{\partial r_j} \lambda_i r_j + 3D\lambda_i \right\} + \left\{ \frac{\partial D}{\partial r_j} \lambda_j r_i + D\lambda_i \right\}$$

$$= \left\{ \left[\frac{r_j}{r} \frac{\partial D}{\partial r} + \left(\frac{\lambda_j}{r} - \frac{\beta r_j}{r^2} \right) \frac{\partial D}{\partial \beta} \right] \lambda_i r_j + 3D\lambda_i \right\}$$

$$+ \left\{ \left[\frac{r_j}{r} \frac{\partial D}{\partial r} + \left(\frac{\lambda_j}{r} - \frac{\beta r_j}{r^2} \right) \frac{\partial D}{\partial \beta} \right] \lambda_j r_i + D\lambda_i \right\}$$

which algebraically reduces to

$$\frac{\partial \left(D\lambda_i r_j + D\lambda_j r_i \right)}{\partial r_j} = \left\{ r\,\frac{\partial D}{\partial r} + 4D \right\} \lambda_i +$$

$$\left\{ \beta\,\frac{\partial D}{\partial r} + \left(\frac{1 - \beta^2}{r} \right) \frac{\partial D}{\partial \beta} \right\} r_i \ . \qquad (C.12)$$

Combining r_i and λ_i terms from Equations (C.9) - (C.12) yields

$$\frac{\partial C_{ij}}{\partial r_j} = \left\{ r\,\frac{\partial A}{\partial r} + 4A + \left\{ \frac{1}{r}\,\frac{\partial B}{\partial r} - \frac{\beta}{r^2}\,\frac{\partial B}{\partial \beta} \right\} \right.$$

$$\left. + \ \beta\,\frac{\partial D}{\partial r} + \left(\frac{1 - \beta^2}{r} \right) \frac{\partial D}{\partial \beta} \right\} r_i \quad +$$

$$\left\{ \frac{1}{r}\,\frac{\partial B}{\partial \beta} + \beta\,\frac{\partial C}{\partial r} + \left(\frac{1 - \beta^2}{r} \right) \frac{\partial C}{\partial \beta} + r\,\frac{\partial D}{\partial r} + 4D \right\} \lambda_i$$

$$(C.13)$$

- a result which matches Equation (2.13) of Reference C1 for D = E.

It is important to note that if $\beta = 0$ and $\underset{\sim}{\lambda} = \{ 0, 0, 0 \}$, Equation (C.13) readily becomes the governing isotropic equation.[C2]

For conciseness, Equation (C.13) will now be written as

$$\frac{\partial C_{ij}}{\partial r_j} = (\text{-----} \mathbb{R} \text{-----})r_i + (\text{-----} \mathbb{S} \text{-----})\lambda_i \quad .$$

(C.14)

Since Kármán and Howarth[C2] have shown that C_{ij} is a solenoidal tensor (i.e., one with a vanishing divergence with respect to one of its indicies), Equation (C.14) becomes

$$(\text{-----} \mathbb{R} \text{-----})r_i = 0$$
(C.15)

and

$$(\text{-----} S \text{-----})\lambda_i = 0 \qquad\qquad (C.16)$$

since r_i can take on an infinite number of values for
constant values of r, β, and λ_i . Equation (C.15) thereby
provides constraints on the mathematical relationships
between the arbitrary functions which make up the
correlation tensor for axisymmetric turbulence.

(··············· APPENDIX C REFERENCES ···············)

[C1]Batchelor, G.K., "Theory of Axisymmetric Turbulence,"
Proceedings of the Royal Society (Series A), Vol. 186, 1946, pp.
480- 502.

[C2]Kármán, Theodore von and Leslie Howarth, "On the
Statistical Theory of Isotropic Turbulence," *Proceedings of the
Royal Society (Series A)*, Vol. 164, 1937, pp.
192-215.

The two-point velocity correlation technique is a method in which the statistical relationship between velocities at two points in a turbulent fluid is defined (reference Figure A1). As stated in the text, the governing equation for the turbulent flow is the Navier-Stokes equation. Steady-state, high Reynolds number turbulence with ignored pressure gradients at point P (cf. Figure A1) is therefore governed by

$$\frac{\partial\,(\,U_i\,U_m\,)}{\partial\,x_m} \cong 0 \quad . \tag{D.1}$$

Since the total flow may be considered to be composed of the linear combination of an underlying mean and a superimposed fluctuating component, it readily follows that Equation (D.1) can be rewritten as

$$\frac{\partial}{\partial\,x_m}\left\{\,(\,\overline{U}_i + u_i\,)\,(\,\overline{U}_m + u_m\,)\,\right\} \cong 0 \tag{D.2}$$

where $\overline{(\cdot)}$ denotes a mean value of $(\cdot)$. Expanding Equation (D.2) then gives

$$\frac{\partial}{\partial x_m} \left\{ \overline{U}_i \overline{U}_m + u_i \overline{U}_m + u_m \overline{U}_i + u_i u_m \right\} \cong 0 \quad . \quad \text{(D.3)}$$

Invoking mass conservation in the term-by-term analysis of Equation (D.3) yields

$$\frac{\partial}{\partial x_m} \left\{ \overline{U}_i \overline{U}_m \right\} = U_i \frac{\partial \overline{U}_m}{\partial x_m} + U_m \frac{\partial \overline{U}_i}{\partial x_m} = U_m \frac{\partial \overline{U}_i}{\partial x_m} \quad \text{(D.4)}$$

$$\frac{\partial}{\partial x_m} \left\{ u_i \overline{U}_m \right\} = u_i \frac{\partial \overline{U}_m}{\partial x_m} + \overline{U}_m \frac{\partial u_i}{\partial x_m} = \overline{U}_m \frac{\partial u_i}{\partial x_m} \quad \text{(D.5)}$$

$$\frac{\partial}{\partial x_m} \left\{ u_m \overline{U}_i \right\} = u_m \frac{\partial \overline{U}_i}{\partial x_m} + \overline{U}_i \frac{\partial u_m}{\partial x_m} = u_m \frac{\partial \overline{U}_i}{\partial x_m} \quad \text{(D.6)}$$

Equation (D.3) can accordingly be restated as

$$\overline{U}_m \frac{\partial \overline{U}_i}{\partial x_m} + \overline{U}_m \frac{\partial u_i}{\partial x_m} + u_m \frac{\partial \overline{U}_i}{\partial x_m} + \frac{\partial (u_i u_m)}{\partial x_m} \cong 0 \ .$$

<div align="right">(D.7)</div>

Navier-Stokes is then applied at point P':

$$\frac{\partial (U_j{}' U_m{}')}{\partial x_m{}'} \cong 0 \quad , \qquad \text{(D.8)}$$

where $(\cdot\cdot)'$ indicates a reference to the primed point in the correlation. Similarly, the expanded version of Equation (D.8) becomes

$$\overline{U}_m{}' \frac{\partial \overline{U}_j{}'}{\partial x_m{}'} + \overline{U}_m{}' \frac{\partial u_j{}'}{\partial x_m{}'} + u_m{}' \frac{\partial \overline{U}_j{}'}{\partial x_m{}'} + \frac{\partial (u_j{}' u_m{}')}{\partial x_m{}'} \cong 0 \ .$$

<div align="right">(D.9)</div>

The method of two-point correlation is implemented by multiplying Equation (D.7) by the jth velocity component at point P' (i.e., u_j'), and stochastic averaging the result. Likewise, Equation (D.9) is multiplied by u_i, and stochastic averaged. Then the results of the separate operations are added.

The first step in the correlation technique yields

$$< u_j' \; \overline{U}_m \; \frac{\partial \overline{U}_i}{\partial x_m} > + < u_j' \; \overline{U}_m \; \frac{\partial u_i}{\partial x_m} > + < u_j' \; u_m \; \frac{\partial \overline{U}_i}{\partial x_m} > +$$

$$< u_j' \; \frac{\partial (u_i u_m)}{\partial x_m} > \cong 0 \; . \qquad (D.10)$$

Each stochastic-averaged term of Equation (D.10) is then considered individually, and the concept of a "mean" variable is invoked:

$$< u_j' \; \overline{U}_m \; \frac{\partial \overline{U}_i}{\partial x_m} > = \overline{U}_m \; \frac{\partial \overline{U}_i}{\partial x_m} < u_j' > \equiv 0 \qquad (D.11)$$

$$\left\langle u_j' \, \bar{U}_m \, \frac{\partial u_i}{\partial x_m} \right\rangle = \bar{U}_m \left\langle u_j' \, \frac{\partial u_i}{\partial x_m} \right\rangle \qquad (D.12)$$

$$\left\langle u_j' \, u_m \, \frac{\partial \bar{U}_i}{\partial x_m} \right\rangle = \frac{\partial \bar{U}_i}{\partial x_m} \left\langle u_j' \, u_m \right\rangle \qquad (D.13)$$

$$\left\langle u_j' \, \frac{\partial (u_i u_m)}{\partial x_m} \right\rangle = \frac{\partial}{\partial x_m} \left\langle u_i u_m u_j' \right\rangle \qquad . \qquad (D.14)$$

Equation (D.7) accordingly simplifies to

$$\bar{U}_m \left\langle u_j' \, \frac{\partial u_i}{\partial x_m} \right\rangle + \frac{\partial \bar{U}_i}{\partial x_m} \left\langle u_j' \, u_m \right\rangle + \frac{\partial}{\partial x_m} \left\langle u_i u_m u_j' \right\rangle \cong 0.$$

$$(D.15)$$

Similarly, the equation for the primed point becomes

- D5 -

$$< u_i \, \overline{U}_m \, \frac{\partial \, \overline{U}_j{}'}{\partial \, x_m{}'} > + < u_i \, \overline{U}_m{}' \, \frac{\partial \, u_j{}'}{\partial \, x_m{}'} > + < u_i \, u_m{}' \, \frac{\partial \, \overline{U}_j{}'}{\partial \, x_m} > +$$

$$< u_i \, \frac{\partial \, (\, u_j{}' u_m{}' \,)}{\partial \, x_m{}'} > \, \cong \, 0 \qquad (D.16)$$

which, like the unprimed equation, can be rewritten:

$$\overline{U}_m{}' \, <u_i \, \frac{\partial \, u_j{}'}{\partial \, x_m{}'}> + \frac{\partial \, \overline{U}_j{}'}{\partial \, x_m{}'} \, <u_i u_m{}'> + \frac{\partial}{\partial \, x_m{}'} \, <u_j{}' u_m{}' \, u_i> \, \cong \, 0 \, .$$

$$(D\,.17)$$

Addition of Equations (D.15) and (D.17) yields the desired result:

$$\overline{U}_m < u_j' \frac{\partial u_i}{\partial x_m} > + \frac{\partial \overline{U}_i}{\partial x_m} < u_j' u_m > + \frac{\partial}{\partial x_m} < u_i u_m u_j' > +$$

$$\overline{U}_m' < u_i \frac{\partial u_j'}{\partial x_m'} > + \frac{\partial \overline{U}_j'}{\partial x_m'} < u_i u_m' > + \frac{\partial}{\partial x_m'} < u_j' u_m' u_i > \cong 0$$

$$(D.18)$$

- a description of the interaction between the velocity at one point with another in a turbulent flow field.

APPENDIX E   DERIVATION OF THE TURBULENT DOWNWASH PSD

The one-dimensional psd for the modelled downwash turbulence is defined as

$$\Phi_{ww}(t,k) = \int_{-\infty}^{\infty} < w(\underset{\sim}{x},t)w(\underset{\sim}{x}+\underset{\sim}{r},t) > e^{-\iota kr} dr \quad . \quad (E.1)$$

Substituting the autocorrelation of Equation (3.17) yields

$$\Phi_{ww}(t,k) = \int_{-\infty}^{\infty} \left\{ \sigma^2 g + a|r| + b \right\} e^{-\iota kr} dr \quad . \quad (E.2)$$

Noting the even nature of the autocorrelation gives

$$\Phi_{ww}(t,k) = 2 \int_{-\infty}^{\infty} \left\{ \sigma^2 g + a|r| + b \right\} \cos(kr) dr \quad . \quad (E.3)$$

- E1 -

C-3

From inspection of (E.3), it follows that

$$\Phi_{ww}^{(i)}(t,k) \equiv 2 \int_{-\infty}^{\infty} \sigma^2 g \, \cos(kr) \, dr \qquad (E.4)$$

and

$$\Phi_{ww}^{(a)}(t,k) \equiv 2 \int_{-\infty}^{\infty} \left\{ a|r| + b \right\} \cos(kr) \, dr \qquad . \qquad (E.5)$$

i)   <u>The Isotropic Psd</u>

First, the isotropic psd will be considered. A functional representation of the transverse correlation function, g, is required. Appendix F provides such a relation, viz.

$$g = f + \frac{1}{2} r \frac{\partial f}{\partial r} \qquad . \qquad (E.6)$$

- E2 -

The longitudinal correlation function, f, can be reasonably approximated by the Dryden exponential form

$$f(r,t) \cong e^{-|r|/\Lambda(t)} \quad .$$

Use of this formulation in Equation (E.6), and subsequent substitution of the result into Equation (E.4) yields

$$\Phi_{ww}^{(i)}(t,k) = 2\sigma^2 \int_0^\infty e^{-|r|/\Lambda} \cos(kr)\, dr -$$

$$\frac{\sigma^2}{\Lambda} \int_0^\infty r\, e^{-|r|/\Lambda} \cos(kr)\, dr \qquad (E.7)$$

Letting $\theta \equiv \dfrac{r}{\Lambda}$ and $\varkappa \equiv k\Lambda$, allows (E.7) to be rewritten as

$$\Phi_{WW}^{(i)}(t,\varkappa) = 2\sigma^2\Lambda \int_0^\infty e^{-\theta}\cos(\varkappa\theta) \ d\theta - \sigma^2\Lambda \int_0^\infty \theta \ e^{-\theta}\cos(\varkappa\theta) \ d\theta \quad .$$

(E.8)

Equation (E.8) integrates to

$$\Phi_{WW}^{(i)}(t,k) = 2\sigma^2\Lambda \left[\frac{1}{1 + \varkappa^2} \right] - \sigma^2\Lambda \left[\frac{1 - \varkappa^2}{(1 + \varkappa^2)^2} \right] \quad .$$

(E.9)

Combining the terms of (E.9) yields the Dryden psd, namely

$$\Phi_{WW}^{(i)}(t,\varkappa) \equiv \sigma^2\Lambda \ \frac{1 + 3\varkappa^2}{(1 + \varkappa^2)^2} \quad .$$
(E.10)

ii) The Anisotropic Psd

Consideration of the anisotropic psd first requires the definition:

$$\int_0^{\infty} (\, a|r| \, + \, b \,) \, dr \equiv \sigma^2 \, \Delta\Lambda(t) \qquad . \qquad (E.11)$$

It follows from Figure E1 - the graphical interpretation of Equation (E.11) - that

$$\sigma^2 \, \Delta\Lambda(t) \; = \; \frac{b^2}{2 \, a} \qquad . \qquad (E.12)$$

Consequently, the anisotropic psd takes the form

$$\Phi_{ww}^{(a)}(t,\varkappa) \; \equiv \; 2 \int_{-\infty}^{\infty} \left\{ - \, a \, r \, + \, b \right\} \cos \frac{\varkappa \, r}{\Lambda} \; dr \qquad (E.13)$$

- E5 -
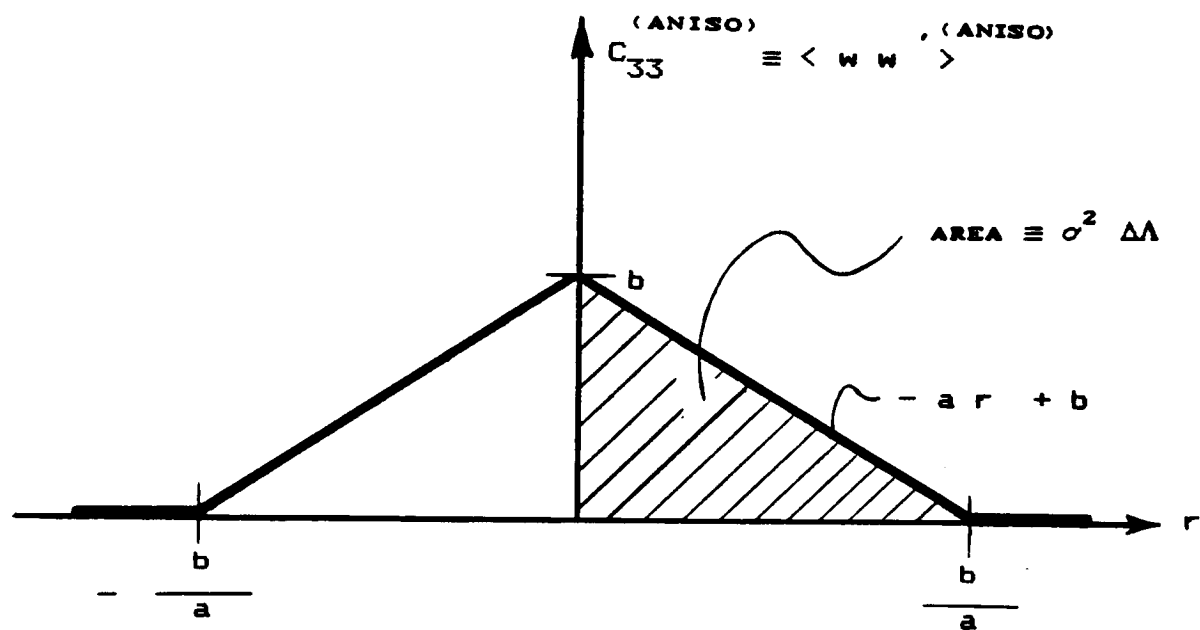
Figure E1 : Definition of $\Delta\Lambda$ from the Anisotropic Component
of the Downwash Autocorrelation Function , C_{33}

since the anisotropic correlation is an even function of
domain { $0 \leq r \leq b/a$ }. Multiplying Equation (E.13) by
Λ/Λ, and recalling that $\varkappa = k\Lambda$ and $\theta \equiv r/\Lambda$ gives

$$\Phi_{WW}^{(a)}(t,\varkappa) = 2\Lambda \int_{0}^{\frac{b}{a\,\Lambda}} \left\{ - a\,r + b \right\} \cos(\varkappa\theta)\, d\theta$$

$$= 2\Lambda \left\{ \int_{0}^{\frac{b}{a\,\Lambda}} - a\Lambda\theta\, \cos(\varkappa\theta)\, d\theta + \int_{0}^{\frac{b}{a\,\Lambda}} b\, \cos(\varkappa\theta)\, d\theta \right\}$$

$$= -2a\Lambda^2 \int_{0}^{\frac{b}{a\,\Lambda}} \theta\, \cos(\varkappa\theta)\, d\theta + \frac{2\Lambda b}{\varkappa} \left[\sin(\varkappa\theta) \right]_{0}^{\frac{b}{a\,\Lambda}}$$

(E.14)

Equation (E.14) integrates by parts to

- E7 -

$$\Phi_{WW}^{(a)}(t,\varkappa) = -2a\Lambda^2 \left[\frac{\theta}{\varkappa} \sin(\varkappa\theta) \Bigg|_0^{\frac{b}{a\,\Lambda}} - \int_0^{\frac{b}{a\,\Lambda}} \frac{1}{\varkappa} \sin(\varkappa\theta)\, d\theta \right]$$

$$+ \quad \frac{2\Lambda b}{\varkappa} \quad \sin \frac{\varkappa b}{a\Lambda}$$

or

$$\Phi_{WW}^{(a)}(t,\varkappa) = \frac{2a\Lambda^2}{\varkappa^2} \quad \frac{1 - \cos(\frac{\varkappa b}{a\Lambda})}{(\frac{\varkappa b}{a\Lambda})^2} \qquad (E.15)$$

Multiplication of Equation (E.15) by $\left[\frac{b}{a\Lambda}\right]^2 \Big/ \left[\frac{b}{a\Lambda}\right]^2$ yields

$$\Phi_{WW}^{(a)}(t,\varkappa) \;=\; \frac{2b^2}{a}\;\frac{1 - \cos(\frac{\varkappa b}{a\Lambda})}{(\frac{\varkappa b}{a\Lambda})^2} \quad , \qquad (E.16)$$

which, with Equation (E.12), gives

$$\Phi_{WW}^{(a)}(t,\varkappa) \;=\; \frac{2(2a\sigma^2\Lambda)}{a}\;\frac{1 - \cos(\frac{\varkappa b}{a\Lambda})}{(\frac{\varkappa b}{a\Lambda})^2}$$

which can be rewritten as

$$\Phi_{WW}^{(a)}(t,\varkappa) \;\equiv\; 4\sigma^2\Lambda\left[\frac{\Delta\Lambda}{\Lambda}\right]\;\frac{1 - \cos(\frac{\varkappa b}{a\Lambda})}{(\frac{\varkappa b}{a\Lambda})^2} \qquad (E.17)$$

- the time-dependent anisotropic power spectral density of the downwash turbulence sensed by the aircraft in low-altitude flight through a wind shear.

Recall that

$$C_{ij}(\underset{\sim}{r},t) = A(\underset{\sim}{r},t)\ r_i r_j\ +\ B(\underset{\sim}{r},t)\ \delta_{ij}\quad,\qquad (F.1)$$

and that isotropy demands symmetry in the indices of the second-order correlation tensor. Consequently, continuity imposes

$$\frac{\partial\ C_{ij}}{\partial\ r_j}\ =\ \frac{\partial\ C_{ij}}{\partial\ r_i}\ =\ 0\quad. \qquad (F.2)$$

Substitution of Equation (F.1) into Equation (F.2) yields

$$\frac{\partial\ (\ A\ r_i r_j\ )}{\partial\ r_i}\ +\ \frac{\partial\ (\ B\ \delta_{ij}\ )}{\partial\ r_i}\ =\ 0\quad. \qquad (F.3)$$

Equation (F.3) will now be considered in components. First, the "A" part will be considered. The chain rule of differentiation demands

$$\frac{\partial\,(\,A\,r_i r_j\,)}{\partial\,r_i} = \frac{\partial\,A}{\partial\,r_i}\,r_i r_j + A\,\frac{\partial\,r_i}{\partial\,r_i}\,r_j + A\,r_i\,\frac{\partial\,r_j}{\partial\,r_i}$$

$$= \frac{\partial\,A}{\partial\,r_i}\,r_i r_j + A\,\delta_{ii}\,r_j + A\,r_i\,\delta_{ij}$$

$$= \frac{\partial\,A}{\partial\,r_i}\,r_i r_j + 3\,A\,r_j + A\,r_j$$

$$= \left[\,\frac{\partial\,r}{\partial\,r_i}\,\frac{\partial\,A}{\partial\,r}\,\right]\,r_i r_j + 4\,A\,r_j$$

$$= \left[\,\frac{r_i}{r}\,\frac{\partial\,A}{\partial\,r}\,\right]\,r_i r_j + 4\,A\,r_j$$

$$= \frac{r_i^2}{r}\,\frac{\partial\,A}{\partial\,r}\,r_j + 4\,A\,r_j$$

or

$$\frac{\partial \, (\, A \, r_i r_j \,)}{\partial \, r_i} \; = \; \left[\; r \, \frac{\partial \, A}{\partial \, r} \; + \; 4 \, A \; \right] r_j \qquad . \qquad \text{(F.4)}$$

Similarly, for the "B" part:

$$\frac{\partial \, (\, B \, \delta_{ij} \,)}{\partial \, r_i} \; = \; \delta_{ij} \, \frac{\partial \, B}{\partial \, r_i}$$

$$= \; \left[\; \frac{\partial \, r}{\partial \, r_i} \, \frac{\partial \, B}{\partial \, r} \; \right] \delta_{ij}$$

$$= \; \frac{r_i}{r} \, \frac{\partial \, B}{\partial \, r} \, \delta_{ij}$$

or

$$\frac{\partial \left(B \, \delta_{ij} \right)}{\partial r_i} = \frac{1}{r} \, \frac{\partial B}{\partial r} \, r_j \quad . \qquad (F.5)$$

Hence, Equation (F.3) rewrites as

$$\left\{ 4 A + r \, \frac{\partial A}{\partial r} + \frac{1}{r} \, \frac{\partial B}{\partial r} \right\} r_j = 0 \quad . \qquad (F.6)$$

Since Equation (F.6) must be satisfied for any arbitrary values of "r," it follows that

$$4 A + r \, \frac{\partial A}{\partial r} + \frac{1}{r} \, \frac{\partial B}{\partial r} = 0 \quad . \qquad (F.7)$$

Furthermore, work done in Appendix B has shown the following:

$$A \equiv \frac{\sigma^2 (f - g)}{r^2} \qquad \text{and} \qquad B \equiv \sigma^2 g \quad ,$$

therefore Equation (F.7) becomes

$$4 \frac{\sigma^2 (f - g)}{r^2} + r \frac{\partial}{\partial r} \left\{ \frac{\sigma^2 (f - g)}{r^2} \right\} + \frac{1}{r} \frac{\partial (\sigma^2 g)}{\partial r} = 0.$$

$$(F.8)$$

Collecting terms and differentiating Equation (F.8) yields the desired result, viz.

$$g = f + \frac{r}{2} \frac{\partial f}{\partial r} \quad . \qquad\qquad (F.9)$$

```
*
      REAL  RATIO,PI,PARAM,INC,K,D,A,IC,DELTA,F,ITR,ATR,TOT,G
      INTEGER I,J,ANSWER
      CHARACTER*16 FILE 1, FILE 2, FILE 3
*
*     ***********************************************************
*     *  AIRCRAFT RESPONSE POWER SPECTRUMS AND COMPONENTS       *
*     ***********************************************************
*     *                                                         *
*     *              MASTER'S THESIS SUPPLEMENT                 *
*     *              FOR NASA - LANGLEY RESEARCH                *
*     *                                                         *
*     *                 TONY R. LAITURI                         *
*     *                                                         *
*     *                                                         *
*     *            **** PROGRAM DESCRIPTION ***                 *
*     *                                                         *
*     *                                                         *
*     *    FOR VARYING NON-DIMENSIONAL WAVE NUMBER, THE POWER   *
*     *    SPECTRAL RESPONSE OF AN AIRCRAFT IS CALCULATED.      *
*     *    THE USER ENTERS delta lambda/lambda, b/(a*lambda),AND*
*     *    A REASONABLE c/lambda RATIO CORRESPONDING TO AIRCRAFT*
*     *    SIZE.  FURTHERMORE, THE WAVE NUMBER RESULTS AND TOTAL*
*     *    RESULTS WILL BE PLACED IN DATA FILES FOR PLOTTING.   *
*     *    ALSO. THIS PROGRAM UTILIZES A MORE GENERAL FORM OF THE*
*     *    SEARS' FUNCTION TO ENSURE ACCURATE MODULUS VALUES OVER*
*     *    THE ENTIRE RANGE OF WAVE NUMBERS.                    *
*     *                                                         *
*     ***********************************************************
*
*
*               PRINT HEADER TO PROGRAM
*
      WRITE(*,*) ' '
      WRITE(*,*) '********************************************'
      WRITE(*,*) 'POWER SPECTRAL DENSITY ANALYSIS OF WIND-SHEAR '
      WRITE(*,*) ' '
      WRITE(*,*) '    ISO, ANISO, AND TOTAL RESPONSE          '
      WRITE(*,*) ' '
      WRITE(*,*) 'TONY R. LAITURI              NASA RESEARCH '
      WRITE(*,*) '********************************************'
*
*
*               QUERY THE PROGRAM USER
*
*
      WRITE(*,*) ' '
      WRITE(*,*) 'PLEASE ENTER KAPPA, TOT OUTPUT FILE NAME '
      READ(*,98) FILE 1
      WRITE(*,*) ' '
      WRITE(*,*) 'PLEASE KAPPA, ISO RESPONSE OUTPUT FILE NAME'
      READ(*,99) FILE 2
      WRITE(*,*) ' '
      WRITE(*,*) 'PLEASE ENTER KAPPA,ANISO RESPONSE OUTPUT FILE NAME'
      READ(*,98) FILE 3
      WRITE(*,*)
*
98    FORMAT(A)
*
      OPEN(81,FILE=FILE 1, STATUS = 'NEW')
      OPEN(82,FILE=FILE 2, STATUS = 'NEW')
      OPEN(83,FILE=FILE 3, STATUS = 'NEW')
*
```

```fortran
*
*
      WRITE(*,*) ' '
      WRITE(*,*) 'PLEASE ENTER B/A*IS'
      READ(*,*) PARAM
      WRITE(*,*) ' '
      WRITE(*,*) 'PLEASE ENTER D IS/IS'
      READ(*,*) RATIO
      WRITE(*,*) ' '
      WRITE(*,*) 'PLEASE ENTER C/IS RATIO'
      READ(*,*) G
      WRITE(*,*) ' '
*
      PI=3.141592654
*
*
*                 MAIN PROGRAM
*
*
*
*
      WRITE(*,*) ' '
      WRITE(*,*) 'FOR RATIO = ',RATIO
      WRITE(*,*) 'FOR b/aIS = ',PARAM
      WRITE(*,*) 'FOR C/IS = ',G
      WRITE(*,*) '*******************************'
      WRITE(*,*) ' '
      WRITE(*,*) '  KAPPA    DELTA     ISOTROPIC ANISOTROPIC  TOTAL'
      WRITE(*,*) '                     RESPONSE   RESPONSE    RESP'
      WRITE(*,*) '--------------------------------------------------'
      WRITE(*,*) ' '
*
      DO 10, I=1,50
          K=I*0.1
          D=K*PARAM
          A=1.0 - COS(D)
          IC=(1.0+3*K**2.)/((1.+K**2.)**2.)
          DELTA=4.0*RATIO*A/(D**2.*IC)
          Z=0.1811
          F=(Z+0.5*G*K)/(Z+(0.78447*G*K)+(1.5708*G**2.*K**2.))
          ITR=F*IC
          ATR=F*DELTA*IC
          TOT=ITR+ATR
          WRITE(*,15) K,DELTA,ITR,ATR,TOT
15    FORMAT(F6.1,3X,E10.4,3X,E10.4,3X,E10.4,3X,E10.4)
*
*
*             WRITE TO DATA FILES
*
*
          WRITE(81,*) K,TOT
          WRITE(82,*) K,ITR
          WRITE(83,*) K,ATR
*
*
10    CONTINUE
      WRITE(*,*) ' '
      WRITE(*,*) 'PROGRAM TERMINATED'
99    END
```

```
*
*          ***********************************************
*          * POWER SPECTRUMS OF ISOTROPIC AND ANISOTROPIC COMPONENTS *
*          ***********************************************
*          *                                                    *
*          *              MASTER'S THESIS SUPPLEMENT            *
*          *              FOR NASA - LANGLEY RESEARCH           *
*          *                                                    *
*          *                   TONY R. LAITURI                  *
*          *                                                    *
*          *                                                    *
*          *            ***** PROGRAM DESCRIPTION *****         *
*          *                                                    *
*          *                                                    *
*          *       THIS PROGRAM GENERATES POWER SPECTRAL VALUES *
*          *       FOR THE ISOTROPIC, ANISOTROPIC, AND THEIR SUM. *
*          *       THESE VALUES ARE PRINTED OUT FOR VALUES OF   *
*          *       KAPPA (THE NONDIMENSIONALIZED WAVE NUMBER)   *
*          *       RANGING FROM 0.1 TO 5.0 THE OUTPUT OF WHICH  *
*          *       BATCHED TO FILES DESIGNATED BY THE USER FOR  *
*          *       LATER USE (PLOTTING).                        *
*          *                                                    *
*          ***********************************************
*
           REAL RATIO,K,ISO,ANISO,SUM,PARAM,DENOM
           INTEGER  I,VALUE
           CHARACTER*16 FILE 1, FILE 2, FILE 3
*
*
           WRITE(*,*) ' '
           WRITE(*,*) '*************************************'
           WRITE(*,*) ' POWER SPECTRAL ANALYSIS PROGRAM FOR'
           WRITE(*,*) ' NASA-LANGLEY RESEARCH. T.R. LAITURI'
           WRITE(*,*) '*************************************'
           WRITE(*,*) ' '
           WRITE(*,*) ' '
*
*
*                        QUERY THE USER
*
*
           WRITE(*,*) ' '
           WRITE(*,*) 'PLEASE ENTER KAPPA-ISO PSD OUTPUT FILE'
           READ(*,2) FILE 1
           WRITE(*,*) ' '
           WRITE(*,*) 'PLEASE ENTER KAPPA-ANISO PSD OUTPUT FILE'
           READ(*,2) FILE 2
           WRITE(*,*) ' '
           WRITE(*,*) 'PLEASE ENTER KAPPA-SUM PSD OUTPUT FILE'
           READ(*,2) FILE 3
*
2          FORMAT(A)
*
           OPEN(71,FILE=FILE 1, STATUS = 'NEW')
           OPEN(72,FILE=FILE 2, STATUS = 'NEW')
           OPEN(73,FILE=FILE 3, STATUS = 'NEW')


           WRITE(*,*) ' '
5          WRITE(*,*) 'PLEASE DELTA LAMBDA/LAMBDA RATIO'
           READ(*,*) RATIO
           WRITE(*,*) ' '
           WRITE(*,*) 'PLEASE ENTER B'(a*LAMBDA)

           WRITE(*,*) ' '
*
           WRITE(*,*) 'FOR DELTA LAMDA / LAMBDA = ',RATIO
           WRITE(*,*) 'FOR b/(a*LAMBDA)        = ',PARAM
           WRITE(*,*) '*************************************'
*
           DO 10, I=1,50
                K=I*0.10
                DENOM = K*PARAM
                ISO = (1.+3.*K**2.)/((1.+K**2.0)**2.0)
                ANISO = 4.*RATIO*(1.-COS(K*PARAM))/((K*PARAM)**2.0)
                SUM = ISO + ANISO
                CHECK=PARAM*K
*
*                WRITE TO DATA FILES
*
                WRITE(71,*) K,ISO
                WRITE(72,*) K,ANISO
                WRITE(73,*) K,SUM
*
10         CONTINUE
*
90         END
```

The input/output relationship for the anisotropic contribution to the entire downwash simulation is

$$w_A(s) = H_A(s)\, n_A(s) \quad . \qquad (H.1)$$

Since H_A has been previously determined to be

$$H_A(s) = \left[\frac{a\,V^2}{\Phi_o}\right]^{1/2} \frac{1 - e^{-s\,(b/(aV))}}{s} \quad , \qquad (H.2)$$

the expression for the anisotropic component of the downwash turbulence is

$$w_A(t) = \left[\frac{a\,V^2}{\Phi_o}\right]^{1/2} \mathcal{L}^{-1}\left\{ \frac{1 - e^{-hs}}{s}\, n_A(s) \right\} \quad , \qquad (H.3)$$

where $h \equiv b/(aV)$ and $\mathcal{L}^{-1}$ is the inverse Laplace transform operator. With the following definitions:

$$\mathbb{L}(s) \equiv \frac{1 - e^{-hs}}{s} \quad \leftarrow \text{ inverse Laplace transform } \rightarrow \quad l(t)$$

(H.4)

and

$$\mathbb{M}(s) \equiv n_{A}(s) \quad \leftarrow \text{ inverse Laplace transform } \rightarrow \quad m(t) \quad ,$$

(H.5)

Equation (H.3) takes the form

$$w_{A}(t) = \left[\frac{a\, V^{2}}{\Phi_{o}} \right]^{1/2} \mathcal{L}^{-1} \left\{ \mathbb{L}(s)\, \mathbb{M}(s) \right\} \quad . \qquad \text{(H.6)}$$

- H2 -

Equation (H.6) can accordingly be rewritten as[H1]

$$w_A(t) = \left[\frac{a\ V^2}{\Phi_o}\right]^{1/2} \int_o^t l(\tau)\ m(t-\tau)\ d\tau \qquad . \qquad (H.7)$$

In order to determine "l," consider the following mathematical relation[H2]

$$\mathcal{L}\left\{I(h,t-t_o)\right\}\ e^{-st_o}\ \frac{1 - e^{-hs}}{hs} \qquad \text{for } t_o \geq 0 \qquad . \qquad (H.8)$$

Here $I(h,t-t_o)$ is the unit finite impulse function and "t" is the onset of the impulse. Incorporating this fact into the present anaysis provides

- H3 -

$$l(t) = \mathcal{L}^{-1}\left\{ \mathbb{L}(s) \right\}$$

$$= \mathcal{L}^{-1}\left\{ \mathcal{L}\left\{ I(h, t-t_o) \right\} \right\}$$

$$= h\, I(h, t-t_o)$$

$$= h\, I(h, t) \quad \text{for } t_o = 0 \quad . \quad (H.9)$$

Consequently, Equation (H.9) yields

$$l(t{=}\tau) = h\, I(h, \tau) \quad . \quad (H.10)$$

Equation (H.10) permits (H.7) to take the form

- H4 -

$$w_{A}(t) \; = \; \left[\frac{a \; V^2}{\Phi_o} \right]^{1/2} \int_o^t h \; I(h, \tau) \; m(t-\tau) \; d\tau \qquad . \qquad (H.11)$$

Considering the mathematical nature of the white noise source and invoking the fact that the product "h I(h,τ)" equals unity over the range $0 \le \tau \le h$ (cf. Figure H1) , allows Equation (H.11) to be written as

$$w_{A}(t) \; = \; \left[\frac{a \; V^2}{\Phi_o} \right]^{1/2} \int_o^h n_{A}(t-\tau) \; d\tau \qquad . \qquad (H.12)$$
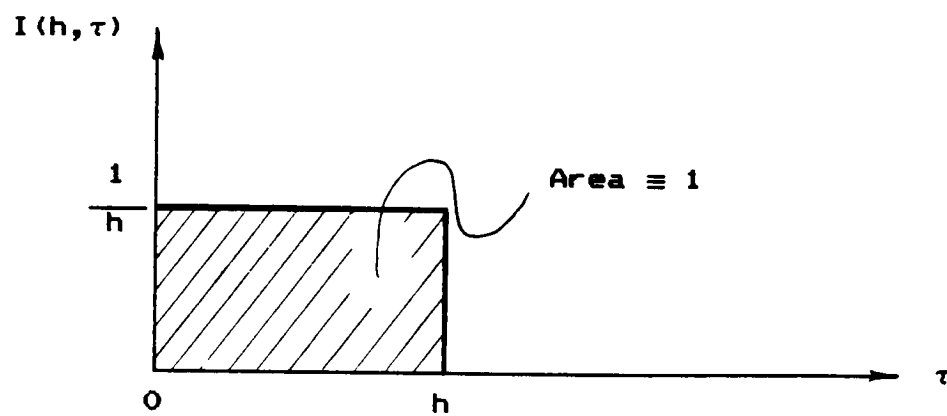
Figure H1 : Unit Finite Impulse Function with $t_o = 0$

(............ APPENDIX H REFERENCES ....)

[H1]Spiegel, Murray R., _Advanced Mathematics for Engineers and Scientists_, Schaum's Outline Series, McGraw-Hill Book Co., Inc., N.Y., 1971, pp. 100-102.

[H2]Churchill, R., _Operational Mathematics_, 2nd ed., McGraw-Hill Book Co., Inc., N.Y., 1958, p. 26.